ADVANCEMENTS IN NEUROIMAGING FOR MILD TRAUMATIC BRAIN INJURY AND MULTI-SITE RELIABILITY

A Dissertation

Submitted to the Faculty

of

Purdue University

by

Sumra Bari

In Partial Fulfillment of the

Requirements for the Degree

of

Doctor of Philosophy

August 2019

Purdue University

West Lafayette, Indiana

THE PURDUE UNIVERSITY GRADUATE SCHOOL
STATEMENT OF DISSERTATION APPROVAL

Dr. Thomas M. Talavage, Chair

School of Electrical and Computer Engineering

Dr. Eric A. Nauman

School of Mechanical Engineering

Dr. Joaquín Goñi

School of Industrial Engineering

Dr. David J. Love

School of Electrical and Computer Engineering

Dr. Edward J. Delp

School of Electrical and Computer Engineering

Approved by:

Dr. Dimitrios Peroulis

Head of the School Graduate Program

Dedicated to my *support system*.

That kept me fighting through times of stress.

ACKNOWLEDGMENTS

I would like to express my sincere gratitude to my advisor Prof. Thomas M. Talavage. Prof. Talavage has always been very supportive and involved in my research projects. I would like to thank him for his mentorship and words of encourgement that led me accomplish this work.

I would like to thank Prof. Eric Nauman and Prof. Joaquín Goñi for their immense support, guidance and encouragement.

I would also like to acknowledge *Purdue Neurotrauma Group* for all their efforts in collecting the data and thank my former and current colleagues Dr. Kausar Abbas, Dr. Trey Shank, Dr. Diana Svaldi, Dr. Ikbeom Jang, (Drs. to be) Nicole Vike, Pratik Kashyap, Andres Llico and Xianglun Mao for stimulating discussions.

I would like to thank my friends (Drs. to be) Hamad Ahmed, Ahmed Zeeshan Pervaiz, Dr. Usman Sadiq, Dr. Umer Iftikhar, Ahsan Shahid, Talal Haider and Dr. Kamran Lodhi for making this place a home away from home and the delicious cooking. I would especially like to thank my best friend Dr. Zeeshan Nadir for his support, help and encouragement during times of stress.

TABLE OF CONTENTS

Page

LIST OF TABLES

Table Page

LIST OF FIGURES

Figure Page

Figure Page

Figure Page

Figure Page

ABBREVIATIONS

mTBI	mild Traumatic Brain Injury
HAE	head acceleration event
fMRI	functional Magnetic Resonance Imaging
MRS	Magnetic Resonance Spectroscopy
CSA	collision sport athlete
NCA	non-collision sport athlete
PTA	peak translational acceleration
rs-fMRI	resting-state functional Magnetic Resonance Imaging
FC	funtional connectome
GSR	global signal regression

ABSTRACT

Bari, Sumra Ph.D., Purdue University, August 2019. Advancements in Neuroimaging for mild Traumatic Brain Injury and Multi-site Reliability. Major Professor: Thomas M. Talavage.

Head injuries in collision sports have been linked to long-term neurological disorders. High school collision sport athletes, a population vulnerable to head injuries, are at a greater risk of chronic damage. Various studies have indicated significant deviations in brain function due to the accumulation of repetitive low-level subconcussive impacts to the head without externally observable cognitive symptoms. The aim of this study was to investigate metabolic changes in asymptomatic collision sport athletes across time within their competition season and as a function of mechanical force to their head. For this purpose, Proton Magnetic Resonance Spectroscopy (MRS) was used as a tool to detect altered brain metabolism in high school collision sport athletes (football and soccer) without diagnosed concussion. Also, sensors were attached to each athletes head to collect the count and magnitude of head impacts during their games and practices. Transient neurometabolic alterations along with prolonged recovery were observed in collision sport athletes.

Multi-site studies are becoming important to increase statistical power, enhance generalizability, and to improve the likelihood of pooling relevant subgroups together, activities which are otherwise limited by the availability of patients or funds at a single site. Even with harmonized imaging sequences, site-dependent variability can mask the advantages of these multi-site studies. The aim of this study was to assess multi-site reproducibility in resting-state functional connectivity fingerprints, and to improve identifiability of obtained functional connectomes. We evaluated individual fingerprints in test- retest visit pairs within and across two sites and present a

generalized framework based on principal component analysis (PCA) to improve identifiability. The optimally reconstructed functional connectomes using PCA showed a substantial improvement in individual fingerprinting of the subjects within and across the two sites and test-retest visit pairs relative to the original data. Results demonstrate that the data-driven method presented in the study can improve identifiability in resting-state functional connectomes in multi-site studies.

1. DEPENDENCE OF BRAIN METABOLISM ON SUBCONCUSSIVE IMPACTS IN COLLISION SPORT ATHLETES: AN MR SPECTROSCOPIC STUDY

The material presented in this chapter is published in [1].

1.1 Introduction

Recent interest in the diagnosis and prognosis of mild traumatic brain injury (mTBI) and concussion in collision sports has grown, driven by a number of disturbing trends related to the short- and long-term health of participating athletes [2, 3]. Until recently, the standard of clinical care for a diagnosis of concussion would allow athletes to return to play as soon as they became symptom free [4]. Athletes with a history of diagnosed concussions often continued participation in practices and games, leading to greater risk of accumulating structural and functional brain alterations [5, 6]. Long term neurological impairments associated with mTBI include early on- set of Alzheimers disease, dementia, depression, and even chronic traumatic encephalopathy [4, 7, 8]. Among male athletes American Football has the highest annual rate of reported concussions, a position held by soccer in female athletes [9, 10]. Extra care and systematic evaluation is required in case of high school athletes before they return to play, because they are more neurologically vulnerable than a collegiate population [11].

Critically, a growing body of research has now demonstrated that asymptomatic athletes are also at the risk of functional and structural brain damage [12–17]. Such findings have raised concerns regarding the many subconcussive impacts experienced by collision-sport athletes. A subconcussive event involves a direct blow to the head or an indirect acceleration or whiplash movement due to an impact elsewhere on the

body, but does not result in clinical symptoms [18] -hereafter referred to as a head acceleration event (HAE).

Repetitive exposure to HAEs is linked to later life-long cognitive and functional impairment [7, 19–21]. Athletes experience hundreds of HAEs during each competition season [22], but these events largely go uninvestigated as they produce no overt symptoms. Continued participation by these seemingly uninjured athletes is hypothesized to increase susceptibility to meaningful brain injury [23,24], with animal models suggesting the increased likelihood of development of neurodegenerative disease [25].

Detection and intervention to reduce the potential long-term consequences of exposure to HAEs is, therefore, a critical direction for the research community [26]. Conventional structural imaging techniques (computed tomography or T_1/T_2 weighted MRI) may not always detect the subtle physiologic changes or cellular injury caused by the accumulation of these events. Functional neuroimaging techniques like functional MRI (FMRI) and diffusion weighted imaging (DWI), however, play a significant role in elucidating the structural and physiologic changes caused by repetitive head trauma in the absence of overt cognitive symptoms. Several studies using these modalities have demonstrated changes in functional connectivity, working memory, cerebrovascular reactivity and white matter in asymptomatic collision sport athletes due to repeated HAE exposure [12,13,15–17,27–31]. Another important non-invasive tool that provides assessment of metabolite profiles and helps in elucidating altered neurometabolism is proton (^{1}H) magnetic resonance spectroscopy (MRS). MRS has been used as a diagnostic tool to investigate changes in physiology in common neuropathologies like multiple sclerosis, dementia, Parkinsons disease, and Alzheimers disease [32–36]. MRS also serves as an ideal biomarker for identifying early brain changes in mTBI, including concussion [37–39,39–46]. We have previously used MRS to determine alterations in neurometabolite concentrations occur during periods of exposure to HAEs [47, 48].

This study of high school-aged male football and female soccer collision sport athlete (CSA) and non-collision athlete (NCA) control populations seeks to evaluate

whether MRS-detected changes exist and are associated with particular HAE characteristics. Observation in asymptomatic athletes of alterations in neurometabolism that are found to be associated with particular HAE mechanical loading profiles would be suggestive of preventable cellular injury. Such a finding would have broad implications for mitigation of the effects of subconcussive events, through which collision-based sports could be made safer for all participants.

1.2 Methods

Purdue Institutional Review Board approved all research methods prior to initiation of the study. Participants of 18 years and above provided written informed consent and participants under the age of 18 provided parental consent and participant assent.

1.2.1 Participants

Ninety (90) high school athletes participated in this study. Two pools comprise this sample, 63 athletes participating in collision sports (CSA) and 27 athletes participating in non-collision sports (NCA).

CSA: 40 male football athletes (ages: 15-18 years, mean=16.4) and 23 female soccer athletes (ages: 14-17 years, mean=15.9), each a member of a high school junior varsity or varsity team, were recruited from two local high schools over two seasons of play (seven football and six soccer players participated in both the seasons, yielding a total of 76 observations for CSA).

NCA: 14 male athletes (ages: 15-18 years, mean=16.21) and 13 female athletes (ages: 14-18 years, mean=16.07), each participating only in non-collision high school sports (e.g. cross-country, swimming, track and field, tennis, basketball, softball) at the junior varsity or varsity level, were recruited (from the same high schools as the CSA participants) to serve as a control for the stability of the measurement process.

Note that participants were not excluded due to history of concussion. Self-reports of prior history of concussion (and associated counts) were 16 of 40 male CSA (1 prior concussion: n = 9; 2 prior concussions: n = 4; 3 prior concussions: n = 3), 6 of 27 female CSA (1: n = 3; 2: n = 1; 3: n = 2), 5 of 14 male NCA (1: n = 3; 2: n = 1; 4: n = 1), and 4 of 13 female NCA (1: n = 3; 3: n = 1).

None of the athletes were diagnosed with a concussion by their athletic trainer or team physician during the period of study.

1.2.2 Imaging Schedule

The CSA pool underwent five imaging sessions: one prior to participation in collision activities (*Pre*), one each during the first (*In1*) and second (*In2*) halves of the competition season, and two following the cessation of collision activities at intervals of 4-8 weeks (*Post1*) and 20-24 weeks (*Post2*). Athletes were physically active during the period prior to collision activities (i.e., *Pre*) and the transition to *In1* was marked by the onset of practices involving collisions (i.e., tackling for football, heading for soccer). Note that data from *Post2* were not used in statistical analyses for our female CSA (soccer) cohort, because a simple survey of activity (conducted prior to each imaging session) revealed most of these athletes had been participating for at least the preceding month in club soccer without associated monitoring of HAE exposure.

NCA participants underwent two MRI scanning sessions (*Test*, *Re-Test*), 5 to 18 weeks apart within their training/competition seasons, maintaining comparable levels of physical activity at both sessions.

1.2.3 Head Acceleration Event (HAE) Monitoring

Soccer: For all 23 participants, HAEs were monitored during all practices and games using the xPatch (X2 Biosystems; Seattle, WA). The xPatch sensor was attached to each athletes head, behind the right ear, using an adhesive patch applied

subsequent to cleaning of the area with rubbing alcohol. On an as-needed basis, a spray adhesive (CavilonTM) was applied. Data from the sensors were downloaded after each practice and game, using the Head Impact Monitoring System software (X2 Biosystems; Seattle, WA). Sensors recorded HAEs having Peak Translational Accelerations (PTA) greater than 10 g as separate events. The software provided Peak Translational Acceleration (PTA) and Peak Angular Acceleration (PAA) for each recorded event. Low-acceleration eventsthose having PTA $\leq$ 20 g [49] – and events outside the valid time window of a practice or a game were discarded. Monitoring was conducted over two seasons of play, yielding 29 observations (six players participating in both seasons).

Football: For one of the two seasons included in this analysis, 24 football athletes had HAEs monitored during all practices and games using the xPatch. During the other season, the commercially-available Vector mouthguard-based telemetry system (i1 Biometrics) was used to monitor HAEs; however, this device failed to reliably capture video-documented impacts, so no HAE data from this season were included in subsequent analyses.

Non-Collision Athletes: Due to substantial anticipated difference in exposure to subconcussive trauma relative to CSA, NCA participants were not monitored for HAEs during training or competition.

1.2.4 MRS Data Acquisition

All imaging sessions were conducted at the Purdue University MRI Facility (West Lafayette, IN), using a 3T General Electric Signa HDx (Waukesha, WI) with a 16-channel brain array (Nova Medical; Wilmington, MA). Single-voxel MR spectra were acquired using the PRESS (Point RESolved Spectroscopy) pulse sequence (TR/TE = 1,500/30 ms, 128 averages, 2.0 x 2.0 x 2.0 cm^3). A high-resolution T1-weighted anatomical scan was acquired for registration and tissue segmentation purposes using

3D spoiled gradient recalled echo (SPGR) sequence (TR/TE = 5.7/1.976 ms, flip angle = 73, 1 mm isotropic resolution).

Spectra were obtained specifically from the left dorsolateral prefrontal cortex (DLPFC) and dominant primary motor cortex (M1), with voxels placed as shown in Fig. 1.1 – see also [47]. DLPFC was monitored due to its role in working memory [50] and our previous findings of altered functional activity [15, 20, 51] and cerebrovascular reactivity [31] in this region for asymptomatic collision sport athletes. M1 has been documented to exhibit neurometabolic alterations subsequent to traumatic brain injury [43, 52].

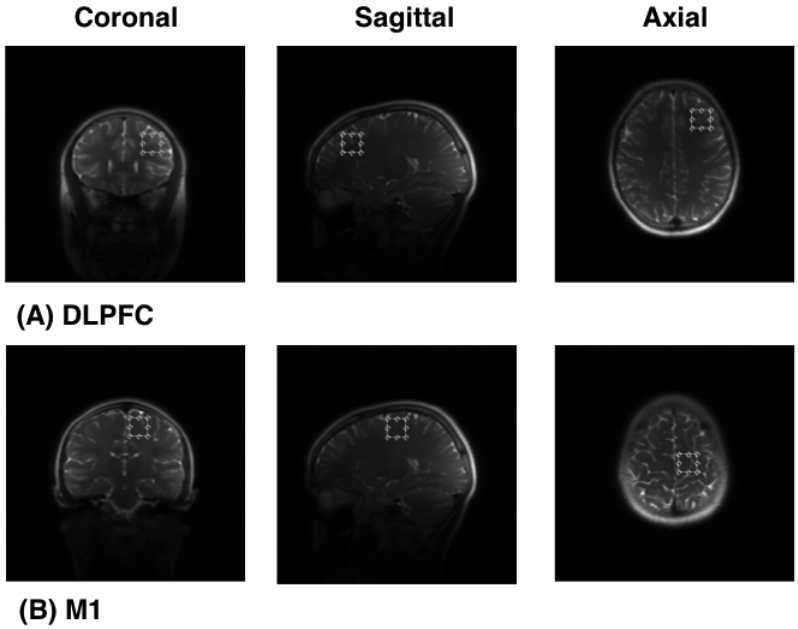

Fig. 1.1.: Three planar views of MRS voxel placement in (A) DLPFC and (B) M1.

1.2.5 Data Processing

Evaluation of HAEs

HAE metrics were determined for the 53 monitored CSA up to the date of each imaging session (*In1, In2* and *Post1*). First, the (to-date) cumulative PTA

($\mathbf{cPTA_{(Th,j,i)}}$) for *i-th* athlete at the *j-th* session (*In1-2*, *Post1*) was obtained by summing the PTA of each of those N_j HAEs which exceeded the threshold (***Th***) experienced by the corresponding athlete from the beginning of the season until either the day of assessment (for *In1* and *In2*) or through the end of the season (*Post1*):

$$cPTA_{Th,j,i} = \sum_{k=1}^{N_j} PTA_{k,i} \cdot u(PTA_{k,i} - Th)$$

where

$$u(x) = \begin{cases} 1 & : x > 0 \\ 0 & : x \leq 0 \end{cases}$$

While a similar procedure was used to compute cumulative PAA (cPAA), only cPTA was considered for further analysis. This decision was made given that cPTA and cPAA were found to be highly correlated (95% CI of sample correlation [0.995; 0.998]), and prior work has demonstrated that measurement of PTA is more accurate [53].

Next, the (to-date) cumulative number of head acceleration events $\boldsymbol{cHAE_{Th,j,i}}$ was obtained by counting each of the N_j head acceleration events exceeding the targeted threshold (Th), as above:

$$cHAE_{Th,j,i} = \sum_{k=1}^{N_j} u(PTA_{k,i} - Th)$$

Finally, the average PTA $\boldsymbol{aPTA_{Th,j,i}}$ as experienced by the *i-th* athlete from the beginning of the season until the date of the *j-th* imaging session for a given threshold level Th was calculated as

$$aPTA_{Th,j,i} = \frac{cPTA_{Th,j,i}}{aHAE_{Th,j,i}}$$

To assess whether a clear threshold existed below which HAEs did not meaningfully contribute to changes in metabolite concentrations, the cPTA and aPTA were computed for three threshold levels: 20g, 50g and 70g (approximately corresponding to 20th, 75th and 90th percentile of all impacts recorded that exceeded 10g).

MRS Data Processing

Tissue water reference concentrations as reported by TARQUIN [54] were used. Since the spectroscopic voxels contained fractions of CSF, grey matter and white matter, the values from TARQUIN were corrected for partial volume effects and for metabolite and water T_1 and T_2 relaxation effects-using AFNI [55] and FSL [56] and [57] – following the procedure described in [47]. Our metabolites of interest include myo-inositol (Ins), an osmolyte involved in glial cell growth; total N-acetyl aspartate and N-acetylaspartylglutamate containing compounds (tNAA), a biomarker of neuronal integrity; total creatine-containing compounds (tCr), key in energy metabolism; total choline-containing compounds (tCho), a measure of inflammation, demyelination and membrane turnover or repair; and glutamate and glutamine (Glx), a neurotransmitter and its precursor that reflect synaptic activity [36, 47, 58, 59]. A typical MRS spectrum of the metabolites of interest is shown in Fig. 1.2.

The placement of spectroscopic voxels in follow-up scans was accomplished by attempting to match the reconstructed voxel location from *Pre/Test* sessions. Since multiple operators were conducting the MRI sessions, any imaging session with inconsistent voxel placement resulting into voxel overlap of less than 30% with the *Pre/Test* session (within same subject) was discarded. The metabolite values from the surviving imaging sessions, with Cramer-Rao lower bounds less than 25% standard deviation as reported by TARQUIN, were included into the statistical analysis. Data from one female NCA were discarded for poor spectra, as detected by visual inspection. The percentage of data points excluded for each population due to these criteria is summarized in Table A.1.

Statistical Analysis

Analyses were conducted in R. To account for missing values (e.g., lost after quality checks or athletes absent from an imaging session) the means of 50 imputations from

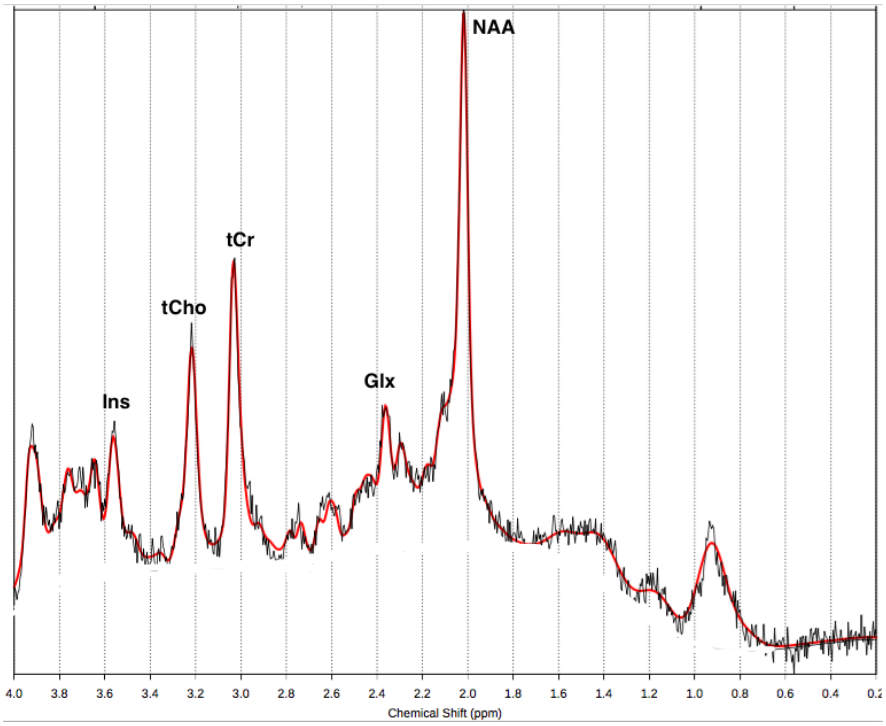

Fig. 1.2.: Raw Spectrum of metabolites of interest (myo-inositol (Ins), N-acetyl aspartate and N-acetylaspartylglutamate (tNAA), creatine-containing compounds (tCr), choline-containing compounds (tCho) and glutamate and glutamine (Glx)).

Amelia II [60] were used to complete the dataset. Because some groups did not satisfy normality (Shapiro-Wilk test; $p < 0.05$) and sphericity (Mauchlys Test; $p < 0.05$) conditions, non-parametric tests were conducted in lieu of ANOVA.

First, the stability of MRS measures across sessions was evaluated on the *Test* and *Re-Test* sessions from the NCA, using a Wilcoxon signed rank test followed by false discovery rate (FDR; [61]) correction. Any pairwise comparison was considered significant if $p_{FDR} < 0.05$. All metabolite concentrations were found to be stable across the two sessions in NCA. In contrast with [47], the total concentrations of tCr were also found to be stable across sessions in both NCA and CSA. Therefore, metabolite concentrations and metabolite ratios to [tCr] from the NCA *Test* and *Re-Test* sessions were pooled for subsequent comparison to the CSA.

Neurometabolite concentrations and ratios for the CSA pool were evaluated for dependence on session by a Friedman Test (the non-parametric version of a one-way repeated measures ANOVA), conducted separately for each metabolite concentration and ratio. Those metabolites and ratios that exhibited significant changes ($p < 0.05$) were further analyzed by pairwise comparisons among all sessions using the Wilcoxon signed rank test, followed by FDR correction.

Those metabolites/sessions in the male and female CSA pools found to be significantly different from the corresponding *Pre* session were further analyzed with linear regression models to examine the association between metabolite concentrations and $aPTA$, at multiple threshold levels. Regressions were performed iteratively by removing each data point, and at each iteration the goodness-of-fit (R^2) was computed and an F-test was used to compare the fit to a constant model. We report here the mean R^2 and p-value associated with the mean F-statistic of all iterations.

While not necessarily expected to differ at the group levelnot all CSA experienced equivalent histories of HAE exposurethe NCA and (asymptomatic) CSA pools were compared at each session, using a Wilcoxon rank sum test followed by FDR correction. Note that only within-gender comparisons were made between NCA and CSA.

1.3 Results

1.3.1 HAE Monitoring

Summary HAE statistics are reported in Appendix A Tables A.2-A.4 for male and female CSA. Table A.2 reports the $25^{th}, 50^{th}, 75^{th}$ and 90^{th} percentiles of PTA of all HAEs experienced by male and female CSA pools. Table A.3 and Table A.4 reports the median $cPTA_{Th,j,i}$ and $aHAE_{Th,j,i}$ for male and female CSA pools at $Th = 20g, 50g$ and $70g$ and *In1-2*, *Post1* sessions respectively. Female CSA experienced statistically significant lower $cPTA_{50g,In2,i}$ than male CSA (Fig. 1.3) as observed by Wilcoxon sign rank test ($p = 0.002$).

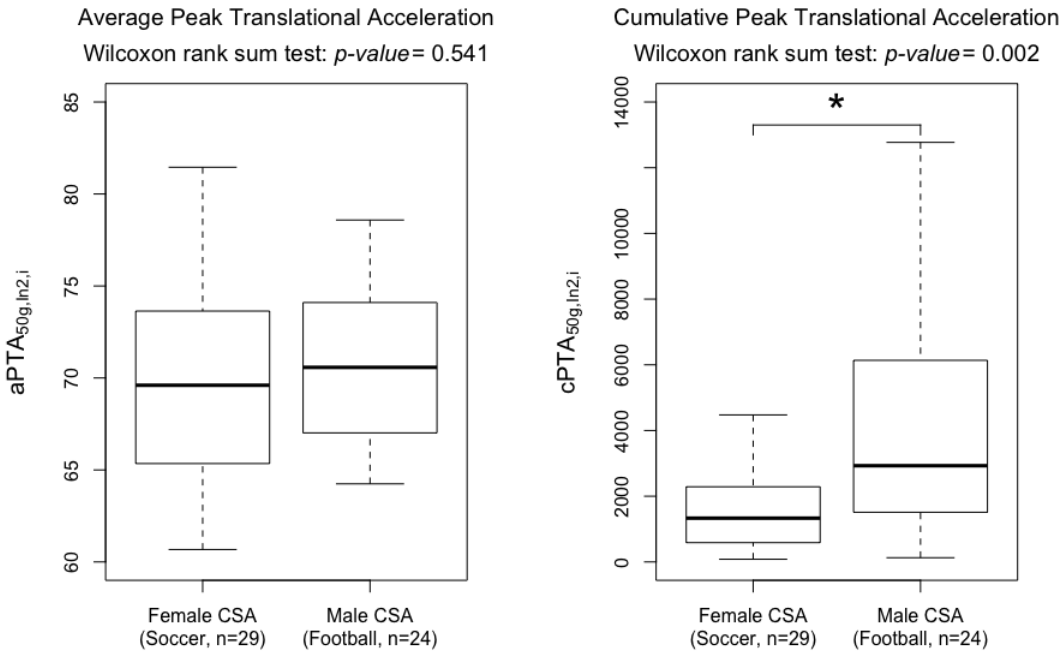

Fig. 1.3.: Boxplots comparing the and experienced by female CSA (Soccer) and male CSA (Football) pools at a threshold of 50g at *In2*.

1.3.2 MR Spectroscopy

Summary statistics documenting stability of the assessed metabolites across sessions in the male and female NCA pools are listed in Tables A.5 and A.6. Comparable measures for session-dependence in male and female CSA pools are presented in Tables A.7 and A.8.

Male and female CSA pools exhibited alterations in metabolite concentration and/or metabolite ratio across sessions. In M1, the female CSA (i.e., soccer) pool exhibited a statistically significant (Friedman $\chi^2 = 11.36$, $p = 0.009$) increase in absolute concentration of M1 Glx at *Post1* relative to *Pre*. (Fig. 1.4A). This change in absolute concentration was accompanied by a statistically significant (Friedman $\chi^2 = 10.99$, $p = 0.012$) increase in the ratio [Glx]:[tCr] at *In2* and *Post1* relative to *Pre*. (Fig. 1.4B). In DLPFC, the male CSA (i.e., football) pool exhibited a statistically

significant (Friedman $\chi^2 = 9.6$, $p = 0.047$) decrease in DLPFC [Glx] at *In2*, relative to each of *Pre*, *In1* and *Post2* (Fig. 1.5A). This group also exhibited a statistically significant (Friedman $\chi^2 = 15.013$, $p = 0.005$) increase in the ratio of DLPFC [tCho] to DLPFC [tCr] (i.e., [tCho]:[tCr]) at *In2* relative to each of *Pre*, *In1* and *Post2* (Fig. 1.5B).

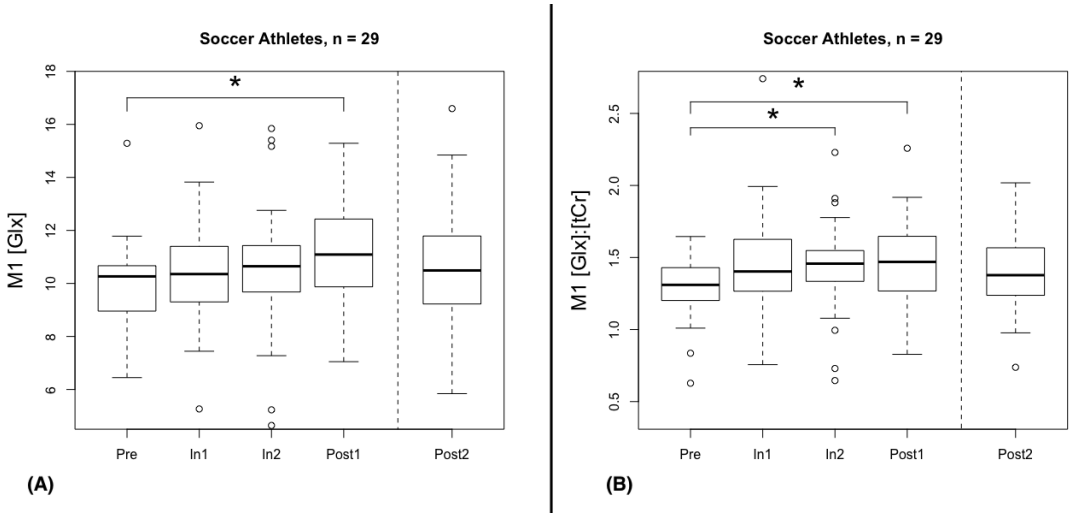

Fig. 1.4.: Box-and-whisker plots of (A) M1 [Glx] and (B) M1 [Glx]:[tCr] for total cohort of soccer athletes (n=29). Session-specific distributions found to be significantly deviant ($p_{FDR} < 0.05$, Wilcoxon signed rank test) by pairwise comparisons are marked by an asterisk.

1.3.3 Regression Analysis

Changes across session within CSA that did not result in group-level differences with the NCA stability measurements motivated assessment whether the across-session changes for CSA were primarily confined to a sub-population of athletes who had experienced greater levels of mechanical loading. Statistical results of the regression analyses are presented in Table 9. Nearly all conducted regressions evidenced their best goodness-of-fit (R^2) with $aPTA$ when optimized for $Th = 50$ g (Figure 6A). At this threshold, the regression for male CSA athletes at *In2* of DLPFC [tCho]:[tCr]

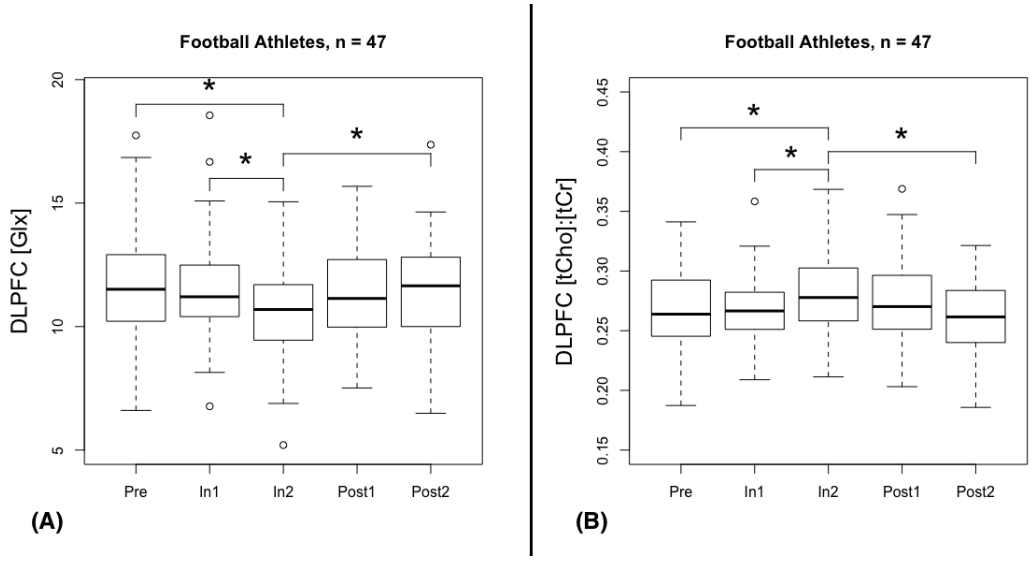

Fig. 1.5.: Box-and-whisker plots of (A) DLPFC [Glx] and (B) DLPFC [tCho]:[tCr] for total cohort of football athletes (n=47). Session-specific distributions found to be significantly deviant ($p_{FDR} < 0.05$, Wilcoxon signed rank test) by pairwise comparisons are marked by an asterisk.

against HAE measures achieved a mean F-statistic across iterations corresponding to an uncorrected significance level of $p < 0.05$ (Figure 6B). No other regressions resulted in a mean F-statistic having $p < 0.05$.

1.4 Discussion

We have investigated metabolic changes in two CSA pools (male football, female soccer) both (*1*) across time, within individual competition seasons; and (*2*) as a function of HAE exposure. Our main findings indicate the presence of session-dependent metabolic alterations in both groups of CSA, suggesting that CSA are combating cellular dysfunction in the absence of observable external symptoms. Further, there is evidence that the time-dependent changes in male football athletes are a function of exposure to the history of mechanical loading. The significantly lesser cumulative exposure to HAEs for female CSA cohort as compared to their male counterparts

(see Fig. 1.3 and Table A.2) presents a likely explanation for the lesser number of metabolic changes for the soccer athletes. These findings suggest that metabolic disturbance is most likely to occur after accumulation of some as-yet-undetermined threshold of mechanical loading to the head.

Evidence for metabolic disturbance

Two versions of metabolic disturbance were observed in this study. Male CSA exhibited changes in DLPFC associated with glutamate+glutamine (Glx) and with total choline containing compounds (tCho), whereas female CSA exhibited changes in M1 associated only with glutamate+glutamine (Glx). These findings are in contrast with stable measurements observed for all metabolites across *Test* and *Re-Test* sessions in male and female NCA.

Football athletes (i.e., male CSA) exhibited changes in DLPFC with the onset of, and sustained exposure to, collision events, with changes disappearing once exposure to collision events ceased. For both [Glx] and [tCho]:[tCr], Fig. 1.5 illustrates clear deviation during the second half of the season (*In2*) relative to *Pre*, with the deviation lessening at *Post1* and returning to baseline levels at *Post2*. Altered metabolite measures trended toward *Pre*-season levels 1-2 months after the season, with return to baseline occurring after approximately five months of reduced (e.g., in the case of wrestling) or non-existent exposure to HAEs. These findings suggest that the sustained exposure to repetitive trauma, caused by subconcussive blows to the head, can trigger transient metabolic disturbance, with gradual return to baseline levels (plausibly reflecting healing of cellular damage) once exposure ends. In particular, the decrease observed in DLPFC [Glx] at *In2* assessment could be associated with the alteration in excitatory synaptic activity, and increased Glx catabolism resulting from hypoglycemia [62]. This decreasing trend has been previously observed in both animal models [62] and studies of concussed and mild TBI patients [39, 42, 43, 45, 47]. Elevation of DLPFC [tCho]:[tCr] suggests ongoing processes of membrane turnover for potential repair of cells and inflammation [37, 38, 40, 41, 46, 63].

Soccer athletes (i.e., female CSA) exhibited changes only in primary motor cortex (M1). The increases in M1 [Glx] and M1 [Glx]:[tCr] at *In2* and *Post1* could be linked to alterations in excitatory synaptic activity in motor area and motor dys-function. The increase in [Glx] could further be associated with a secondary response to injury [64, 65] which can cause excitotoxic accumulation. This last has been previously observed or postulated in patients with mild TBI or concussion [45, 47, 66]. Two possible factors that could have led to this increase in Glx in female CSA include a gender effect associated with the menstrual cycle, and a sport-related effect arising from the significantly lesser cumulative exposure to HAEs for the females, relative to their male counterparts. (See below for further discussion of these matters.) Note from Fig. 1.4 that the altered metabolite measures trended toward *Pre*-season levels approximately five months after the season, even with known (but uncharacterized) recent HAE exposure for many of the athletes.

In general, the neurochemical deviations observed in both groups of clinically asymptomatic CSA during and subsequent to accumulation of HAEs indicate the presence of an altered metabolic state. The combination of impaired neuro-transmission and hypermetabolism (associated with [Glx]) with evidence of inflammation and increased membrane turnover (associated with [tCho]:[tCr]) arising from HAE exposure strongly argue for cellular injury to the brain preceding the overt cognitive symptoms typically observed in clinically-diagnosed concussion.

Prolonged neurometabolic recovery period supported by other biomarkers

These findings of neurometabolic alterations in the presence of HAEs are consistent with previous biomarker findings suggesting that repetitive head trauma can produce disturbances in brain physiology in the absence of diagnosable cognitive symptoms. The timeline of metabolic deviations in this study are similar to aberrations observed in cerebrovascular reactivity (CVR) in asymptomatic female soccer athletes [31], and all of resting-state fMRI [27, 67], working memory task-based fMRI [29], and diffusion weighted imaging [28] in asymptomatic football athletes. In

all cases, deviations from pre-participation measurements (i.e., *Pre*) persisted for at least two months following the end of the season, sometimes being observed as late as five months after cessation of HAE exposure. This suggests that the asymptomatic CSA in this study are likely to have a transient injury from which it takes several months for natural repair processes to return physiologic health to baseline levels. The presence of a mismatch between injury accumulation and repair raises concerns for the neural health of all adolescent collision-sport athletes.

Dependence of metabolic disturbance on HAE exposure

Alterations in cellular signaling and inflammation observed in football athletes were correlated with the average acceleration per HAE. The deviant metabolite distributions of DLPFC [Glx] and [tCho]:[tCr] at *In2* exhibited negative and positive correlations, respectively, with the aPTA experienced by the football athletes during the second half of their competition season. These relationships with HAEs imply that greater mechanical stress may induce impaired neuro-transmission, an acute state of hypermetabolism and increased membrane turnover and inflammation [62, 68]. Of particular interest, the best modeling prediction was associated with an HAE threshold of 50 g, and is comparable to findings in the study of cerebrovascular reactivity in female soccer athletes [69]. These results support the hypothesis that with accumulation of HAEs there is continual increment in neurometabolic alterations, which could ultimately exceed a threshold beyond which the metabolic disturbances never return to baseline levels.

Metabolic disturbances causing state of brain vulnerability

Considering a longer perspective, the absence of immediate symptoms could predispose athletes to alterations in brain physiology that appear later in life, or under particular circumstances [23, 24]. The neural health of young athletes suffering from transient metabolic disturbances in the absence of diagnosable cognitive symptoms is therefore of concern, as these athletes are more likely to continue participation with

associated accumulation of strain at the cellular level. The subsequent neurometabolic cascade of mild TBI follows a sequence of initial ionic fluxes, impaired neurotransmission and changes in glucose metabolism resulting in high energy demands and a period of metabolic crisis [70, 71]. The critical mismatch between supply and demand of energy during repeated exposure to HAEs could result in a positive feedback loop with negative consequences. In particular, increasing energy demands due to metabolic crisis could be exacerbated by progressively more impaired metabolite delivery, as suggested by changes in CVR [31]. Such an escalation of the energy crisis could readily result in a prolonged recovery period from transient metabolic disturbances, similar to those observed in this study. Further, it would be expected that during the condition of energy crisis caused by repetitive head trauma, cellular metabolism would be stretched to its limits and cells could become more vulnerable. Overstimulation of the adolescent brain in this condition could cause long lasting effects on the complex sequence of neurochemical and anatomical events occurring during normal development [72, 73]. It is further feasible that young athletes suffering multiple instances of transient metabolic injury might never return to baseline levels, potentially leading to learning, memory, or cognition deficits. In addition, transient metabolic disturbances that lead to dysfunctional neurotransmission could increase the risk of diminished attention and cognitive performance, making adolescent collision-sport athletes susceptible to greater numbers and magnitudes of HAE, exacerbating the problem.

Reflections on the present study and future directions

The primary methodological limitation of this study was the imperfect voxel placement in longitudinal scans of the same athlete. Manual voxel placement by multiple MRI operators resulted in variable locations from measurement to measurement, leading to changes in the relative proportion of gray matter, white matter, and cerebrospinal fluid in the assessed voxel. Such errors would be expected to increase the variance across the measurements, but should not produce systematic biases in any

specific metabolite concentration as a function of time. Future work will seek to eliminate this issue through use of automatic repositioning of MRS voxel e.g., [74,75].

Another limitation of the present study is derived from the focus on specific anatomic locations, leaving a large portion of the brain unexamined. Incorporation of newer MR spectroscopic imaging (MRSI) techniques would permit investigation of changes over a larger region of the brain, providing spatial indifference [76,77], while also permitting separate examination of disturbances in white and gray matter [78,79].

Additional factors potentially contributing to the differences observed between male (football) and female (soccer) CSA include the relatively modest sample sizes in this work, a possible gender effect given there was no control for the menstrual cycle stage at the time of imaging of female CSA, and a sport-related effect due to the significantly lesser cumulative exposure to HAEs for the females, relative to their male counterparts.

The modest population for which both MRS and HAE measurements were available was potentially exacerbated by the small number of teams from which athletes were recruited. Both football and soccer athletes were recruited from two local high school teams, wherein each team had different playing style [80], skill and athletic level of competition. A study involving more teams could sample a greater range of playing styles, and thus could better quantify dose-response thresholds between HAE exposure and neurometabolic changes. Such a dose-response model will be critical in instituting exposure regulations that may best protect adolescent athletes from the long-term risks associated with repetitive head trauma. Further, an increase in the number of athletes studied would increase the chances of having participants who are diagnosed with a concussion, eventually enabling relative assessment of the severity of metabolic injury for asymptomatic athletes.

Some changes (or the absence thereof) in the female CSA neurometabolic concentrations could be affected by alterations occurring throughout the menstrual cycle. Previous studies have shown significant differences in metabolite concentrations in males and females [81, 82]. These neurometabolic differences are not structural but

are due to sex hormones between the two genders. In females the ovarian steroid hormones like estrogens and progesterone are widespread in brain and have modulating effect on the brain physiology, producing metabolite concentrations variations with the phase of the menstrual cycle. Significant changes in ratios of [tNAA], [tCho], [Ins] and [Glx] to [tCr] have been observed from the follicular to the luteal phase of menstrual cycle [83, 84]. Such changes could have affected the concentrations and ratios observed in this study, particularly given the modest sample sizes, and should be accounted for in future longitudinal studies.

The lesser cumulative HAE exposure for the female CSAa consequence of appreciably fewer and lesser cumulative magnitude of HAEs per practice/game – does not necessarily guarantee safety or neural health. Rather, this lesser daily exposure has likely only put the female CSA at a reduced risk of physiologic changes and delayed crossing of the head impact exposure thresholds proposed to exist for cognitive and behavioral impairment [21], and white matter microstructural and cognitive abnormalities [19]. While both of these studies found that athletes did not exhibit significant changes in brain physiology while exposure remained below the identified thresholds, a constant base- line risk existed. Even a small number of additional HAE exposures could push an athlete above these thresholds, rapidly increasing the risk for later cognitive and behavioral impairment.

1.5 Conclusion

Asymptomatic male (football) and female (soccer) CSA, were found to exhibit statistically significant, albeit transient, neurometabolic disturbances in (male) dorsolateral prefrontal cortex and (female) motor cortex during a period of appreciable exposure to head acceleration events. Extending previous work [47, 48], neurometabolic alterations observed in football athletes during the second half of the season were found to be significantly associated with the average acceleration per HAE, being best predicted by the accumulation of events exceeding 50 g. While a smaller sample

of female CSA (soccer) also exhibited significant changes in metabolite concentrations, these changes were not found to be well-linked to their significantly lesser HAE exposure. Marked deviations in neurometabolism, in the absence of overt symptoms, raise concern about the neural health of adolescent collision-sport athletes. These findings suggest that limiting HAE exposure and allowing adequate rest following the competition season are likely to be beneficial for the neural health of these athletes, and may help to ameliorate the risk of subsequent cognitive impairment.

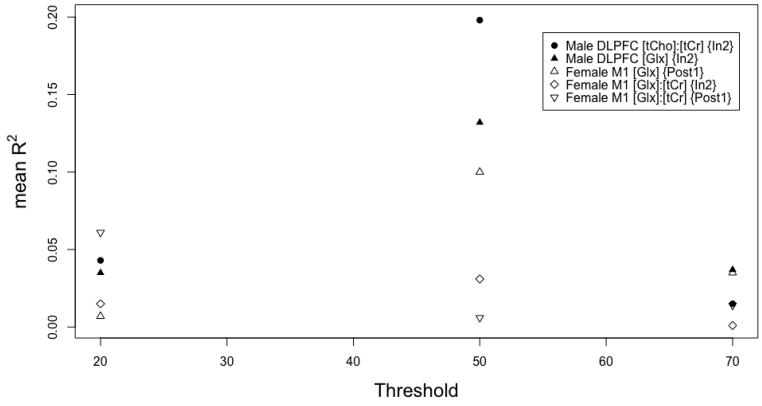

A

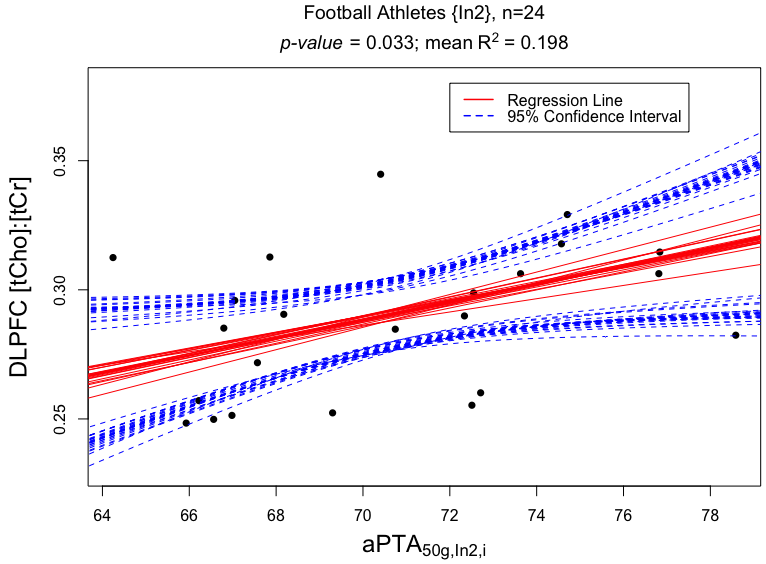

B

Fig. 1.6.: Evaluation of regressions in male and female CSA groups plots for neurometabolite concentrations and ratios against *aPTA* across HAE thresholds. (**A**) Mean R^2 as a function of evaluated threshold value (Th = 20, 50 and 70 g) for all sessions found to significantly differ from their corresponding *Pre* measurement in Figures 1.4 and 1.5. (**B**) The regression fit in male CSA (football) athletes for *In2* DLPFC [tCho]:[tCr] vs. *aPTA* at Th = 50 g – the maximal point in (**A**) – was the only fit to achieve a mean F-statistic that was associated with a p-value of less than 0.05 ($p = 0.033$; uncorrected).

2. UNCOVERING MULTI-SITE IDENTIFIABILITY BASED ON RESTING-STATE FUNCTIONAL CONNECTOMES

The material presented in this chapter is available online at [85] and is under review in NeuroImage, Special Issue *'Reproducibility in Neuroimaging'*.

2.1 Introduction

Multi-site functional magnetic resonance imaging (fMRI) studies are increasingly important for understanding the structure and function of a healthy brain and also subsequent to neuropathology. Recent examples of multi-site imaging initiatives include The Human Connectome Project [86, 87], the 1,000 Functional Connectomes Project (http://fcon_1000.projects.nitrc.org), and disease-oriented initiatives such as the Functional Biomedical Informatics Research Network for schizophrenia [88] and the Alzheimer's Disease Neuroimaging Initiative [89], among others [90]. Multi-site studies achieve larger sample sizes by including cohorts recruited at the different sites. On one hand this allows for higher statistical power and better generalization of the results than may be achieved with potentially limited availability of patients or funds at a single site. On the other hand proper assessment of these data requires principled methodologies, including multivariate analyses coupled with cross-validation designs [89–93]. Known challenges in multi-site acquisitions and their subsequent analyses include the scanner-dependent variability that can mask true underlying changes in brain structure and function. Even when using identical (let alone "comparable") imaging sequences and parameters, potential site-dependent differences might arise due to a range of physical variables, including field inhomogeneities, transmit and receive coil configurations, system stability, system maintenance, scan-

ner drift over time and many others [90, 91, 94]. Determining and minimizing these unwanted site-dependent variations have become critical elements in the design of multi-site fMRI studies.

Many studies have investigated the variation and stability of simple behavioral, motor or memory tasks in multiple sites using fMRI. Such studies have typically used ANOVA models or variance component analysis to examine the variability and extent of overlap of activation maps in task-based fMRI scans acquired across multiple sites [93–100]. In contrast, only a few studies have assessed the variations in resting-state fMRI across sites [101]. These studies used variance component analysis, intra class correlation (ICC) coefficient and/or coefficient of variance to evaluate inter-site and inter-subject variability in connectivity scores, cluster size and temporal signal-to-noise ratio in regions of interest for default mode networks derived from seed-based or independent component analysis [101–109].

Resting-state fMRI (rs-fMRI) measures the spontaneous neural activity in the brain and determines the default functional connectivity between brain regions. rs-fMRI has gained wide-spread attention and is used to investigate brain functional connectivity in the normal healthy brain [110–114] as well as in many clinical populations [115–117]. In recent years, the research areas of network neuroscience and brain connectomics have become central to the understanding of the human brain as a network. In consequence, graph theory and network science methods have been widely used to investigate functional connectivity [118–124]. A functional connectome (FC) is a symmetric square matrix that estimates the level of functional coupling between pairs of brain regions. Each entry is the correlation between the blood oxygenation level dependent (BOLD) signals observed in two different brain regions. Various graph theoretical measures may be used to investigate FC networks [122].

One important avenue of investigation is to explore differences in FC profiles at an individual, rather than group, level [125]. Group averages represent robust connectivity patterns, but inherently mask subject-specific features. Differences in FC profiles in individuals, relative to the group level, have been demonstrated [126–138] and may

help in developing robust neuroimaging-based biomarkers, or even for making subject-level inferences. Robust individual differences in functional connectivity have been termed "fingerprints", and may be demonstrated by the self-identification of subjects by correlating test and retest visits over a body of subjects [127, 136, 139–142]. Fingerprinting relies on the fact that subjects are expected to exhibit an inter-session variability that is less than the inter-subject variability (i.e., they resemble themselves across visits more strongly than they resemble other subjects). The ability to pair the FCs coming from the same subject reflects the inherent level of identifiability of the connectivity dataset.

This study explores the question of variability in the identifiability of subjects in a multi-site scenario, providing a framework to minimize the unwanted site-dependent variations and enhance identifiability on functional connectomes. To do so, we evaluated two independent multi-site resting-state fMRI datasets. To date, identifiability has been studied where test and retest rs-fMRI scans have been conducted in the strictly controlled scenario involving the same scanner, the same imaging sequences, same-day image acquisitions, and constant processing over all data [127, 136, 141]. For example, Amico et al., [136] determined the identifiability of subjects based on test-retest visits on one site. Herein we extend the investigation of identifiability by relaxing a number of these conditions. In particular, one dataset (Purdue) used two different scanners and varied in the number of days between visits, whereas the second dataset (Yale) involved two identically configured imaging-sites. For all cases, the impact of global signal regression as part of the data processing pipeline was also assessed. We optimally reconstructed the FCs using those principal components that maximized multi-site identifiability across all visits, thereby and serving as an orthogonal basis for the functional connectivity. This was performed both with and without global signal regression. For each of these cases, we then compared the multi-site identifiability obtained from the original and optimal reconstructed FCs. In all cases, the reconstruction process produced significantly enhanced identifiability across imaging

systems, providing strong motivation for application of this approach to increase the statistical power and generalizability of results for multi-site fMRI studies.

2.2 Methods

2.2.1 Participants

Purdue dataset

A cohort consisting of 23 undergraduate and graduate students (12 male and 11 female; ages 18-28 years) participated in a total of four imaging sessions (0-21 days apart) at two sites. None of the participants reported any history of neurological disorders. At *site1* two imaging sessions were conducted using a 3T General Electric Signa HDx and a 16-channel brain array (Nova Medical). At *site2* two imaging sessions were conducted using a 3T GE Discovery MR750 and a 32-channel brain array (Nova Medical). The two imaging sessions at a given site were conducted on the same day (i.e., 0 days apart).

Yale dataset

An open source dataset available at http://fcon_1000.projects.nitrc.org/indi/retro/yale_trt.html consisting of 12 (six male and six female; ages 27-56 years) participants was used in the study. The subjects participated in a total of four imaging sessions at two sites approximately one week apart. Data were acquired on two identically configured Siemens 3T Tim Trio scanners at Yale University using a 32-channel head coil [103].

2.2.2 MRI Data Acquisition

Purdue dataset

Each imaging session (independent of site) consisted of a structural T_1 weighted scan and two rs-fMRI scans (*test* and *retest*, eyes open and 9 min and 48 sec). The high-resolution T_1 scan used for registration and segmentation purposes consisted of 3D fast spoiled gradient recalled echo sequence: TR/TE = 5.7/1.976 msec; flip angle = 73°; 1 mm isotropic resolution and the rs-fMRI scans with common imaging parameters across sites consisted of blipped echo-planar imaging: TR/TE = 2,000/26 msec; flip angle = 35°; 34 slices; acceleration factor = 2; Field of View = 20 cm; voxel size = 3.125 x 3.125 x 3.80 mm and 294 volumes.

Note that eight rs-fMRI scans were conducted in total on each subject (184 total scans; see Figure 2.1) and divided into a *training* and a *validation* sets. The two runs acquired in the first session at each of the two sites (four total) were incorporated into the *training* set. Similarly the remaining four rs-fMRI scans, those corresponding to the two runs acquired in the second imaging session at that each site, were incorporated into the *validation* set.

Yale dataset

Each imaging session (independent of site) consisted of a structural T_1 weighted scan and six rs-fMRI scans (eyes open and 6 min). T_1-weighted 3D anatomical scans were acquired using a magnetization prepared rapid gradient echo (MPRAGE) sequence: TR/TE = 2400/1.18 msec; flip angle = 8°; 1 mm isotropic resolution and the rs-fMRI scans with multiband echo-planar imaging: TR/TE = 1000/30 msec; flip angle=55°; 75 slices; acceleration factor = 5; Field of View = 22 cm; voxel size = 2 x 2 x 2 mm and 360 volumes [103].

Two of the six rs-fMRI scans from each imaging session were used as the *test* and *retest*. The imaging sessions were divided in to *training* and *validation* sets in the same way as Figure 2.1.

2.2.3 Data Processing

Both Purdue and Yale datasets were processed with the same processing pipeline, as described below.

rs-fMRI data were processed using functions from AFNI [55] and FSL [56, 57] using in-house MATLAB code following steps from [143]. Structural T_1 images were first denoised using the filters described in [144–146] (using FSL *fsl_anat*) to improve signal-to-noise ratio and effect bias-correction. Images also underwent intensity normalization (AFNI *3dUnifize*). Structural images were then segmented (FSL FAST) into gray matter (GM), white matter (WM) and cerebrospinal fluid (CSF) tissue masks.

rs-fMRI BOLD timeseries were processed in the subject's native space. The first four volumes were discarded to remove spin history effects, leaving 290 volumes for processing. The 4D BOLD timeseries was then passed through outlier detection (AFNI *3dToutcount*), despiking (AFNI *3dDespike*), slice timing correction (AFNI *3dTshift*), and subsequently underwent volume registration (AFNI *3dvolreg*) to the minimized bounding volume. The rs-fMRI BOLD timeseries were then aligned to the T_1 structural scan (AFNI *align_epi_anat.py*). Voxel-wise spatial smoothing was applied independently within each of the GM, WM and CSF masks, using a 4mm full-width-at-half-maximum isotropic Gaussian Kernel (AFNI *3dBlurinMask*). The resulting BOLD timeseries were then scaled to a maximum (absolute value) of 200, and data were censored to remove outlier timepoints. Censoring of individual rs-fMRI volumes occurred if the motion derivatives had a Euclidean norm [147] above 0.4. Censoring involved removal not only of the volume at which this high norm was observed, but also the immediately preceding and following volumes, given that

effects of motion may be carried across timepoints. Entire rs-fMRI timeseries were discarded if more than 100 volumes (34% of the volumes) were censored. Only the subjects for which all eight rs-fMRI scans survived motion censoring were included in the analysis.

Purdue dataset: Out of 23 subjects, a final pool of 18 subjects (144 rs-fMRI scans) was retained for analysis. Three of the original 184 rs-fMRI scans—and their associated three subjects—were rejected due to excessive motion. An additional two subjects were rejected due to poor registration to the template of at least one of the sessions. Yale dataset: 11 out of 12 subjects were included. One subject was dropped after failure in the NIFTI reconstruction of the raw DICOM images.

To assess the impact of global signal regression on the reconstruction procedure and subsequently identifiability, all included fMRI runs were evaluated both after being detrended with (*GSR*) and without (*NoGSR*) global signal regression. Each detrending (AFNI *3dDeconvolve*) approach incorporated the following common regressors: (1) very low frequency fluctuations as derived from a bandpass [0.002-0.01Hz] filter (AFNI *1dBport*); (2) the 12 motion parameters, consisting of three linear translations [x,y,z], three rotations [pitch, yaw, roll] and the corresponding set of first derivatives [148, 149]; and (3) the voxel-wise local neighborhood (40mm) mean WM timeseries (AFNI *3dTproject*) [150]. The data at this point represent the *NoGSR* dataset. Incorporation of a fourth regressor source—the whole-brain mean GM timeseries—in the detrending stage results in the *GSR* dataset.

For connectivity analysis on a regional basis, the grey matter brain atlas from [151] was warped to each subject's native space by linear and non-linear registration (AFNI *auto_warp.py* and *3dAllineate*). This brain parcellation consists of 278 regions of interest (ROIs). Note that data from the cerebellum (including a total of 30 ROIs) were discarded, because the acquired data did not completely cover this structure for all subjects. This resulted in a final GM partition of 248 ROIs.

A functional connectivity matrix (namely the functional connectome; FC) was computed for each rs-fMRI scan through correlation of the mean time series from

each of the 248 ROIs (*MATLAB* command *corr*). The resulting square, symmetric FC matrices were not thresholded or binarized. Each FC matrix was ordered into seven cortical sub-networks, as proposed by Yeo et al. [152], and an additional eighth sub-network comprising sub-cortical regions was added [143]. For each dataset (Purdue and Yale), this resulted in eight functional connectomes per subject (four from each site; two *training* and two *validation*).

2.2.4 Differential Identifiability extended for Multi-Site studies

The upper triangular of each FC (test and retest) for the *training* data was vectorized and added to a matrix where the columns were runs and the rows represent the functional connectivity patterns. Hence, this matrix had $\binom{248}{2}$ rows and $N*4$ columns (4 runs per subject; N subjects). Principal component analysis (PCA) was used to extract $M = N*4$ principal components (i.e., functional connectivity eigenmodes) from the vectorized *training* dataset (*MATLAB* command *pca*). The principal components (PCs) were arranged in descending order of their explained variance. These PCs were then projected back into each subject's FC space to obtain individual reconstructed functional connectomes as analogously done by Amico et al. [136]. Below we extend this approach for multi-site acquisitions.

For individual fingerprints of subjects within and across sites, the identifiability matrix ($\mathbf{I}$) was created by correlating the subjects test and retest FCs within and across the two sites. This gave rise to a multi-site identifiability matrix, $\mathbf{I}$ which consisted of Pearson's correlation coefficients. For the particular case of two imaging sites, the test-retest combinations created four blocks ($\mathbf{I}^{ij}$) in the identifiability matrix $\mathbf{I}$,

$$\mathbf{I} = \begin{bmatrix} \mathbf{I}^{11} & \mathbf{I}^{12} \\ \mathbf{I}^{21} & \mathbf{I}^{22} \end{bmatrix}$$

where $\mathbf{I}^{ij}$ contained Pearson's correlation coefficient obtained by correlating FCs from the site$i$ test session with the FCs from the site$j$ retest session. $\mathbf{I}^{11}$ and $\mathbf{I}^{22}$ represent

the fingerprinting of the subjects within the two sites and $\mathbf{I}^{12}$ and $\mathbf{I}^{21}$ represent the fingerprinting of the subjects across the two sites.

For each test-retest [site$i$, site$j$] pair, differential identifiability ($< I^{ij}_{diff} >$) was calculated from the block $\mathbf{I}^{ij}$ following the procedure from [136]

$$< I^{ij}_{diff} > = < I^{ij}_{self} > - < I^{ij}_{others} >$$

where

$$< I^{ij}_{self} > \; = \; \frac{1}{N} \sum_{k=1}^{N} I^{ij}_{self}(k)$$

$$I^{ij}_{self}(k) \; = \; I^{ij}_{kk} \; , \qquad \forall \; k = 1, 2, \ldots, N$$

where N is the number of subjects (N=18 for Purdue dataset; N=11 for Yale dataset).

$\mathbf{I}^{ij}_{self}$, defined as *self identifiability*, is a vector of length N and contains the main diagonal elements $I^{ij}_{self}(k)$ of the block $\mathbf{I}^{ij}$, and denotes the correlation between the repeat visits of the same subject. The average of the main diagonal elements for the block $\mathbf{I}^{ij}$, $< I^{ij}_{self} >$, represents the overall self correlation for the [site$i$, site$j$] pair.

$$< I^{ij}_{others} > \; = \; \frac{1}{N} \sum_{k=1}^{N} I^{ij}_{others}(k)$$

$$I^{ij}_{others}(k) \; = \; \frac{1}{2} \left(\frac{1}{N-1} \sum_{l=1}^{N} I^{ij}_{kl} + \frac{1}{N-1} \sum_{l=1}^{N} I^{ij}_{lk} \right) \; , \; \forall \; l \neq k$$

For the *k-th* subject $I^{ij}_{others}(k)$ is an element of the vector $\mathbf{I}^{ij}_{others}$ and is obtained by the average of the *k-th* row and *k-th* column, excluding the main diagonal entry of the block $\mathbf{I}^{ij}$, and defines the average correlation of the *k-th* subject's FCs (test and retest) with all other subjects. $< I^{ij}_{others} >$ is the average of all $I^{ij}_{others}(k)$ of the block $\mathbf{I}^{ij}$, and defines an overall mean correlation between visits of different subjects for the [site$i$, site$j$] pair.

For visits associated with the [site$i$, site$j$] pair, $< I_{diff}^{ij} >$ characterizes the difference between the average within-subject FC similarity and the average between-subject FC similarity. The higher the value of $< I_{diff}^{ij} >$, the stronger is the overall fingerprinting of the population for the [site$i$, site$j$] pair.

To maximize the fingerprinting of the population across all the [site$i$, site$j$] visit pairs, the average of the four $< I_{diff}^{ij} >$ values was used, where

$$<< I_{diff} >> = \frac{1}{n} \sum_{i=1}^{n} \sum_{j=1}^{n} < I_{diff}^{ij} >$$

Here, n=2 is the number of sites for both Purdue and Yale datasets.

Multi-site differential identifiability $<< I_{diff} >>$ is then maximized by the selection of subsets of **m** PCs from the total number ($M = N * 4$) of PCs obtained from the training set. For each subset of the first **m** PCs, the subjects test-retest FCs were reconstructed, and $<< I_{diff} >>$ was calculated from these data. The optimal number of PCs, **m***, maximizes the value of $<< I_{diff} >>$, namely $<< I_{diff}^{*} >>$, as given by [136]:

$$<< I_{diff}^{*} >> = \ argmax_{m \in M} \ << I_{diff} >> (m)$$

The **m*** PCs were used to reconstruct the individual FCs (for both visits—i.e., test and retest) for the *training* and *validation* sets. The identifiability matrices computed from the original and reconstructed data for each of the *training* and *validation* sets were then compared.

Analogously, when focused on a particular [site$i$, site$j$] visit pair, we may obtain m^{ij*} as

$$< I_{diff}^{ij\ *} > = \ argmax_{m^{ij} \in M} \ < I_{diff}^{ij} > (m)$$

2.2.5 Statistical Analysis

Differential Identifiability ($\mathbf{I}_{diff}^{ij}$) was computed for each [site$i$, site$j$] pair from $\mathbf{I}^{ij}$ as follows

$$\mathbf{I}_{diff}^{ij} = \mathbf{I}_{self}^{ij} - \mathbf{I}_{others}^{ij}$$

For the *k-th* subject the value of $I^{ij}_{diff}(k)$ was calculated as

$$I^{ij}_{diff}(k) = I^{ij}_{self}(k) - I^{ij}_{others}(k)$$

$I^{ij}_{diff}(k)$ characterizes the differential identifiability on a subject level and quantifies the difference between the *k-th* subject's FC *self identifiability* and its similarity with other subjects' functional connectomes. The higher the value of $I^{ij}_{diff}(k)$, the higher is the identifiability of the *k-th* subject among the cohort.

Pairwise comparisons were done on the distributions of $\mathbf{I}^{ij}_{diff}$ obtained from the original and reconstructed data, for both the *training* and *validation* sets, using the Wilcoxon signed rank test followed by a Bonferroni correction on each subset of tests (e.g., four tests were conducted on the each of the *NoGSR* and *GSR training* and *validation* sets, so a correction for four tests was performed). All such analyses were conducted in R [153]. Any pairwise comparison was considered significant if $p_{Bonferroni} < 0.05$. Similar comparisons were also made between the distributions of $\mathbf{I}^{ij}_{diff}$ as obtained from reconstructions for original data with (*GSR*) and without (*NoGSR*) global signal regression.

The intraclass correlation coefficient (ICC) was used to assess the agreement of an edge (functional connectivity value between two brain regions) between visits of subjects on each [site$i$, site$j$] pair. ICC [154, 155] is generally used to assess the agreement between measurements for different groups. The stronger the resemblance between the measurements, the higher is the ICC value. Furthermore, a bootstrap procedure was applied when computing ICC to avoid biases induced by a small subset of the population. In each of 100 iterations 75% of the population was selected at random, and the ICC was calculated for each edge. The averages over all iterations were used to compare the edgewise ICC values of the original and the reconstructed data. ICC values for the resting-state functional networks of [156], for both the original and reconstructed data, were computed by averaging over the ICC values for the edges that belonged to each functional network. Using the aforementioned bootstrap procedure, edgewise ICC was also computed from all 4 visits across the two sites and these edgewise ICC were averaged over each brain region from [151] to

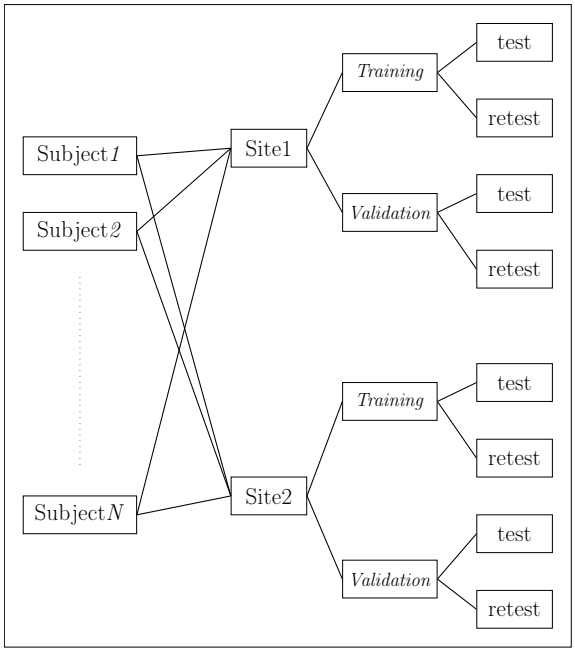

Fig. 2.1.: Diagram of the resting-state fMRI acquisitions for both datasets. Subjects underwent two imaging sessions (*Training* and *Validation*) at each of two MRI sites (Site1 and Site2), wherein each session comprised two resting-state runs (test and retest). After quality checks, the Purdue dataset included 18 subjects and the Yale dataset included 11 subjects. This setup produced a total of eight runs and associated functional connectomes (FC) per subject.

compare the reproducibility, between training and validation sets, of connectivity in each brain region across the original and reconstructed data. This entire edgewise ICC procedure was repeated for each of the *GSR* and *NoGSR* modalities.

2.3 Results

The Purdue dataset used for this study consisted of two fMRI sessions (each session consisted of test and retest pair of rs-fMRI scans) per subject on two different sites. After quality checks, 18 subjects with eight FCs per subject were used for Purdue dataset (see Methods). Building upon [136], we here expanded the concept of

identifiability for multiple acquisitions on multiple sites. We evaluated this method by splitting our dataset (see Figure 2.1) into *training* and *validation* sets. The *training* dataset consisted of four FCs per subject (test-retest at site1, test-retest at site2). Analogously, the *validation* dataset consisted of another four FCs per subject (for the same subjects as the *training* dataset; test-retest at site1, test-retest at site2).

When assessing the Purdue *training* dataset, FCs were decomposed and subsequently reconstructed based on PCA by using each subset of first **m** number of components out of the total (M = 72). For each number of PCA components **m**, $<< I_{diff} >>$ was computed from the reconstructed data (see Methods) and compared to $<< I_{diff} >>$ obtained from original data. Figure 2.2 shows $<< I_{diff} >>$ computed from the original and, iteratively, from the reconstructed data as a function of (**m**), the number of PCs preserved. $<< I_{diff} >>$ peaked at $\mathbf{m^*} = 21$ for *NoGSR* and $\mathbf{m^*} = 22$ for *GSR* datasets. These $\mathbf{m^*}$ PCs extracted from the *training* set were used as a fixed orthogonal connectivity basis (i.e. PCA loadings) to reconstruct the functional connectomes (denoted by Recon) of the *training* and *validation* sets for comparing identifiability obtained from the original FCs (Orig).

When looking at $< I^{ij}_{diff} >$ for different [site$i$, site$j$] visit pairs for *NoGSR* and *GSR*, we found different optimal numbers of components (m^{ij}). Within-site configurations peaked at 29 and 31 components respectively (*NoGSR*) and at 35 components (*GSR*). Between-sites configurations both peaked at 20 components (*NoGSR*) and at 21 components ((*GSR*)). Briefly, more components were included in the optimal reconstruction (and hence more variance was preserved) for within-site configurations whereas less components were included for between-site configurations (and hence less variance was preserved) for optimal identifiability. A summary of $< I^{ij}_{diff} >$ and the corresponding m^{ij*} for all configurations is shown in Table 2.1.

Identifiability matrices (**I**) consisting of Pearsons correlation coefficient between FCs of subjects' test and retest visits across and within the two sites were computed, expanding on [136]. The identifiability matrices obtained from reconstructed FCs using $\mathbf{m^*}$ PCs were compared to the ones obtained from original data. Figure

2.3 illustrates that the identifiability matrices obtained from optimally reconstructed functional connectomes outperformed the original FCs. The individual fingerprint of the subjects (main diagonal of each block $\mathbf{I}^{ij}$) within and across the sites were always higher at the optimal reconstruction for both *NoGSR* and *GSR* datasets.

Differential Identifiability ($\mathbf{I}^{ij}_{diff}$)) for each [site$i$, site$j$] pair was computed from $\mathbf{I}^{ij}$ blocks (see Methods). The distributions of $\mathbf{I}^{ij}_{diff}$ obtained from original and optimally reconstructed data were compared. Figure 2.4 shows that the distributions of $\mathbf{I}^{ij}_{diff}$ for each [site$i$, site$j$] pair was significantly higher ($p_{Bonferroni} < 0.05$, Wilcoxon signed rank test) after optimal reconstruction of the data, indicating higher identifiability of the subjects among the cohort. This result held for both the *NoGSR* and *GSR* cases.

The group averages of original and optimally reconstructed FCs using $\mathbf{m^*}$ PCs were computed. Figure 2.5 shows that the group average of original and reconstructed functional connectomes were almost identical, indicating that the optimal PCA reconstruction preserved the main group-level characteristics of the functional connectomes for both *NoGSR* (Figure 2.5 A-B) and *GSR* (Figure 2.5 C-D) datasets.

ICC was used to assess the reproducibility of edges in functional connectomes between visits of subjects within and across the two sites. The average ICC value, over 100 iterations obtained from the bootstrap procedure (see Methods for details), from original and optimally reconstructed FCs were compared. ICC for each functional network was computed by averaging over ICC values for all the edges that belonged to a functional network. Figures 2.6,B.1 show the edgewise ICC averaged over 100 iterations for the original and the reconstructed data. The edgewise ICC largely increased after optimal reconstruction for almost all edges (Tables 2.2, 2.3) for each [site$i$, site$j$] pair for *NoGSR* (Figures 2.6,B.1 A-B) and *GSR* (Figures 2.6,B.1 C-D) datasets. Figure 2.7 shows that the average ICC for each functional network in the reconstructed data was also higher than in the original data.

When integrating test-retest FC data from both imaging sites, we measured edgewise ICC, pooling all four visits per subject. Figure 2.8 shows the edgewise ICC and histograms for average ICC for each brain region (using the atlas from [151])

for the original and reconstructed data in the validation set. Figure 2.9 presents a brain rendering overlaid with the averaged edgewise ICC values of each brain region as computed from all four test-retest visits across the two sites using the validation dataset. The edgewise ICC and value per brain region for optimally reconstructed data indicated higher reproducibility of the functional connectomes. Both edgewise and average brain region ICC values increased after optimal reconstruction from **m*** PCs, indicating higher reproducibility and identifiability of the reconstructed functional connectomes as compared to the original ones.

Notably, all these findings were replicated in the Yale dataset. The results obtained for the Yale dataset are shown in Supplementary material (see Figures B.2, B.3, B.4 and B.5 and Table B.1). Specifically, Figure B.2 shows $<< I_{diff} >>$ as a function of the number of PCs (**m**) and it peaks at $\mathbf{m^*} = 12$ for both *NoGSR* and *GSR*. The identifiability matrices obtained from reconstructed FCs using these **m*** PCs as compared to the original ones are shown in Figure B.3. Figures B.4, B.5 depicts the edgewise ICC results when pooling all four visits together.

The effect of number of fMRI volumes on multi-site differential identifiability was assessed. To that end, processed BOLD time-series were shortened (by dropping fMRI volumes) to mimic different scan lengths. For each scan length evaluated, FCs were estimated, decomposed and subsequently reconstructed based on **m*** PCs. Optimal multi-site differential identifiability ($<< I^*_{diff} >>$) was computed from optimally reconstructed FCs and compared to that obtained from original FCs. Figure 2.10 shows that the method presented in this study improved $<< I^*_{diff} >>$ for both Purdue and Yale datasets for *NoGSR* and *GSR* for all scan lengths evaluated.

In order to assess the generalizability of the optimal orthogonal basis for each dataset, a leave-one-out experiment was performed. Briefly, each subject's FCs were reconstructed using the **m*** PCs when all the sessions of that subject were excluded from the PCA framework. For each dataset (Purdue and Yale), the optimally reconstructed FCs of each subject were compared to the leave-one-out reconstructed FCs. Histograms of the correlations of optimally reconstructed FCs from training vs

Table 2.1.: Purdue dataset. Maximum percentage differential identifiability ($< I^{ij*}_{diff} > *100$), number of principal components for each [site$i$, site$j$] pair (m^{ij*}), explained variance (R^2), mean (μ) and standard deviation (σ) of edgewise ICC values for Original (Orig) and optimally reconstructed (Recon) for Training datasets without global signal regression (*NoGSR*) and with global signal regression (*GSR*).

	[site$i$, site$j$]	$< I^{ij*}_{diff} >$	m^{ij*}	R^2	ICC μ_{Orig}	ICC σ_{Orig}	ICC μ_{Recon}	ICC σ_{Recon}
NoGSR	[site1, site1]	45.1	29	0.82	0.46	0.20	0.75	0.12
	[site1, site2]	31.0	20	0.74	0.14	0.24	0.34	0.22
	[site2, site1]	31.5	20	0.74	0.20	0.23	0.44	0.22
	[site2, site2]	45.7	31	0.84	0.44	0.20	0.72	0.11
GSR	[site1, site1]	43.6	35	0.84	0.35	0.24	0.77	0.13
	[site1, site2]	30.8	21	0.73	0.18	0.25	0.49	0.22
	[site2, site1]	32.8	21	0.73	0.17	0.25	0.53	0.20
	[site2, site2]	45.5	35	0.84	0.42	0.23	0.81	0.08

leave-one out for all subjects are shown for Purdue and Yale datasets in the Figure 2.11. Median values were 0.79 for Purdue *NoGSR*, 0.77 for Purdue *GSR*, 0.74 for Yale *NoGSR* and 0.73 for Yale *GSR*.

2.4 Discussion

Recently the concepts of brain fingerprinting and identifiability [157] have been investigated based on repeated measures of individual whole-brain estimates of resting-state functional connectivity [126, 127] and between fMRI tasks [128, 134, 141]. More recently, Amico et al. [136] introduced the concept of an identifiability matrix to assess the fingerprinting of a dataset through a functional denominated identifiability score (see Methods). Further they introduced a data-driven method to uncover identifiability in whole-brain functional connectomes (FCs) based on principal component decomposition and subsequent reconstruction. Here, we extended this framework for multi-site repeated measurements experiments and show how high identifiability on an inter-scanner basis is achievable at the whole-brain level, as well as at the pairwise

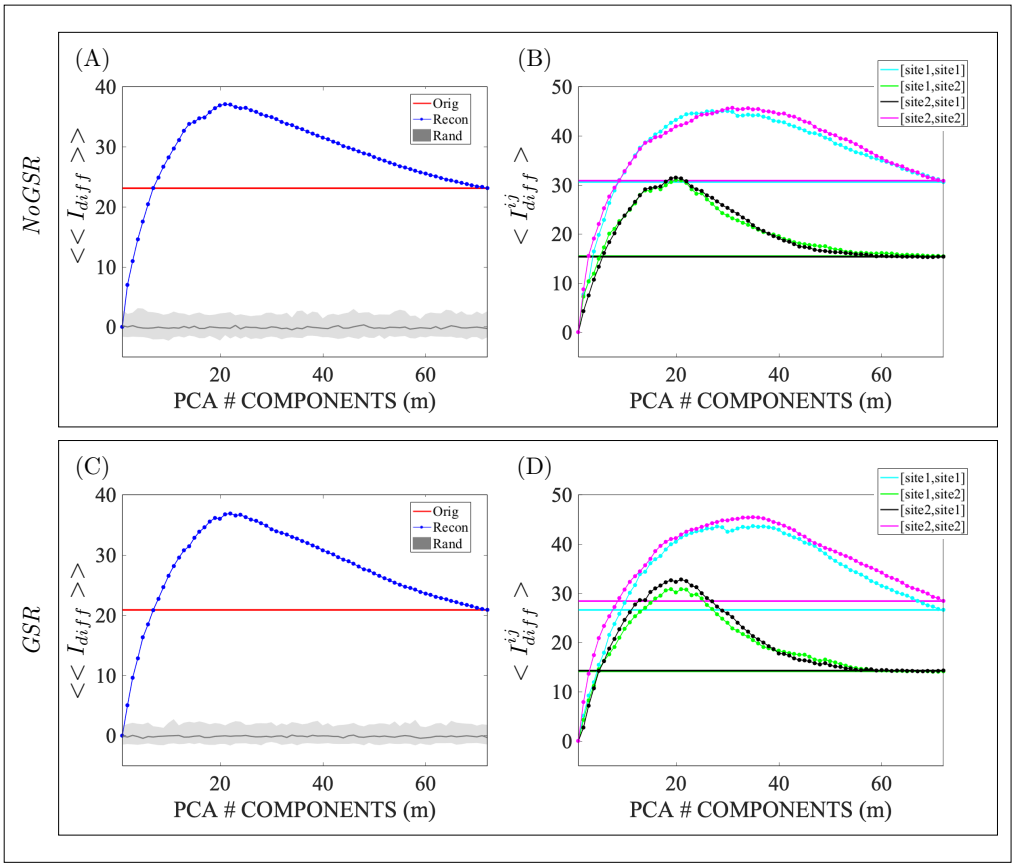

Fig. 2.2.: Purdue dataset. Multi-site differential identifiability ($<< I_{diff} >> *100$) and differential identifiability of each [site$i$, site$j$] pair, ($< I^{ij}_{diff} > *100$) for training data as a function of the number of principal components (PCs) used for reconstruction for resting-state data without global signal regression (*NoGSR*; (A) and (B)); and with global signal regression (*GSR*; (C) and (D)). In all figures solid lines denote $<< I_{diff} >>$ and $< I^{ij}_{diff} >$ as computed from the original FCs, whereas lines with circles denote the differential identifiability for reconstructed FCs as a function of **m**, the included number of components. In (A) and (C), the gray (shaded) area denotes the 95% confidence interval for $<< I_{diff} >>$ over 100 random permutations of the test-retest FC pairs at each value of **m**. It may be observed that the benefit of reconstruction on differential identifiability was not dependent on the exclusion/inclusion of global signal regression.

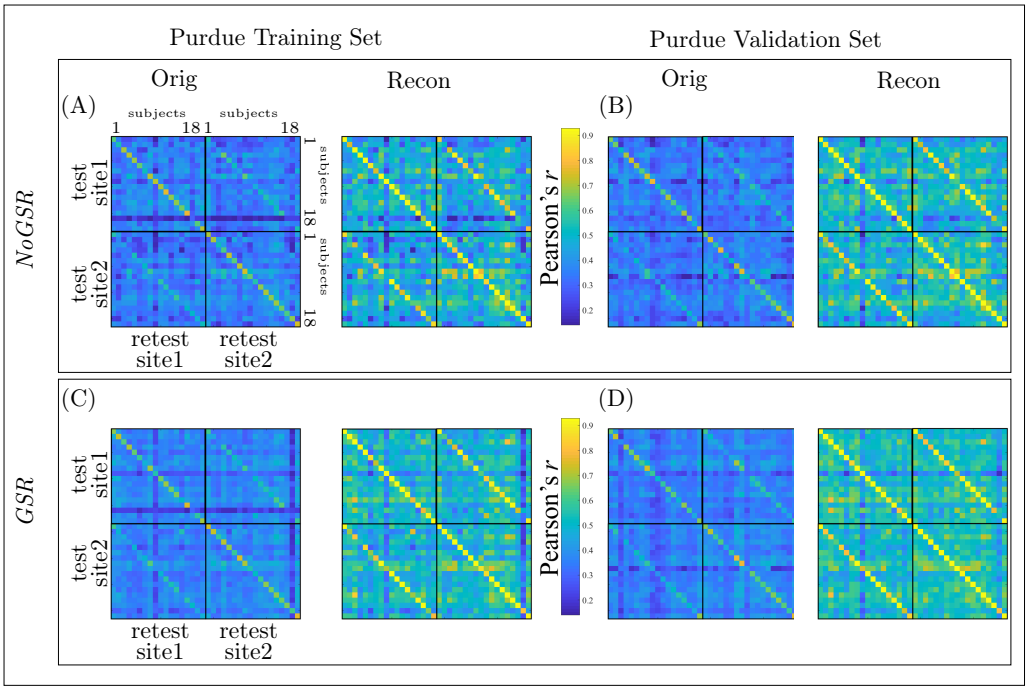

Fig. 2.3.: Purdue dataset. Identifiability matrices (**I**) of the original (Orig) and reconstructed (Recon) data for the *Training*, (A) and (C), and *Validation*, (B) and (D) sets of resting-state functional connectomes without global signal regression (*NoGSR*; (A) and (B)) and with global signal regression (*GSR*; (C) and (D)). The Identifiability matrix (**I**) has a blockwise structure where each block is I^{ij}, representing the identifiability for the [site$i$, site$j$] pair. Note that identifiability was meaningfully improved across sites regardless of the exclusion/inclusion of global signal regression.

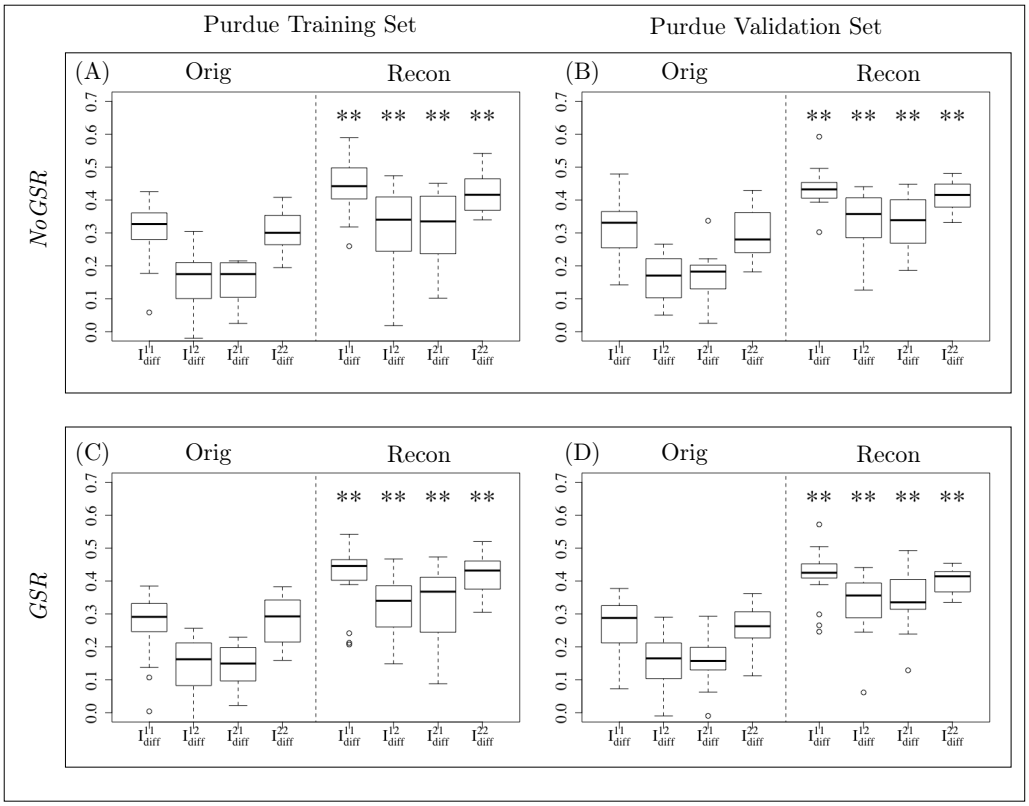

Fig. 2.4.: Purdue dataset. Box plots of Differential Identifiability ($\mathbf{I}^{ij}_{diff}$) computed from each block of the Identifiability matrix (i.e., $\mathbf{I}^{ij}$) for the original (Orig) and optimally reconstructed (Recon) data without global signal regression (*NoGSR*; (A) and (B)) and with global signal regression (*GSR*; (C) and (D)). Values of Pearson's r that are significantly higher ($p_{Bonferroni}$ ¡ 0.05, Wilcoxon signed rank) for Recon relative to Orig are marked by double asterisks. Note that distributions of $\mathbf{I}^{ij}_{diff}$ were found to be unaffected by exclusion/inclusion of global signal regression.

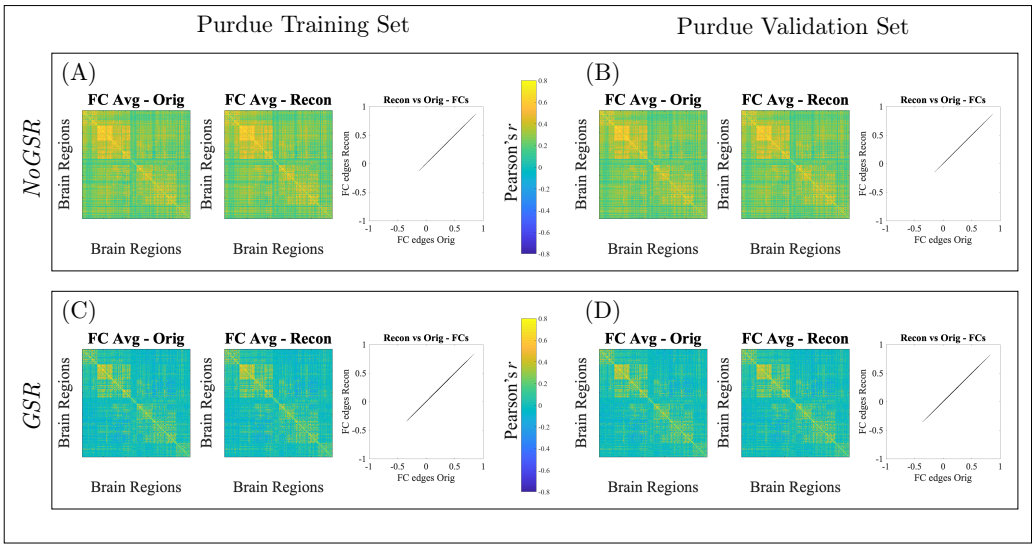

Fig. 2.5.: Purdue dataset. Evaluation of PCA reconstruction at the optimal number of components ($\mathbf{m^*} = 21$) for resting-state functional connectomes (FCs) data without global signal regression (*NoGSR*; (A) and (B)) and ($\mathbf{m^*} = 22$) with global signal regression (*GSR*; (C) and (D)). Left-to-right in each of (A)-(D): the group averaged FC of the original (Orig) data; the group averaged FC of the reconstructed (Recon) data; the scatter plot (for all edges) of the Recon group-averaged FC (y-axis) vs. the Orig group-averaged FC (x-axis). Again, exclusion/inclusion of global signal regression did not alter the benefit of the reconstruction to enhance identifiability.

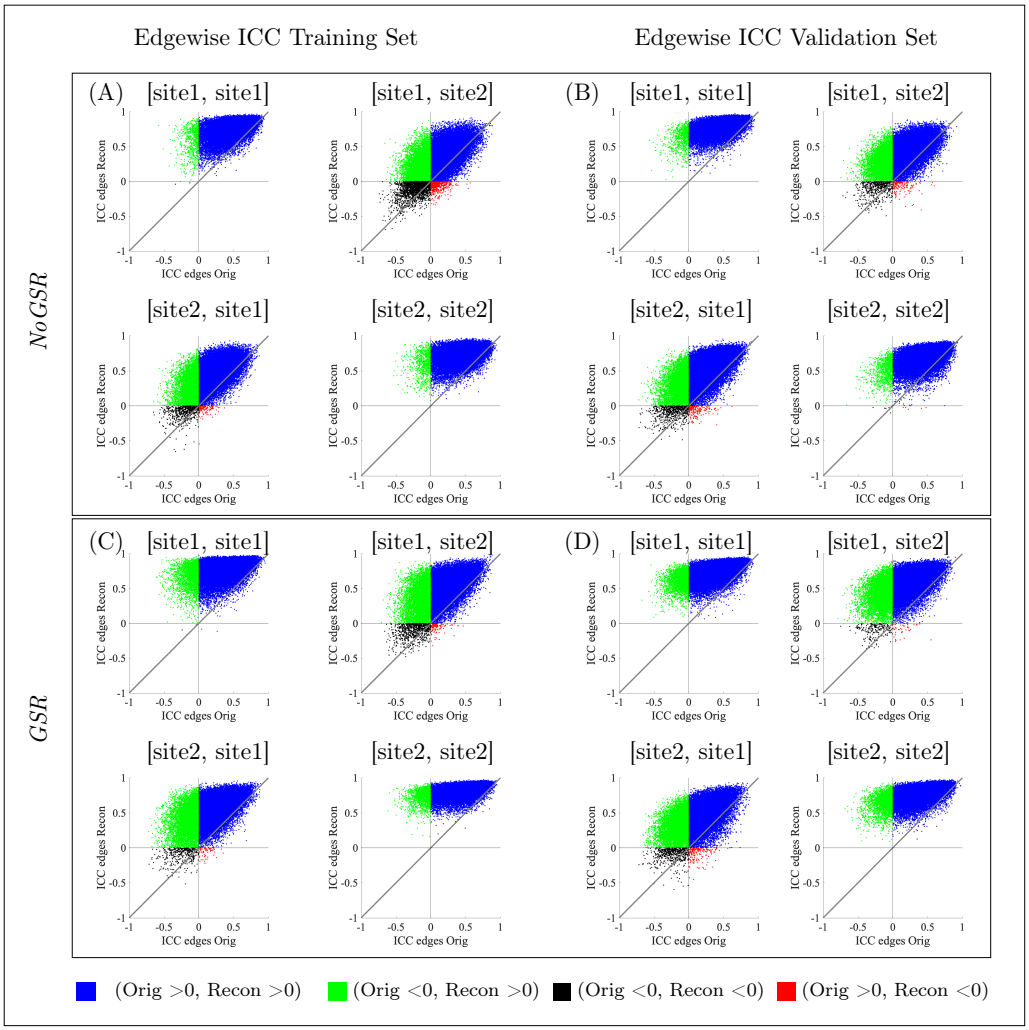

Fig. 2.6.: Purdue dataset. Scatter plots of averaged (100 iterations) intra-class correlation coefficient (ICC) values, computed over each FC edge, for the reconstructed (Recon) data (y-axis) versus the edgewise ICC for the original (Orig) data (x-axis). Plots are presented for data without global signal regression (*NoGSR*; (A) and (B)) and with global signal regression (*GSR*; (C) and (D)). In each plot, quadrants are colored for clarity of the effect of reconstruction on ICC values. Blue represents positive values in both Orig and Recon; green represents negative Orig and positive Recon; black represents negative values for both Orig and Recon; and red represents positive Orig and negative Recon. Note that the vast majority of ICC values have been made more positive by the reconstruction process.

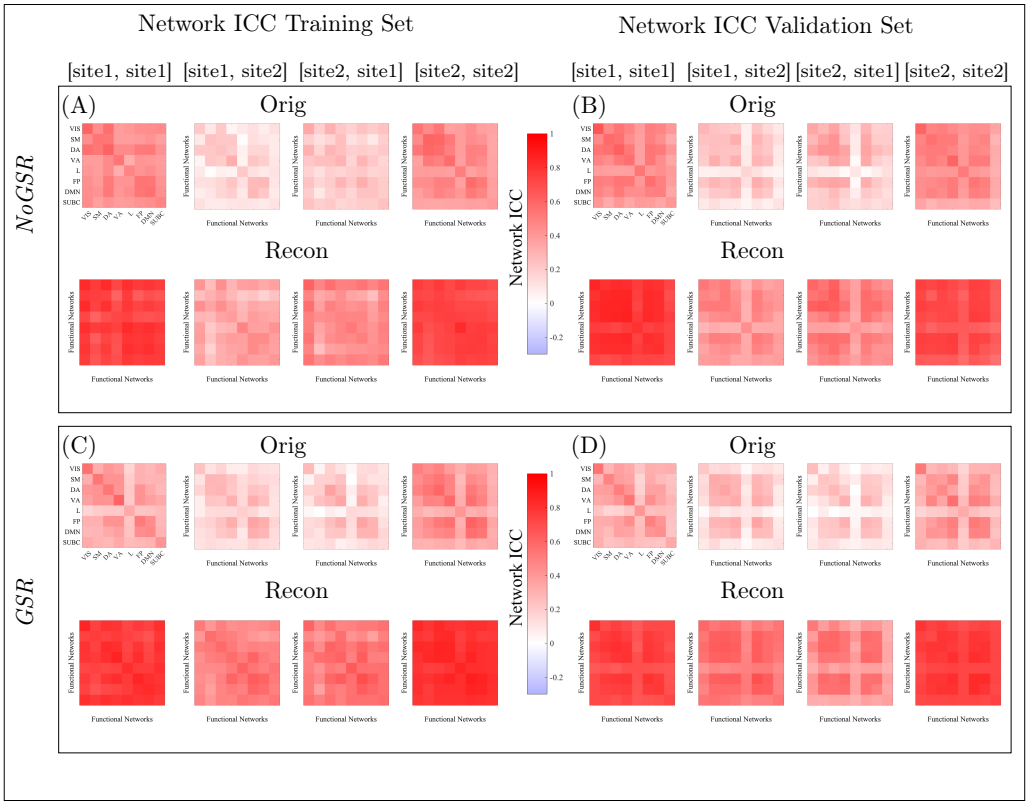

Fig. 2.7.: Purdue dataset. Intra-class correlation coefficient (ICC) values for each functional network, computed as the average of edgewise ICC over each of Yeo's resting-state functional networks in the original (Orig) and reconstructed (Recon) data for *Training* and *Validation* sets on resting-state functional connectomes without global signal regression (*NoGSR*; (A) and (B)) and with global signal regression (*GSR*; (C) and (D)). Yeo's resting functional networks [156]: Visual (VIS), Somato-Motor (SM), Dorsal Attention (DA), Ventral Attention (VA), Limbic system (L), Fronto-Parietal (FP), Default Mode Network (DMN), and subcortical regions (SUBC). Once again, no meaningful effect of exclusion/inclusion of global signal regression is observed on the benefit from reconstruction to enhance identifiability.

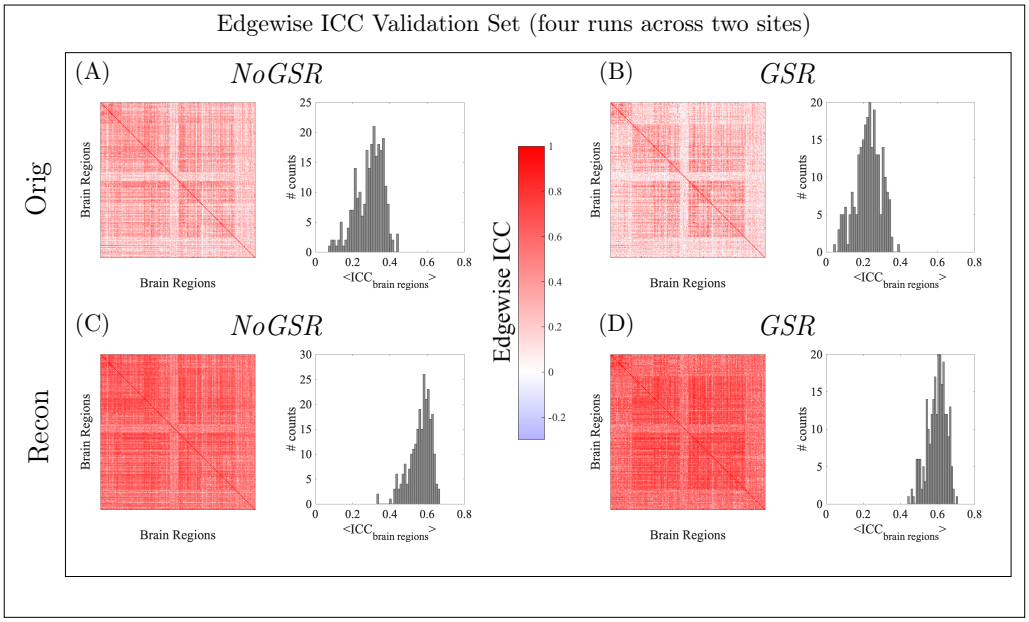

Fig. 2.8.: Purdue dataset. Averaged (100 iterations; see Methods for bootstrap details) intra-class correlation coefficient (ICC) values, computed for each FC edge from four visits across two sites, for the *Validation* set original (Orig; (A) and (B)) and reconstructed (Recon; (C) and (D)) data without global signal regression (*NoGSR*; (A) and (C)) and with global signal regression (*GSR*; (B) and (D)). Note that the benefit from reconstruction to enhance identifiability is, again, not dependent on exclusion/inclusion of global signal regression.

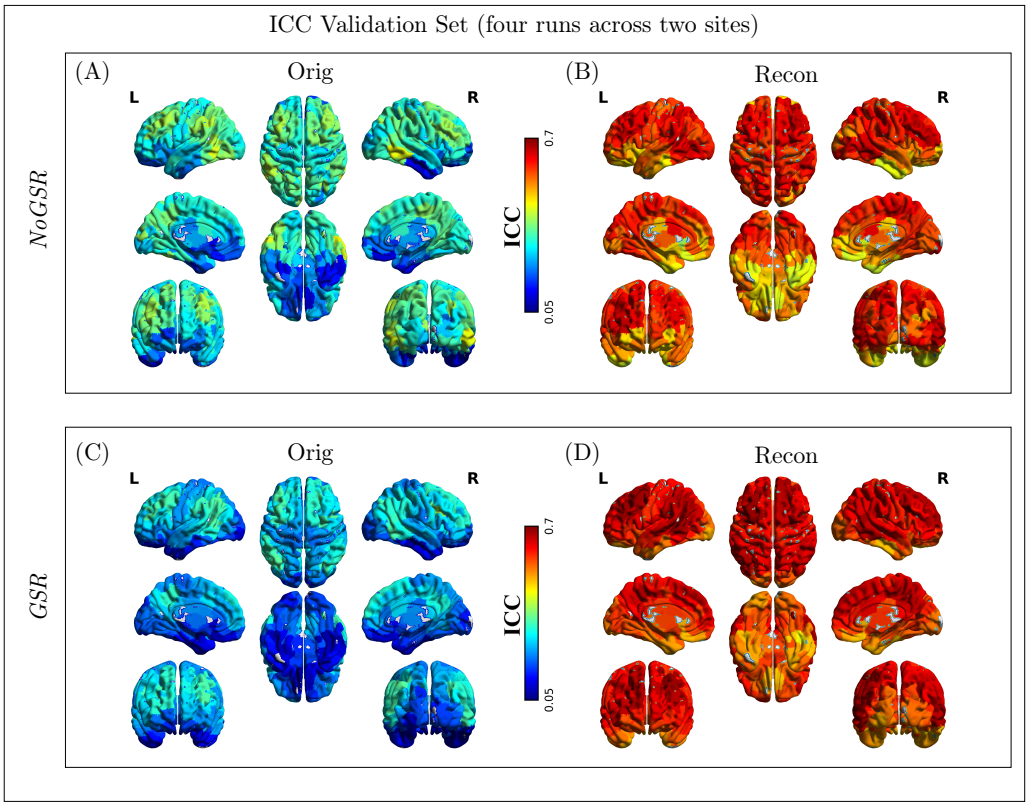

Fig. 2.9.: Purdue dataset. Brain rendering of intraclass correlation coefficient (ICC), computed from all four visits across the two sites for the *Validation* set original (Orig; (A) and (C)) and reconstructed (Recon; (B) and (D)) data without global signal regression (*NoGSR*; (A) and (B)) and with global signal regression (*GSR*; (C) and (D)). The strength per brain region—computed as the mean of edgewise ICC values (ICC computed for each FC edge and averaged over 100 iterations; see Methods for Bootstrap procedure)—provides an assessment of overall reproducibility of the functional connections of each brain region. FC reproducibility was appreciably improved, regardless of exclusion/inclusion of global signal regression.

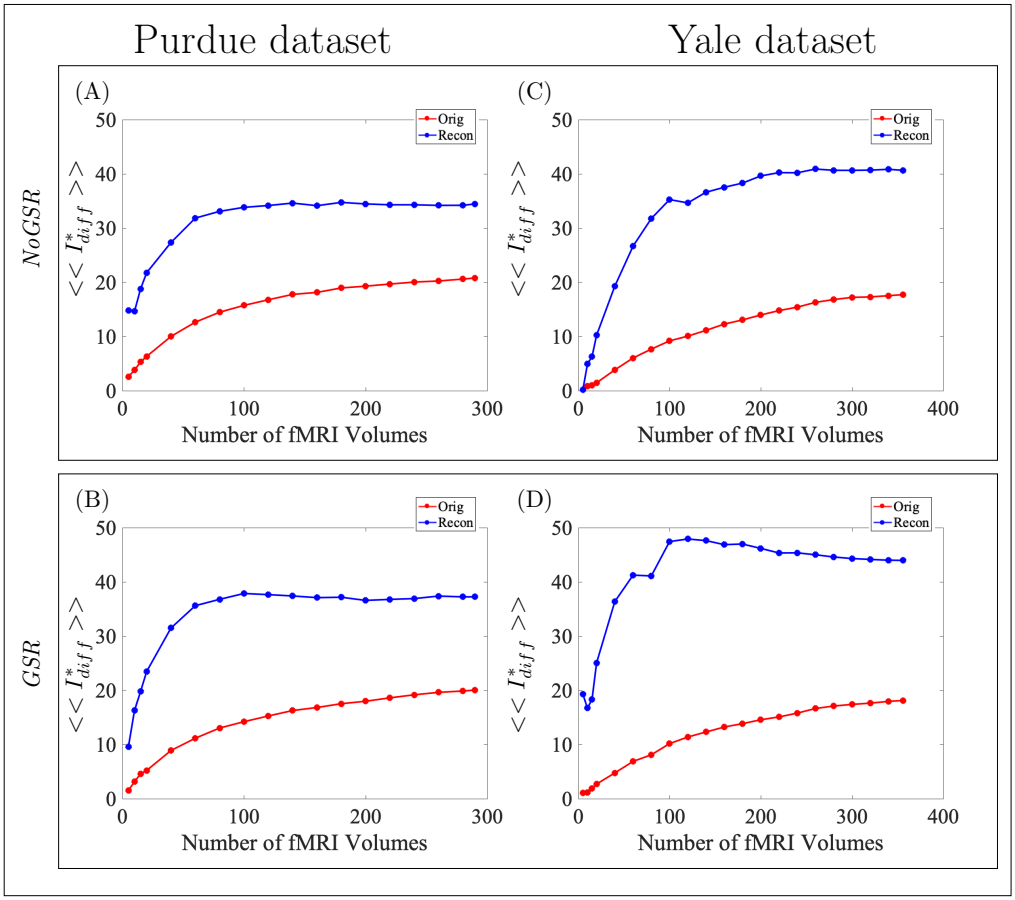

Fig. 2.10.: Optimal multi-site differential identifiability ($<< I^*_{diff} >> *100$) as a function of the number of fMRI volumes used for reconstruction for resting-state Purdue and Yale datasets without global signal regression (*NoGSR*; (A) and (C)) and with global signal regression (*GSR*; (B) and (D)). It may be observed that the benefit of reconstruction on differential identifiability was not dependent on the exclusion/inclusion of global signal regression.

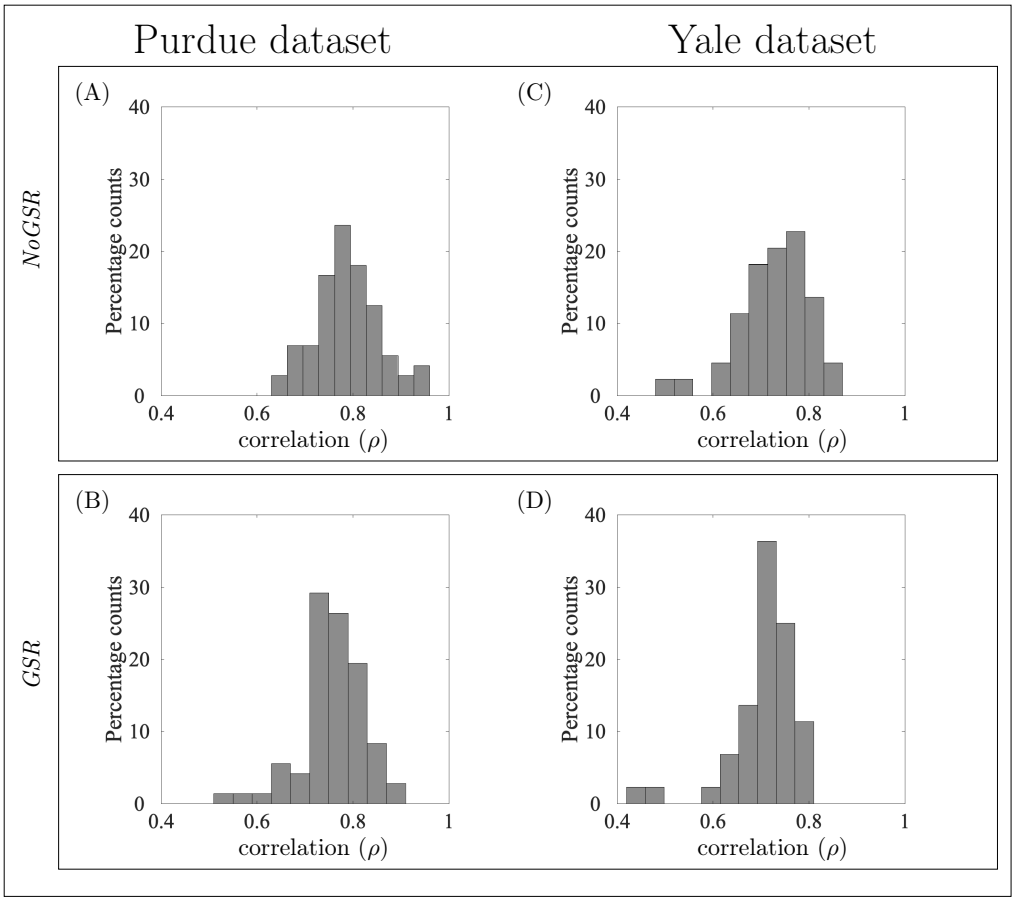

Fig. 2.11.: Histograms of similarity between optimally reconstructed FCs (complete dataset for PCA framework) and with leave-one-out (LOO) reconstructed FCs. (A) Purdue without global signal regression (*NoGSR*), (B) Purdue with global signal regression (*GSR*), (C) Yale *NoGSR* and (D) Yale *GSR*.

Table 2.2.: Purdue dataset. Percentage of positive and negative edgewise intra-class correlation coefficient (ICC) values (computed for each FC edge and averaged over 100 iterations; see Methods for Bootstrap procedure) of original (Orig) data that were converted to positive or negative edgewise ICC in reconstructed (Recon) data for resting-state functional connectomes without global signal regression (*NoGSR*).

[site$i$, site$j$]	Purdue Training Set			Purdue Validation Set		
[site1, site1]		Recon			Recon	
	Orig	Negative	Positive	Orig	Negative	Positive
	Negative	0.28	99.72	Negative	0.00	100.00
	Positive	0.0	100.00	Positive	0.00	100.0
[site1, site2]		Recon			Recon	
	Orig	Negative	Positive	Orig	Negative	Positive
	Negative	20.56	79.44	Negative	7.72	92.28
	Positive	1.85	98.15	Positive	0.65	99.34
[site2, site1]		Recon			Recon	
	Orig	Negative	Positive	Orig	Negative	Positive
	Negative	9.75	90.25	Negative	10.50	89.50
	Positive	0.47	99.53	Positive	0.72	99.28
[site2, site2]		Recon			Recon	
	Orig	Negative	Positive	Orig	Negative	Positive
	Negative	0.00	100.00	Negative	0.61	99.39
	Positive	0.00	100.00	Positive	0.02	99.98

Table 2.3.: Purdue dataset. Percentage of positive and negative edgewise intra-class correlation coefficient (ICC) values (computed for each FC edge and averaged over 100 iterations; see Methods for Bootstrap procedure) of original (Orig) data that were converted to positive or negative edgewise ICC in reconstructed (Recon) data for resting-state functional connectomes with global signal regression (*GSR*).

[site$i$, site$j$]	Purdue Training Set			Purdue Validation Set		
[site1, site1]		Recon			Recon	
	Orig	Negative	Positive	Orig	Negative	Positive
	Negative	0.08	99.92	Negative	0.00	100.00
	Positive	0.01	99.99	Positive	0.00	100.00
[site1, site2]		Recon			Recon	
	Orig	Negative	Positive	Orig	Negative	Positive
	Negative	10.61	89.39	Negative	2.78	97.22
	Positive	0.46	99.54	Positive	0.18	99.82
[site2, site1]		Recon			Recon	
	Orig	Negative	Positive	Orig	Negative	Positive
	Negative	4.80	95.20	Negative	6.34	93.66
	Positive	0.27	99.73	Positive	0.80	99.20
[site2, site2]		Recon			Recon	
	Orig	Negative	Positive	Orig	Negative	Positive
	Negative	0.00	100.00	Negative	0.00	100.00
	Positive	0.00	100.00	Positive	0.00	100.00

level for functional edges. This approach to uncover identifiability was equally effective for rs-fMRI data processed with and without global signal regression. Results indicate that the individual fingerprints obtained from optimally reconstructed FCs were robust, and improved identifiability among the cohort. Further, the method improved the reproducibility of the functional connectivity profiles across visits, both on an edgewise and functional network basis. We discuss below all the results related to the Purdue dataset.

Multi-site differential identifiability $<< I_{diff} >>$ was used as a quality function to maximize the fingerprinting of individual subjects within a cohort by exploring connectivity subspaces over a range of M principal components. The identifiability of a connectivity profile of a subject relies on the fact that individual subjects are expected to be most similar to themselves across visits or scanning sessions, relative to others. We used a continuous identifiability score as defined by [136] for individual fingerprinting of subjects in test-retest sessions for two sites. The continuous identifiability score, $< I^{ij}_{diff} >$, quantified the difference between average within-subject similarity and average between-subject similarity for a single [site$i$, site$j$] visit pair. $<< I_{diff} >>$ quantified the overall fingerprinting of the population across all test-retest visits. $<< I_{diff} >>$ was then maximized over subsets of M PCs to find the **m*** PCs that maximized differential identifiability and provided the optimal orthogonal basis to reconstruct the FCs. For both the *NoGSR* and *GSR* datasets, $<< I_{diff} >>$ and $< I^{ij}_{diff} >$ (Figure 2.2) showed a significant improvement over the identifiability score computed from the original FCs. The higher value of average differential identifiability indicates stronger overall individual fingerprinting of the population.

When assessing $< I^{ij}_{diff} >$ and m^{ij*} (see Table 2.1), it can be seen that there are differences in the proportion of the dimensionality of the data that are kept for maximizing identifiability. In particular, visit pairs including different sites (i.e., [site1, site2] and [site2, site1]) had m^{ij*} values very close to the number of subjects (i.e., 16) whereas visit pairs including just one site (i.e., [site1, site1] and [site2, site2] were able to keep a larger number of components, indeed approximately the

number visits within an imaging site (i.e., twice the number of subjects). These results emphasize how important it is to formalize a data-driven framework for reconstruction of FCs that is not based on fixing certain number of components or ultimately a percentage of variance, since identifiability might peak at very different configurations depending on multiple factors, including number of subjects, number of imaging sites, baseline similarity between test-retest on the sites, etc.

Identifiability matrices ($\mathbf{I}$) computed from optimally reconstructed data outperformed those computed from the original data. Identifiability matrices consisted of Pearsons correlation coefficient between FCs corresponding to subjects' test and retest visits, within and across the two sites. The main diagonal of each of the four blocks ($\mathbf{I}^{ij}$) consisted of correlations between visits of the same subject within and across the two sites. These self correlations had higher values in $\mathbf{I}$ obtained from optimally reconstructed data as compared to the ones obtained from original data (Figure 2.3). One of the noteworthy facts about Figure 2.3 is the substantial increase in self correlations for the challenging problem of test-retest visits between the two sites. This indicates stronger individual fingerprints of subjects after optimal reconstruction of the FCs, not only in repeated visits within the same site, but also among visits across two sites.

Statistically higher values for the distributions of $\mathbf{I}^{ij}_{diff}$ for all test-retest [site$i$, site$j$] pairs of the reconstructed data as compared to the original data illustrated stronger fingerprinting of the population. $\mathbf{I}^{ij}_{diff}$ quantified the differential identifiability on a subject level for the test-retest [site$i$, site$j$] pairs. Higher $\mathbf{I}^{ij}_{diff}$ values indicated improved identifiability of subjects. Differential identifiability increased for all subjects within the same site visits, and also between the two sites after optimal reconstruction of the FCs. No difference was found in the reconstructed data between distributions for *NoGSR* and *GSR* $\mathbf{I}^{ij}_{diff}$, suggesting that both approaches benefit from this framework, both within and between-sites in a similar way.

The group averages of the original and optimally reconstructed FCs were almost identical, indicating that the main group level features of the functional connectivity

profiles were preserved by the optimal reconstruction. The **m*** PCs that maximized the $<< I_{diff} >>$ obtained from the training data, were used as an optimal orthogonal basis to reconstruct the functional connectivity profiles for subjects' test and retest sessions in both the training and validation sets. In general PCA is used to transform a set of correlated variables into a set of linearly uncorrelated variables, namely the principal components. The principal components are arranged in descending order of their explained variance and provide a new basis to represent the data. Keeping the subset of the first **m*** PCs helps to provides a simpler representation of the data through dimensionality reduction while still retaining critical information. Here we rely on the fact, as pointed out by [136], that the highest variance principal components carry cohort-level functional connectivity information, while lower variance PCs carry finer subject-level functional connectivity information, and the lowest variance PCs carry information regarding noise and artifacts. By using the set of first **m*** PCs, which maximized averaged differential identifiability, for reconstruction provided a denoised version of the original FCs by keeping the cohort and finer subject level functional connectivity information.

To assess identifiability at a finer grain perspective, we considered the pairwise intraclass correlation coefficient (ICC) at the level of functional edges. Optimally reconstructed FCs systematically showed increased ICC values as compared to original FCs. At the meso-scale of looking at resting-state networks and their interactions, analogous ICC increases were found. In this study the groups were the test-retest visits within a site or between the two sites, whereas the measurements were the values of each functional connectivity edge from all subjects. The reconstructed FCs represent a denoised version of the original data, having lower variance between measurements on different groups. ICC values in Figures 2.6-2.9 and Tables 2.2-2.3 indicated higher reproducibility of the functional connectivity profiles after optimal reconstruction. The reproducibility of the edges also helped to distinguish subjects and augment identifiability. In other words, higher ICC values led to higher identifiability of the functional connectivity edges. There was a notable increase in ICC values of the

reconstructed data for the challenging problem of between-site test-retest visit pairs. Thus, the significant increase in ICC values for the reconstructed data denoted higher identifiability in all test-retest visit pairs for both *NoGSR* and *GSR* datasets after optimal reconstruction with **m*** PCs.

Notably, these findings were replicated in a second independent dataset, here denominated the Yale dataset (see Figures B.2, B.3, B.4 and B.5 and Table B.1). Indeed, $<< I_{diff} >>$ reached even higher values when compared to the Purdue dataset. It is possible that this is because of the identically configured imaging sites as well as because of the shorter TR. Both characteristics might facilitate higher identifiability scores.

When assessing the effect of scan lengths on multi-site differential identifiability, we noticed that the optimally reconstructed FCs systematically provided higher levels of $<< I^*_{diff} >>$ for both datasets, with and without GSR, and for all scan lengths evaluated (see Figure 2.10). These multi-site results are in the line of those observed in [136] for single-site evaluations and emphasize not only the importance of maximizing identifiability but also the generalizability of this extended framework to different imaging sites, TRs as well as scan lengths or number of fMRI volumes acquired.

The modest cohort-sizes of the two datasets assessed in this paper (Purdue $N = 18$, Yale $N = 11$) limited our ability to further explore the universality of the sets of orthogonal basis obtained at the optimal reconstruction levels. A leave-one-out procedure (Figure 2.11) showed that both sets of orthogonal basis had limited generalizability, with Purdue (the largest cohort) having higher generalizability than Yale (the smallest one). These results suggest that cohort-size could be critical for this venue. Further work with large inter-scanner datasets should uncover the plausibility of obtaining truly generalizable sets of orthogonal components for single- and multi-scanner fMRI datasets that would optimally reconstruct unseen subjects while preserving their connectivity fingerprints [158].

This work has several limitations. A limitation of the method is that this data-driven method requires the availability of test-retest sessions on all subjects and each

site, which is usually not available in cross-sectional clinical studies. A limitation of the study is the modest sample size and small number of available sites. However, several multi-site fMRI studies were performed with less than 10 subjects [95,96,100–102]. A larger multi-site study involving more subjects and sites will help to generalize the results. Further, better acquisition parameters for rs-fMRI may improve the results of the study.

This study expanded on the emerging field of fingerprinting in resting-state functional connectomes (FCs), by opening it to a less controlled scenario wherein repeated measurements are obtained from different imaging sites. To do so, it extended a recently proposed method to assess and ultimately improve identifiability in multi-site studies. Future studies could use this method to examine the reproducibility of fingerprinting in resting-state functional networks and structural connectivity across more than two sites. Another avenue of exploration would be to investigate the reliability of graph theory measures (e.g., clustering coefficient, characteristic path length, modularity, etc.) in the denoised FCs. Further use of this extended PCA methodology could be used to denoise T_1 and T_2 structural images at the voxel level by reconstructing test-retest MNI registered volumes at the optimal level of differential identifiability. Another important investigation would be to test the method presented in this study on scanners from different vendors, allowing combination of data for larger multi-site studies.

2.5 Conclusion

Multi-site fMRI studies have great appeal as a means of generating larger datasets, but the site-dependent variability can mask the advantages of such studies. Individual fingerprinting is a critical and emerging field in resting-state functional connectivity. Here we evaluated fingerprinting of the subjects in test-retest visit pairs, within and across two sites. We presented a framework based on principal component analysis to denoise the FCs and improve identifiability. We used principal components

that maximized differential identifiability on the *training* data as an orthogonal basis to reconstruct subjects' individual FCs for *training* and *validation* datasets. These optimally reconstructed FCs resulted in substantial improvement in individual fingerprinting within same-site visit pairs and also for the challenging problem of between-site visits, relative to the original data. Optimally reconstructed FCs systematically showed a notable increase in ICC values as compared to the original FCs, at the levels of functional edges, resting-state networks, and network interactions. Results showed that it is possible to use the data-driven method presented in this study to improve identifiability in the functional connectivity domain for multi-site studies. This would pave the way to pool subjects recruited at different sites, allowing for better assessments of brain structure and function in the healthy and diseased brain.

3. FUTURE WORK

The first part of this work demonstrated transient neurometabolic alterations in collision sport athletes which were associated with the head acceleration events they experienced during the season. Future work will seek to include larger sample sizes for study population recruited from more teams to incorporate different playing styles [80], skill and athletic level of competition. A study involving more teams could sample a greater range of playing styles, and thus could better quantify dose-response thresholds between HAE exposure and neurometabolic changes. Such a dose-response model will be critical in instituting exposure regulations that may best protect adolescent athletes from the long-term risks associated with repetitive head trauma. Further, an increase in the number of athletes studied would increase the chances of having participants who are diagnosed with a concussion, eventually enabling relative assessment of the severity of metabolic injury for asymptomatic athletes.

Future work will seek to control for gender effect due to sex hormones between the two genders. Previous studies have shown significant differences in metabolite concentrations in males and females [81,82]. Such changes could affect the concentrations and ratios observed in MRS studies, particularly for modest sample size studies, and should be accounted for in future longitudinal studies.

Future studies should include the use of automatic repositioning of MRS voxel e.g., [74,75] which would eliminate variable locations of voxel placement from measurement to measurement, leading to changes in the relative proportion of gray matter, white matter, and cerebrospinal fluid in the assessed voxel. Automatic voxel placement can reduce the variance for longitudinal measurements.

Also, future work will look to incorporate the newer MR spectroscopic imaging (MRSI) techniques that would permit investigation of changes over a larger region of the brain rather than focusing on specific anatomic locations and providing spatial

indifference [76, 77], while also permitting separate examination of disturbances in white and gray matter [78, 79].

This second part of the study expanded on the emerging field of fingerprinting in resting-state functional connectomes (FCs), by opening it to a less controlled scenario wherein repeated measurements were obtained from different imaging sites. To do so, it extended a recently proposed method to assess and ultimately improve identifiability in multi-site studies. Future studies could use this method to examine the reproducibility of fingerprinting in resting-state functional networks and structural connectivity across more than two sites. Another avenue of exploration would be to investigate the reliability of graph theory measures (e.g., clustering coefficient, characteristic path length, modularity, etc.) in the denoised FCs. Further use of this extended PCA methodology could be used to denoise T_1 and T_2 structural images at the voxel level by reconstructing test-retest MNI registered volumes at the optimal level of differential identifiability. Another important investigation would be to test the method presented in this study on scanners from different vendors, allowing combination of data for larger multi-site studies.

REFERENCES

REFERENCES

[1] S. Bari, D. O. Svaldi, I. Jang, T. E. Shenk, V. N. Poole, T. Lee, U. Dydak, J. V. Rispoli, E. A. Nauman, and T. M. Talavage, "Dependence on subconcussive impacts of brain metabolism in collision sport athletes: an MR spectroscopic study," *Brain Imaging and Behavior*, vol. 13, no. 3, pp. 735–749, 6 2019. [Online]. Available: http://link.springer.com/10.1007/s11682-018-9861-9

[2] P. S. Auerbach and W. H. Waggoner, "Its Time to Change the Rules," *JAMA*, vol. 316, no. 12, p. 1260, 9 2016. [Online]. Available: http://jama.jamanetwork.com/article.aspx?doi=10.1001/jama.2016.8184

[3] A. Schwartz, "N.F.L. Players Shaken by Duersons Suicide Calculation - The New York Times," 2011. [Online]. Available: https://www.nytimes.com/2011/02/21/sports/football/21duerson.html

[4] P. McCrory, W. Meeuwisse, M. Aubry, B. Cantu, J. Dvořák, R. Echemendia, L. Engebretsen, K. Johnston, J. Kutcher, M. Raftery, A. Sills, B. Benson, G. Davis, R. Ellenbogen, K. Guskiewicz, S. A. Herring, G. Iverson, B. Jordan, J. Kissick, M. McCrea, A. McIntosh, D. Maddocks, M. Makdissi, L. Purcell, M. Putukian, K. Schneider, C. Tator, and M. Turner, "Consensus statement on Concussion in Sport - The 4th International Conference on Concussion in Sport held in Zurich, November 2012," *Physical Therapy in Sport*, vol. 14, no. 2, pp. 250–258, 2013.

[5] K. M. Guskiewicz, S. W. Marshall, J. Bailes, M. McCrea, R. C. Cantu, C. Randolph, and B. D. Jordan, "Association between Recurrent Concussion and Late-Life Cognitive Impairment in Retired Professional Football Players," *Neurosurgery*, vol. 57, no. 4, pp. 719–726, 2005. [Online]. Available: http://content.wkhealth.com/linkback/openurl?sid=WKPTLP:landingpage&an=00006123-200510000-00012

[6] C. M. Baugh, J. M. Stamm, D. O. Riley, B. E. Gavett, M. E. Shenton, A. Lin, C. J. Nowinski, R. C. Cantu, A. C. McKee, and R. A. Stern, "Chronic traumatic encephalopathy: Neurodegeneration following repetitive concussive and subconcussive brain trauma," *Brain Imaging and Behavior*, vol. 6, no. 2, pp. 244–254, 2012.

[7] A. C. McKee, R. C. Cantu, C. J. Nowinski, E. T. Hedley-Whyte, B. E. Gavett, A. E. Budson, V. E. Santini, H.-S. Lee, C. A. Kubilus, and R. A. Stern, "Chronic Traumatic Encephalopathy in Athletes: Progressive Tauopathy After Repetitive Head Injury," *Journal of Neuropathology & Experimental Neurology*, vol. 68, no. 7, pp. 709–735, 2009. [Online]. Available: https://academic.oup.com/jnen/article-lookup/doi/10.1097/NEN.0b013e3181a9d503

[8] B. Gavett, R. Stern, and A. McKee, "Chronic Traumatic Encephalopathy," *Neurosurgery*, vol. 30, no. 1, pp. 1–10, 2012. [Online]. Available: http://journals.lww.com/neurosurgery/Abstract/2012/04000/Chronic_Traumatic_Encephalopathy.44.aspx

[9] L. M. Gessel, S. K. Fields, C. L. Collins, R. W. Dick, and R. D. Comstock, "Concussions among United States high school and collegiate athletes." *Journal of Athletic Training (National Athletic Trainers' Association)*, vol. 42, no. 4, pp. 495–503, 2007. [Online]. Available: http://spot.lib.auburn.edu/login?url=http://search.ebscohost.com/login.aspx?direct=true&db=cin20&AN=2009759920&site=ehost-live

[10] S. L. Zuckerman, Z. Y. Kerr, A. Yengo-Kahn, E. Wasserman, T. Covassin, and G. S. Solomon, "Epidemiology of Sports-Related Concussion in NCAA Athletes From 2009-2010 to 2013-2014," *The American Journal of Sports Medicine*, vol. 43, no. 11, pp. 2654–2662, 2015. [Online]. Available: http://journals.sagepub.com/doi/10.1177/0363546515599634

[11] M. Field, M. W. Collins, M. R. Lovell, and J. Maroon, "Does age play a role in recovery from sports-related concussion? A comparison of high school and collegiate athletes." [Online]. Available: https://www.impacttest.com/ArticlesPage_images/Articles_Docs/7DHSvsCollegeAthleteJPediatrics2003.pdf

[12] J. J. Bazarian, T. Zhu, J. Zhong, D. Janigro, E. Rozen, A. Roberts, H. Javien, K. Merchant-Borna, B. Abar, and E. G. Blackman, "Persistent, Long-term Cerebral White Matter Changes after Sports-Related Repetitive Head Impacts," *PLoS ONE*, vol. 9, no. 4, p. e94734, 4 2014. [Online]. Available: http://dx.plos.org/10.1371/journal.pone.0094734

[13] E. M. Davenport, C. T. Whitlow, J. E. Urban, M. A. Espeland, Y. Jung, D. A. Rosenbaum, G. A. Gioia, A. K. Powers, J. D. Stitzel, and J. A. Maldjian, "Abnormal White Matter Integrity Related to Head Impact Exposure in a Season of High School Varsity Football," *Journal of Neurotrauma*, vol. 31, no. 19, pp. 1617–1624, 10 2014. [Online]. Available: http://online.liebertpub.com/doi/abs/10.1089/neu.2013.3233

[14] T. W. McAllister, J. C. Ford, L. A. Flashman, A. C. Maerlender, R. M. Greenwald, N. Lincoln McAllister, J. G. Beckwith, R. P. Bolander, T. D. Tosteson, J. H. Turco, R. Raman, S. Jain, A. Maerlender, M. P. Richard Bolander, and S. H. John Turco, "Effect of head impacts on diffusivity\r\nmeasures in a cohort of collegiate contact\r\nsport athletes," pp. 63–69, 2013.

[15] T. M. Talavage, E. A. Nauman, E. L. Breedlove, U. Yoruk, A. E. Dye, K. E. Morigaki, H. Feuer, and L. J. Leverenz, "Functionally-Detected Cognitive Impairment in High School Football Players without Clinically-Diagnosed Concussion," *Journal of Neurotrauma*, vol. 31, no. 4, pp. 327–338, 2014. [Online]. Available: http://online.liebertpub.com/doi/abs/10.1089/neu.2010.1512

[16] S. M. Slobounov, A. Walter, H. C. Breiter, D. C. Zhu, X. Bai, T. Bream, P. Seidenberg, X. Mao, B. Johnson, and T. M. Talavage, "The effect of repetitive subconcussive collisions on brain integrity in collegiate football players over a single football seasonA multi-modal neuroimaging study," *NeuroImage: Clinical*, vol. 14, no. March, pp. 708–718, 2017. [Online]. Available: http://dx.doi.org/10.1016/j.nicl.2017.03.006

[17] B. B. Reynolds, A. N. Stanton, S. Soldozy, H. P. Goodkin, M. Wintermark, and T. J. Druzgal, "Investigating the effects of subconcussion on functional connectivity using mass-univariate and multivariate approaches," *Brain Imaging and Behavior*, vol. 12, no. 5, pp. 1332–1345, 10 2018. [Online]. Available: http://link.springer.com/10.1007/s11682-017-9790-z

[18] J. E. Bailes, A. L. Petraglia, B. I. Omalu, E. Nauman, and T. Talavage, "Role of subconcussion in repetitive mild traumatic brain injury," *Journal of Neurosurgery*, vol. 119, no. 5, pp. 1235–1245, 2013. [Online]. Available: http://thejns.org/doi/10.3171/2013.7.JNS121822

[19] M. L. Lipton, N. Kim, M. E. Zimmerman, M. Kim, W. F. Stewart, C. A. Branch, and R. B. Lipton, "Soccer Heading Is Associated with White Matter Microstructural and Cognitive Abnormalities," *Radiology*, vol. 268, no. 3, pp. 850–857, 2013. [Online]. Available: http://pubs.rsna.org/doi/10.1148/radiol.13130545

[20] E. L. Breedlove, M. Robinson, T. M. Talavage, K. E. Morigaki, U. Yoruk, K. O'Keefe, J. King, L. J. Leverenz, J. W. Gilger, and E. A. Nauman, "Biomechanical correlates of symptomatic and asymptomatic neurophysiological impairment in high school football," *Journal of Biomechanics*, vol. 45, no. 7, pp. 1265–1272, 2012. [Online]. Available: http://dx.doi.org/10.1016/j.jbiomech.2012.01.034

[21] P. H. Montenigro, M. L. Alosco, B. M. Martin, D. H. Daneshvar, J. Mez, C. E. Chaisson, C. J. Nowinski, R. Au, A. C. McKee, R. C. Cantu, M. D. McClean, R. A. Stern, and Y. Tripodis, "Cumulative Head Impact Exposure Predicts Later-Life Depression, Apathy, Executive Dysfunction, and Cognitive Impairment in Former High School and College Football Players," *Journal of Neurotrauma*, vol. 34, no. 2, pp. 328–340, 2017. [Online]. Available: http://online.liebertpub.com/doi/10.1089/neu.2016.4413

[22] S. P. Broglio, J. T. Eckner, D. Martini, J. J. Sosnoff, J. S. Kutcher, and C. Randolph, "Cumulative Head Impact Burden in High School Football," *Journal of Neurotrauma*, vol. 28, no. 10, pp. 2069–2078, 2011. [Online]. Available: http://www.liebertonline.com/doi/abs/10.1089/neu.2011.1825

[23] R. A. Stern, D. O. Riley, D. H. Daneshvar, C. J. Nowinski, R. C. Cantu, and A. C. McKee, "Long-term Consequences of Repetitive Brain Trauma: Chronic Traumatic Encephalopathy," *PM and R*, vol. 3, no. 10 SUPPL. 2, pp. S460–S467, 2011. [Online]. Available: http://dx.doi.org/10.1016/j.pmrj.2011.08.008

[24] M. L. Alosco, Y. Tripodis, J. Jarnagin, C. M. Baugh, B. Martin, C. E. Chaisson, N. Estochen, L. Song, R. C. Cantu, A. Jeromin, and R. A. Stern, "Repetitive head impact exposure and later-life plasma total tau in former National Football League players," *Alzheimer's & Dementia: Diagnosis, Assessment & Disease Monitoring*, vol. 7, pp. 33–40, 2017. [Online]. Available: http://linkinghub.elsevier.com/retrieve/pii/S2352872916300598

[25] C. A. Tagge, A. M. Fisher, O. V. Minaeva, A. Gaudreau-Balderrama, J. A. Moncaster, X.-L. Zhang, M. W. Wojnarowicz, N. Casey, H. Lu, O. N. Kokiko-Cochran, S. Saman, M. Ericsson, K. D. Onos, R. Veksler, V. V. Senatorov, A. Kondo, X. Z. Zhou, O. Miry, L. R. Vose, K. R. Gopaul, C. Upreti, C. J. Nowinski, R. C. Cantu, V. E. Alvarez, A. M.

Hildebrandt, E. S. Franz, J. Konrad, J. A. Hamilton, N. Hua, Y. Tripodis, A. T. Anderson, G. R. Howell, D. Kaufer, G. F. Hall, K. P. Lu, R. M. Ransohoff, R. O. Cleveland, N. W. Kowall, T. D. Stein, B. T. Lamb, B. R. Huber, W. C. Moss, A. Friedman, P. K. Stanton, A. C. McKee, and L. E. Goldstein, "Concussion, microvascular injury, and early tauopathy in young athletes after impact head injury and an impact concussion mouse model," *Brain*, vol. 141, no. 2, pp. 422–458, 2 2018. [Online]. Available: https://academic.oup.com/brain/article/141/2/422/4815697

[26] J. Bailes, S. Bravo, H. Breiter, D. Kaufman, Z. Lu, D. Molfese, T. Perrish, S. Slobounov, T. Talavage, and D. Zhu, "A Call to Arms: The Need to Create an Inter-Institutional Concussion Neuroimaging Consortium to Discover Clinically Relevant Diagnostic Biomarkers and Develop Evidence-Based Interventions to Facilitate Recovery," *Developmental Neuropsychology*, vol. 40, no. 2, pp. 59–62, 2 2015. [Online]. Available: http://www.tandfonline.com/doi/full/10.1080/87565641.2015.1018090

[27] K. Abbas, T. E. Shenk, V. N. Poole, E. L. Breedlove, L. J. Leverenz, E. A. Nauman, T. M. Talavage, and M. E. Robinson, "Alteration of Default Mode Network in High School Football Athletes Due to Repetitive Subconcussive Mild Traumatic Brain Injury: A Resting-State Functional Magnetic Resonance Imaging Study," *Brain Connectivity*, vol. 5, no. 2, pp. 91–101, 2015. [Online]. Available: http://online.liebertpub.com/doi/10.1089/brain.2014.0279

[28] I. Y. Chun, X. Mao, E. L. Breedlove, L. J. Leverenz, E. A. Nauman, and T. M. Talavage, "DTI detection of longitudinal WM abnormalities due to accumulated head impacts," *Developmental Neuropsychology*, vol. 40, no. 2, pp. 92–97, 2015.

[29] T. E. Shenk, M. E. Robinson, D. O. Svaldi, K. Abbas, K. M. Breedlove, L. J. Leverenz, E. A. Nauman, and T. M. Talavage, "FMRI of visual working memory in high school football players," *Developmental Neuropsychology*, vol. 40, no. 2, pp. 63–68, 2015.

[30] D. O. Svaldi, C. Joshi, M. E. Robinson, T. E. Shenk, K. Abbas, E. A. Nauman, L. J. Leverenz, and T. M. Talavage, "Cerebrovascular reactivity alterations in asymptomatic high school football players," *Developmental Neuropsychology*, vol. 40, no. 2, pp. 80–84, 2015.

[31] D. O. Svaldi, E. C. McCuen, C. Joshi, M. E. Robinson, Y. Nho, R. Hannemann, E. A. Nauman, L. J. Leverenz, and T. M. Talavage, "Cerebrovascular reactivity changes in asymptomatic female athletes attributable to high school soccer participation," *Brain Imaging and Behavior*, vol. 11, no. 1, pp. 98–112, 2017.

[32] A. Lin, B. D. Ross, K. Harris, and W. Wong, "Efficacy of proton magnetic resonance spectroscopy in neurological diagnosis and neurotherapeutic decision making." *NeuroRx : the journal of the American Society for Experimental NeuroTherapeutics*, vol. 2, no. 2, pp. 197–214, 2005. [Online]. Available: http://www.pubmedcentral.nih.gov/articlerender.fcgi?artid=1064986&tool=pmcentrez&rendertype=abstract

[33] A. Grö Ger, R. Kolb, R. Schä, and U. Klose, "Dopamine Reduction in the Substantia Nigra of Parkinson's Disease Patients Confirmed by In Vivo Magnetic Resonance Spectroscopic Imaging," *PLoS ONE*, vol. 9, no. 1, 2014. [Online]. Available: http://journals.plos.org/plosone/article/file?id=10.1371/journal.pone.0084081&type=printable

[34] G. Öz, J. R. Alger, P. B. Barker, R. Bartha, A. Bizzi, C. Boesch, P. J. Bolan, K. M. Brindle, C. Cudalbu, A. Dinçer, U. Dydak, U. E. Emir, J. Frahm, R. G. González, S. Gruber, R. Gruetter, R. K. Gupta, A. Heerschap, A. Henning, H. P. Hetherington, F. A. Howe, P. S. Hüppi, and R. E. Hurd, "Clinical Proton MR spectroscopy in central nervous system Disorders 1," *Radiology*, vol. 270, no. 3March, 2014. [Online]. Available: http://pubs.rsna.org/doi/pdf/10.1148/radiol.13130531

[35] B. Zhang, T. J. Ferman, B. F. Boeve, G. E. Smith, M. Maroney-Smith, A. J. Spychalla, D. S. Knopman, C. R. Jack, R. C. Petersen, and K. Kantarci, "MRS in Mild Cognitive Impairment: Early Differentiation of Dementia with Lewy Bodies and Alzheimer's Disease," *Journal of Neuroimaging*, vol. 25, no. 2, pp. 269–274, 2015.

[36] S. K. Gujar, S. Maheshwari, I. Bj??rkman-Burtscher, and P. C. Sundgren, "Magnetic Resonance Spectroscopy," *Journal of Neuro-Ophthalmology*, vol. 25, no. 3, pp. 217–226, 9 2005. [Online]. Available: https://insights.ovid.com/crossref?an=00041327-200509000-00015

[37] R. Ricci, G. Barbarella, P. Musi, P. Boldrini, C. Trevisan, and N. Basaglia, "Localised proton MR spectroscopy of brain metabolism changes in vegetative patients," *Neuroradiology*, vol. 39, no. 5, pp. 313–319, 1997.

[38] S. Friedman, W. Brooks, R. Jung, B. Hart, and R. Yeo, "Proton MR spectroscopic findings correspond to neuropsychological function in traumatic brain injury," *American Journal of Neuroradiology*, vol. 19, no. 10, pp. 1879–1885, 1998.

[39] P. Newsholme, J. Procopio, M. M. Ramos Lima, T. C. Pithon-Curi, and R. Curi, "Glutamine and glutamate - Their central role in cell metabolism and function," *Cell Biochemistry and Function*, vol. 21, no. 1, pp. 1–9, 2003.

[40] V. Govindaraju, G. E. Gauger, G. T. Manley, A. Ebel, M. Meeker, and A. a. Maudsley, "Volumetric proton spectroscopic imaging of mild traumatic brain injury." *AJNR. American journal of neuroradiology*, vol. 25, no. 5, pp. 730–737, 2004.

[41] L. Shutter, K. A. Tong, and B. A. Holshouser, "Proton MRS in acute traumatic brain injury: role for glutamate/glutamine and choline for outcome prediction." *Journal of neurotrauma*, vol. 21, no. 12, pp. 1693–1705, 2004.

[42] C. Gasparovic, R. Yeo, M. Mannell, J. Ling, R. Elgie, J. Phillips, D. Doezema, and A. R. Mayer, "Neurometabolite concentrations in gray and white matter in mild traumatic brain injury: an 1H-magnetic resonance spectroscopy study." *Journal of neurotrauma*, vol. 26, no. 10, pp. 1635–43, 10 2009. [Online]. Available: http://www.ncbi.nlm.nih.gov/pubmed/19355814http://www.pubmedcentral.nih.gov/articlerender.fcgi?artid=PMC2822798

[43] L. C. Henry, S. Tremblay, Y. Boulanger, D. Ellemberg, and M. Lassonde, "Neurometabolic Changes in the Acute Phase after Sports Concussions Correlate with Symptom Severity," *Journal of Neurotrauma*, vol. 27, no. 1, pp. 65–76, 2010. [Online]. Available: https://www.researchgate.net/profile/Sebastien_Tremblay3/publication/26819013_Neurometabolic_Changes_in_the_Acute_Phase_

after_Sports_Concussions_Correlate_with_Symptom_Severity/links/0912f505cb65bf38f3000000.pdfhttp://www.liebertonline.com/doi/abs/10.108

[44] R. Vagnozzi, S. Signoretti, L. Cristofori, F. Alessandrini, R. Floris, E. Isgró, A. Ria, S. Marziale, G. Zoccatelli, B. Tavazzi, F. Del Bolgia, R. Sorge, S. P. Broglio, T. K. McIntosh, and G. Lazzarino, "Assessment of metabolic brain damage and recovery following mild traumatic brain injury: A multicentre, proton magnetic resonance spectroscopic study in concussed patients," *Brain*, vol. 133, no. 11, pp. 3232–3242, 2010.

[45] R. A. Yeo, C. Gasparovic, F. Merideth, D. Ruhl, D. Doezema, and A. R. Mayer, "A Longitudinal Proton Magnetic Resonance Spectroscopy Study of Mild Traumatic Brain Injury," *Journal of Neurotrauma*, vol. 28, no. 1, pp. 1–11, 2011. [Online]. Available: http://www.liebertonline.com/doi/abs/10.1089/neu.2010.1578

[46] A. Maudsley, V. Govind, B. Levin, G. Saigal, L. T. Harris, and S. Sheriff, "Distributions of MR Diffusion and Spectroscopy Measures with Traumatic Brain Injury," *Journal of neurotrauma*, vol. 1063, no. Md, pp. 1–25, 2014. [Online]. Available: http://www.ncbi.nlm.nih.gov/pubmed/25333480

[47] V. N. Poole, K. Abbas, T. E. Shenk, E. L. Breedlove, K. M. Breedlove, M. E. Robinson, L. J. Leverenz, E. A. Nauman, T. M. Talavage, and U. Dydak, "MR spectroscopic evidence of brain injury in the non-diagnosed collision sport athlete," *Developmental Neuropsychology*, vol. 39, no. 6, pp. 459–473, 2014.

[48] V. N. Poole, E. L. Breedlove, T. E. Shenk, K. Abbas, M. E. Robinson, L. J. Leverenz, E. A. Nauman, U. Dydak, T. M. Talavage, B. Danielle, M. Sholly, D. Activity, N. Digestibility, E. L. Adams, J. Mcgrew, B. Danielle, M. Sholly, D. Activity, N. Digestibility, T. E. Shenk, M. E. Robinson, D. O. Svaldi, K. Abbas, K. M. Breedlove, L. J. Leverenz, E. A. Nauman, T. M. Talavage, E. A. Nauman, E. L. Breedlove, U. Yoruk, A. E. Dye, K. E. Morigaki, H. Feuer, L. J. Leverenz, E. L. Breedlove, U. Yoruk, A. E. Dye, K. E. Morigaki, H. Feuer, L. J. Leverenz, M. E. Robinson, T. E. Shenk, E. L. Breedlove, L. J. Leverenz, E. A. Nauman, T. M. Talavage, K. Abbas, T. E. Shenk, V. N. Poole, M. E. Robinson, L. J. Leverenz, E. A. Nauman, T. M. Talavage, E. L. Breedlove, L. J. Leverenz, E. A. Nauman, T. M. Talavage, M. E. Robinson, L. Hou, P. Yang, F. Jiang, Q. Liu, X. Wang, L. Kang, I. Jang, S. Bari, Y. Zou, N. L. Vike, P. Kashyap, T. M. Talavage, P. Number, S. Type, E. McCuen, D. O. Svaldi, K. M. Breedlove, N. Kraz, B. Cummiskey, E. L. Breedlove, J. Traver, K. F. Desmond, R. E. Hannemann, E. Zanath, A. Guerra, L. J. Leverenz, T. M. Talavage, E. A. Nauman, I. Y. Chun, X. Mao, E. L. Breedlove, L. J. Leverenz, E. A. Nauman, T. M. Talavage, K. M. Breedlove, E. L. Breedlove, M. E. Robinson, V. N. Poole, J. R. K. Iii, P. Rosenberger, M. Rasmussen, T. M. Talavage, L. J. Leverenz, E. A. Nauman, I. Y. Chun, S. Bari, L. J. Leverenz, E. A. Nauman, and T. M. Talavage, "The role of location of subconcussive head impacts in fMRI brain activation change," *Developmental Neuropsychology*, vol. 40, no. 2, pp. 74–79, 2015. [Online]. Available: http://dx.doi.org/10.1016/j.jbiomech.2015.08.003http://online.liebertpub.com/doi/10.1089/brain.2014.0279http://dx.doi.org/10.1080/87565641.2014.990455http://dx.doi.org/10.1080/87565641.2015.1012204http://online.liebertpub.com/doi/abs/10.1089/neu.2010.

[49] E. McCuen, D. Svaldi, K. Breedlove, N. Kraz, B. Cummiskey, E. L. Breedlove, J. Traver, K. F. Desmond, R. E. Hannemann, E. Zanath, A. Guerra, L. Leverenz, T. M. Talavage, and E. A. Nauman, "Collegiate women's soccer players suffer greater cumulative head impacts than their high school counterparts," *Journal of biomechanics*, vol. 48, no. 13, pp. 3720–3723, 2015. [Online]. Available: http://dx.doi.org/10.1016/j.jbiomech.2015.08.003

[50] C. E. Curtis and M. D'Esposito, "Persistent activity in the prefrontal cortex during working memory," *Trends in Cognitive Sciences*, vol. 7, no. 9, pp. 415–423, 9 2003. [Online]. Available: https://www.sciencedirect.com/science/article/pii/S1364661303001979

[51] K. Morigaki Breedlove, E. L. Breedlove, M. Robinson, V. N. Poole, J. R. King III, P. Rosenberger, M. Rasmussen, T. M. Talavage, L. J. Leverenz, and E. A. Nauman, "Detecting Neurocognitive and Neurophysiological Changes as a Result of Subconcussive Blows in High School Football Athletes," *Athletic Training & Sports Health Care —*, vol. 6, 2014. [Online]. Available: http://www.impacttest.

[52] L. C. Henry, S. Tremblay, S. Leclerc, A. Khiat, Y. Boulanger, D. Ellemberg, and M. Lassonde, "Metabolic changes in concussed American football players during the acute and chronic post-injury phases," *BMC Neurology*, vol. 11, no. 1, p. 105, 12 2011. [Online]. Available: http://bmcneurol.biomedcentral.com/articles/10.1186/1471-2377-11-105

[53] B. Cummiskey, D. Schiffmiller, T. M. Talavage, L. Leverenz, J. J. Meyer, D. Adams, and E. A. Nauman, "Reliability and accuracy of helmet-mounted and head-mounted devices used to measure head accelerations," *Proceedings of the Institution of Mechanical Engineers, Part P: Journal of Sports Engineering and Technology*, vol. 231, no. 2, pp. 144–153, 6 2017. [Online]. Available: http://journals.sagepub.com/doi/10.1177/1754337116658395

[54] M. Wilson, G. Reynolds, R. A. Kauppinen, T. N. Arvanitis, and A. C. Peet, "A constrained least-squares approach to the automated quantitation of in vivo ¡sup¿1¡/sup¿ H magnetic resonance spectroscopy data," *Magnetic Resonance in Medicine*, vol. 65, no. 1, pp. 1–12, 2011. [Online]. Available: http://doi.wiley.com/10.1002/mrm.22579

[55] R. W. Cox, "AFNI: Software for Analysis and Visualization of Functional Magnetic Resonance Neuroimages," *COMPUTERS AND BIOMEDICAL RESEARCH*, vol. 29, pp. 162–173, 1996. [Online]. Available: https://ac.els-cdn.com/S0010480996900142/1-s2.0-S0010480996900142-main.pdf?_tid=b367069c-c8b8-11e7-b3a0-00000aacb361&acdnat=1510608308_13001f4d4f6a65ca677dde5e54983c4a

[56] M. Jenkinson, C. F. Beckmann, T. E. J. Behrens, M. W. Woolrich, and S. M. Smith, "FSL," 2012. [Online]. Available: https://ac.els-cdn.com/S1053811911010603/1-s2.0-S1053811911010603-main.pdf?_tid=e4e2f3c0-c8b8-11e7-a08e-00000aacb361&acdnat=1510608391_06c25cc0a16fd17f0eeb1e5983958656

[57] S. M. Smith, M. Jenkinson, M. W. Woolrich, C. F. Beckmann, T. E. Behrens, H. Johansen-Berg, P. R. Bannister, M. De Luca, I. Drobnjak, D. E. Flitney, R. K. Niazy, J. Saunders, J. Vickers, Y. Zhang,

N. De Stefano, J. M. Brady, and P. M. Matthews, "Advances in functional and structural MR image analysis and implementation as FSL," in *NeuroImage*, vol. 23, no. SUPPL. 1, 2004. [Online]. Available: https://ac.els-cdn.com/S1053811904003933/1-s2.0-S1053811904003933-main.pdf?_tid=09306906-c8b9-11e7-b5b6-00000aab0f6c&acdnat=1510608452_48c28dee6fe74c89b722cc61d698b12a

[58] E. A. Wilde, S. Bouix, D. F. Tate, A. P. Lin, M. R. Newsome, B. A. Taylor, J. R. Stone, J. Montier, S. E. Gandy, B. Biekman, M. E. Shenton, and G. York, *Advanced neuroimaging applied to veterans and service personnel with traumatic brain injury: state of the art and potential benefits*, 2015, vol. 9, no. 3.

[59] H. Zhu and P. B. Barker, "MR Spectroscopy and Spectroscopic Imaging of the Brain." Humana Press, 2011, pp. 203–226. [Online]. Available: http://link.springer.com/10.1007/978-1-61737-992-5_9

[60] J. Honaker, G. King, and M. Blackwell, "Amelia {\smrm II}: A program for missing data," *Journal of Statistical Software*, vol. 45, no. 7, p. 47, 2006. [Online]. Available: http://www.jstatsoft.org/http://gking.harvard.edu/amelia/docs/amelia.pdf

[61] Y. Benjamini, Y. Hochberg, and Y. Benjaminit, "Controlling the False Discovery Rate: A Practical and Powerful Approach to Multiple Controlling the False Discovery Rate: a Practical and Powerful Approach to Multiple Testing," *Source Journal of the Royal Statistical Society. Series B (Methodological) Journal of the Royal Statistical Society. Series B J. R. Statist. Soc. B*, vol. 57, no. 1, pp. 289–300, 1995. [Online]. Available: http://www.jstor.org/stable/2346101http://about.jstor.org/terms

[62] M. U. Schuhmann, D. Stiller, M. Skardelly, J. Bernarding, P. M. Klinge, A. Samii, M. Samii, and T. Brinker, "Metabolic Changes in the Vicinity of Brain Contusions: A Proton Magnetic Resonance Spectroscopy and Histology Study," *Journal of neurotrauma*, vol. 20, no. 8, pp. 725–743, 2003. [Online]. Available: http://www.liebertonline.com/doi/abs/10.1089/089771503767869962%5Cnhttp://online.liebertpub.com/doi/pdfplus/10.1089/089771503767869962

[63] M. R. Garnett, A. M. Blamire, R. G. Corkill, T. a. Cadoux-Hudson, B. Rajagopalan, and P. Styles, "Early proton magnetic resonance spectroscopy in normal-appearing brain correlates with outcome in patients following traumatic brain injury." *Brain : a journal of neurology*, vol. 123 (Pt 1, pp. 2046–54, 2000. [Online]. Available: http://www.ncbi.nlm.nih.gov/pubmed/11004122

[64] R. Bullock, A. Zauner, J. J. Woodward, J. Myseros, S. C. Choi, J. D. Ward, A. Marmarou, and H. F. Young, "Factors affecting excitatory amino acid release following severe human head injury," *Journal of Neurosurgery*, vol. 89, no. 4, pp. 507–518, 10 1998. [Online]. Available: http://thejns.org/doi/10.3171/jns.1998.89.4.0507

[65] R. A. Ruppel, P. M. Kochanek, P. Adelson, M. E. Rose, S. R. Wisniewski, M. J. Bell, R. S. Clark, D. W. Marion, and S. H. Graham, "Excitatory amino acid concentrations in ventricular cerebrospinal fluid after severe traumatic brain injury in infants and children: The role of child abuse," *The Journal of Pediatrics*, vol. 138, no. 1, pp. 18–25, 1 2001. [Online]. Available: https://www.sciencedirect.com/science/article/pii/S0022347601518508

[66] S. Ashwal, B. Holshouser, K. Tong, T. Serna, R. Osterdock, M. Gross, and D. Kido, "Proton MR Spectroscopy Detected Glutamate / Glutamine Is Increased in Children with Traumatic Brain Injury," *Journal of Neurotrauma*, vol. 21, no. 11, pp. 1539–1552, 2004.

[67] K. Abbas, T. E. Shenk, V. N. Poole, M. E. Robinson, L. J. Leverenz, E. A. Nauman, and T. M. Talavage, "Effects of Repetitive Sub-Concussive Brain Injury on the Functional Connectivity of Default Mode Network in High School Football Athletes," *Developmental Neuropsychology*, vol. 40, no. 1, pp. 51–56, 1 2015. [Online]. Available: http://www.tandfonline.com/doi/abs/10.1080/87565641.2014.990455

[68] M. R. Garnett, A. M. Blamire, B. Rajagopalan, P. Styles, and T. A. D. Cadoux-Hudson, "Evidence for cellular damage in normal-appearing white matter correlates with injury severity in patients following traumatic brain injury. A magnetic resonance spectroscopy study," *Brain*, vol. 123, no. 7, pp. 1403–1409, 2000. [Online]. Available: http://ezproxy.newcastle.edu.au/login?url=http://ovidsp.ovid.com?T=JS&CSC=Y&NEWS=N&PAGE=fulltext&D=emed5&AN=2000228411%5Cnhttp://library.newcastle.edu.au/resserv?sid=OVID:embase&id=pmid:&id=&issn=0006-8950&isbn=&volume=123&issue=7&spage=1403&pages=1403-14

[69] D. O. Svaldi, C. Joshi, E. C. McCuen, J. P. Music, R. Hannemann, L. J. Leverenz, E. A. Nauman, and T. M. Talavage, "Accumulation of high magnitude acceleration events predicts cerebrovascular reactivity changes in female high school soccer athletes," *Brain Imaging and Behavior*, pp. 1–11, 10 2018. [Online]. Available: http://link.springer.com/10.1007/s11682-018-9983-0

[70] C. C. Giza and D. A. Hovda, "The Neurometabolic Cascade of Concussion." *Journal of athletic training*, vol. 36, no. 3, pp. 228–235, 2001. [Online]. Available: http://www.ncbi.nlm.nih.gov/pubmed/12937489%0Ahttp://www.pubmedcentral.nih.gov/articlerender.fcgi?artid=PMC155411

[71] S. M. DeLellis, S. Kane, and K. Katz, "The neurometabolic cascade and implications of mTBI: mitigating risk to the SOF community." *Journal of special operations medicine : a peer reviewed journal for SOF medical professionals*, vol. 9, no. 4, pp. 36–42, 2009. [Online]. Available: http://www.ncbi.nlm.nih.gov/pubmed/20112647

[72] H. C. Klonoff C.; Klonoff, P. S., K. H., C. C., H. Klonoff, C. Clark, and P. S. Klonoff, "Long-term outcome of head injuries: A 23 year follow up study of children with head injuries," *Journal of Neurology Neurosurgery and Psychiatry*, vol. 56, no. 4, pp. 410–415, 1993. [Online]. Available: http://ovidsp.ovid.com/ovidweb.cgi?T=JS&PAGE=reference&D=med3&NEWS=N&AN=8482963%5Cnhttp://ovidsp.ovid.com/ovidweb.cgi?T=JS&PAGE=reference&D=emed6&NEWS=N&AN=23120533%5Cnhttp://ovidsp.ovid.com/ovidweb.cgi?T=JS&CSC=Y&NEWS=N&PAGE=fulltext&D=emed6&AN=23120533

[73] A. McKinlay, R. C. Grace, L. J. Horwood, D. M. Fergusson, and M. R. MacFarlane, "Long-term behavioural outcomes of pre-school mild traumatic brain injury," *Child: Care, Health and Development*, vol. 36, no. 1, pp. 22–30, 2010.

[74] I. Hancu, D. J. Blezek, and M. C. Dumoulin, "Automatic repositioning of single voxels in longitudinal 1H MRS studies," *NMR in Biomedicine*, vol. 18, no. 6, pp. 352–361, 2005.

[75] W. Dou, O. Speck, T. Benner, J. Kaufmann, M. Li, K. Zhong, and M. Walter, "Automatic voxel positioning for MRS at 7 T," *Magma (New York, N.Y.)*, vol. 28, no. 3, pp. 259–270, 2015. [Online]. Available: http://dx.doi.org/10.1007/s10334-014-0469-9

[76] X. Q. Ding, A. A. Maudsley, M. Sabati, S. Sheriff, P. R. Dellani, and H. Lanfermann, "Reproducibility and reliability of short-TE whole-brain MR spectroscopic imaging of human brain at 3T," *Magnetic Resonance in Medicine*, vol. 73, no. 3, pp. 921–928, 2015.

[77] A. A. Maudsley, C. Domenig, and S. Sheriff, "Reproducibility of serial whole-brain MR Spectroscopic Imaging," *NMR in Biomedicine*, vol. 23, no. 3, pp. 251–256, 2010.

[78] D. T. Chard, "Brain metabolite changes in cortical grey and normal-appearing white matter in clinically early relapsing-remitting multiple sclerosis," *Brain*, vol. 125, no. 10, pp. 2342–2352, 2002. [Online]. Available: https://academic.oup.com/brain/article-lookup/doi/10.1093/brain/awf240

[79] X. Zhu, N. Schuff, J. Kornak, B. Soher, K. Yaffe, J. H. Kramer, F. Ezekiel, B. L. Miller, W. J. Jagust, and M. W. Weiner, "Effects of Alzheimer Disease on Fronto-parietal Brain N-acetyl Aspartate and Myo-Inositol Using Magnetic Resonance Spectroscopic Imaging," *Alzheimer Disease & Associated Disorders*, vol. 20, no. 2, pp. 77–85, 2006. [Online]. Available: http://content.wkhealth.com/linkback/openurl?sid=WKPTLP:landingpage&an=00002093-200604000-00001

[80] D. Martini, J. Eckner, J. Kutcher, and S. P. Broglio, "Subconcussive head impact biomechanics: comparing differing offensive schemes." *Medicine and science in sports and exercise*, vol. 45, no. 4, pp. 755–61, 4 2013. [Online]. Available: http://www.ncbi.nlm.nih.gov/pubmed/23135370http://www.pubmedcentral.nih.gov/articlerender.fcgi?artid=PMC3605196

[81] R. L. O'Gorman, L. Michels, R. A. Edden, J. B. Murdoch, and E. Martin, "In vivo detection of GABA and glutamate with MEGA-PRESS: Reproducibility and gender effects," *Journal of Magnetic Resonance Imaging*, vol. 33, no. 5, pp. 1262–1267, 5 2011. [Online]. Available: http://doi.wiley.com/10.1002/jmri.22520

[82] D. Endres, L. Tebartz van Elst, B. Feige, S. Backenecker, K. Nickel, A. Bubl, T. Lange, I. Mader, S. Maier, and E. Perlov, "On the Effect of Sex on Prefrontal and Cerebellar Neurometabolites in Healthy Adults: An MRS Study," *Frontiers in Human Neuroscience*, vol. 10, p. 367, 8 2016. [Online]. Available: http://journal.frontiersin.org/Article/10.3389/fnhum.2016.00367/abstract

[83] N. L. Ragson, M. A. Thomas, B. H. Guze, L. A. Fairbanks, K. Yue, J. G. Curran, and A. J. Rapkin, "Menstrual cycle-related brain metabolite changes using H magnetic resonance spectroscopy in premenopausal women: A pilot study." *Psychiatry Research: Neuroimaging*, vol. 106, no. 1, pp. 47–57, 2001. [Online]. Available: http://search.ebscohost.com.proxy-ub.rug.nl/login.aspx?direct=true&db=psyh&AN=2001-14932-005&site=ehost-live&scope=site

[84] N. A. Batra, J. Seres-Mailo, C. Hanstock, P. Seres, J. Khudabux, F. Bellavance, G. Baker, P. Allen, P. Tibbo, E. Hui, and J. M. Le Melledo, "Proton Magnetic Resonance Spectroscopy Measurement of Brain Glutamate Levels in Premenstrual Dysphoric Disorder," *Biological Psychiatry*, vol. 63, no. 12, pp. 1178–1184, 2008.

[85] S. Bari, E. Amico, N. Vike, T. M. Talavage, and J. Goñi, "Uncovering Multi-Site Identifiability Based on Resting-State Functional Connectomes," 9 2018. [Online]. Available: http://arxiv.org/abs/1809.08959

[86] D. C. Van Essen, K. Ugurbil, E. Auerbach, D. Barch, T. E. Behrens, R. Bucholz, A. Chang, L. Chen, M. Corbetta, S. W. Curtiss, S. Della Penna, D. Feinberg, M. F. Glasser, N. Harel, A. C. Heath, L. Larson-Prior, D. Marcus, G. Michalareas, S. Moeller, R. Oostenveld, S. E. Petersen, F. Prior, B. L. Schlaggar, S. M. Smith, A. Z. Snyder, J. Xu, and E. Yacoub, "The Human Connectome Project: A data acquisition perspective," *NeuroImage*, vol. 62, no. 4, pp. 2222–2231, 2012.

[87] D. C. Van Essen, S. M. Smith, D. M. Barch, T. E. Behrens, E. Yacoub, and K. Ugurbil, "The WU-Minn Human Connectome Project: An overview," *NeuroImage*, vol. 80, pp. 62–79, 2013.

[88] D. B. Keator, T. G. van Erp, J. A. Turner, G. H. Glover, B. A. Mueller, T. T. Liu, J. T. Voyvodic, J. Rasmussen, V. D. Calhoun, H. J. Lee, A. W. Toga, S. McEwen, J. M. Ford, D. H. Mathalon, M. Diaz, D. S. O'Leary, H. Jeremy Bockholt, S. Gadde, A. Preda, C. G. Wible, H. S. Stern, A. Belger, G. McCarthy, B. Ozyurt, and S. G. Potkin, "The Function Biomedical Informatics Research Network Data Repository," *NeuroImage*, vol. 124, pp. 1074–1079, 2016. [Online]. Available: http://dx.doi.org/10.1016/j.neuroimage.2015.09.003

[89] C. R. Jack, M. A. Bernstein, N. C. Fox, P. Thompson, G. Alexander, D. Harvey, B. Borowski, P. J. Britson, J. L. Whitwell, C. Ward, A. M. Dale, J. P. Felmlee, J. L. Gunter, D. L. Hill, R. Killiany, N. Schuff, S. Fox-Bosetti, C. Lin, C. Studholme, C. S. DeCarli, G. Gunnar Krueger, H. A. Ward, G. J. Metzger, K. T. Scott, R. Mallozzi, D. Blezek, J. Levy, J. P. Debbins, A. S. Fleisher, M. Albert, R. Green, G. Bartzokis, G. Glover, J. Mugler, and M. W. Weiner, "The Alzheimer's disease neuroimaging initiative (ADNI): MRI methods," *Journal of Magnetic Resonance Imaging*, vol. 27, no. 4, pp. 685–691, 4 2008. [Online]. Available: http://doi.wiley.com/10.1002/jmri.21049

[90] J. D. Van Horn and A. W. Toga, "Multisite neuroimaging trials." *Current opinion in neurology*, vol. 22, no. 4, pp. 370–8, 8 2009. [Online]. Available: http://www.ncbi.nlm.nih.gov/pubmed/19506479http://www.pubmedcentral.nih.gov/articlerender.fcgi?artid=PMC2777976

[91] L. Friedman, G. H. Glover, and The FBIRN Consortium, "Reducing interscanner variability of activation in a multicenter fMRI study: Controlling for signal-to-fluctuation-noise-ratio (SFNR) differences," *NeuroImage*, vol. 33, no. 2, pp. 471–481, 11 2006. [Online]. Available: https://www.sciencedirect.com/science/article/pii/S1053811906007944

[92] R. V. Mulkern, P. Forbes, K. Dewey, S. Osganian, M. Clark, S. Wong, U. Ramamurthy, L. Kun, and T. Y. Poussaint, "Establishment and Results

of a Magnetic Resonance Quality Assurance Program for the Pediatric Brain Tumor Consortium," *Academic Radiology*, vol. 15, no. 9, pp. 1099–1110, 9 2008. [Online]. Available: https://www.sciencedirect.com/science/article/pii/S1076633208002183

[93] G. G. Brown, D. H. Mathalon, H. Stern, J. Ford, B. Mueller, D. N. Greve, G. McCarthy, J. Voyvodic, G. Glover, M. Diaz, E. Yetter, I. B. Ozyurt, K. W. Jorgensen, C. G. Wible, J. A. Turner, W. K. Thompson, and S. G. Potkin, "Multisite reliability of cognitive BOLD data," *NeuroImage*, vol. 54, no. 3, pp. 2163–2175, 2011. [Online]. Available: http://dx.doi.org/10.1016/j.neuroimage.2010.09.076

[94] J. T. Voyvodic, "Activation mapping as a percentage of local excitation: fMRI stability within scans, between scans and across field strengths," *Magnetic Resonance Imaging*, vol. 24, no. 9, pp. 1249–1261, 11 2006. [Online]. Available: https://www.sciencedirect.com/science/article/pii/S0730725X06002207

[95] L. Friedman, H. Stern, G. G. Brown, D. H. Mathalon, J. Turner, G. H. Glover, R. L. Gollub, J. Lauriello, K. O. Lim, T. Cannon, D. N. Greve, H. J. Bockholt, A. Belger, B. Mueller, M. J. Doty, J. He, W. Wells, P. Smyth, S. Pieper, S. Kim, M. Kubicki, M. Vangel, and S. G. Potkin, "Test-retest and between-site reliability in a multicenter fMRI study," *Human Brain Mapping*, vol. 29, no. 8, pp. 958–972, 2008.

[96] B. J. Casey, J. D. Cohen, K. O'Craven, R. J. Davidson, W. Irwin, C. A. Nelson, D. C. Noll, X. Hu, M. J. Lowe, B. R. Rosen, C. L. Truwitt, and P. A. Turski, "Reproductibility of fMRI results across four institutions using a spatial working memory task," *Neuroimage*, vol. 8, no. 3, pp. 249–261, 1998.

[97] V.-E. Gountouna, D. E. Job, A. M. McIntosh, T. W. J. Moorhead, G. K. L. Lymer, H. C. Whalley, J. Hall, G. D. Waiter, D. Brennan, D. J. McGonigle, T. S. Ahearn, J. Cavanagh, B. Condon, D. M. Hadley, I. Marshall, A. D. Murray, J. D. Steele, J. M. Wardlaw, and S. M. Lawrie, "Functional Magnetic Resonance Imaging (fMRI) reproducibility and variance components across visits and scanning sites with a finger tapping task," *NeuroImage*, vol. 49, no. 1, pp. 552–560, 1 2010. [Online]. Available: https://www.sciencedirect.com/science/article/pii/S1053811909007988

[98] J. Suckling, D. Ohlssen, C. Andrew, G. Johnson, S. C. Williams, M. Graves, C.-H. Chen, D. Spiegelhalter, and E. Bullmore, "Components of variance in a multicentre functional MRI study and implications for calculation of statistical power," *Human Brain Mapping*, vol. 29, no. 10, pp. 1111–1122, 10 2008. [Online]. Available: http://doi.wiley.com/10.1002/hbm.20451

[99] A. Yendiki, D. N. Greve, S. Wallace, M. Vangel, J. Bockholt, B. A. Mueller, V. Magnotta, N. Andreasen, D. S. Manoach, and R. L. Gollub, "Multi-site characterization of an fMRI working memory paradigm: Reliability of activation indices," *NeuroImage*, vol. 53, no. 1, pp. 119–131, 10 2010. [Online]. Available: https://www.sciencedirect.com/science/article/pii/S1053811910006920

[100] K. H. Zou, D. N. Greve, M. Wang, S. D. Pieper, S. K. Warfield, N. S. White, S. Manandhar, G. G. Brown, M. G. Vangel, R. Kikinis, and W. M. Wells, "Reproducibility of Functional MR Imaging: Preliminary Results of Prospective Multi-institutional Study Performed by Biomedical Informatics

Research Network," *Radiology*, vol. 237, no. 3, pp. 781–789, 12 2005. [Online]. Available: http://pubs.rsna.org/doi/10.1148/radiol.2373041630

[101] S. Noble, D. Scheinost, E. S. Finn, X. Shen, X. Papademetris, S. C. McEwen, C. E. Bearden, J. Addington, B. Goodyear, K. S. Cadenhead, H. Mirzakhanian, B. A. Cornblatt, D. M. Olvet, D. H. Mathalon, T. H. McGlashan, D. O. Perkins, A. Belger, L. J. Seidman, H. Thermenos, M. T. Tsuang, T. G. van Erp, E. F. Walker, S. Hamann, S. W. Woods, T. D. Cannon, and R. T. Constable, "Multisite reliability of MR-based functional connectivity," *NeuroImage*, vol. 146, pp. 959–970, 2 2017. [Online]. Available: https://www.sciencedirect.com/science/article/pii/S1053811916305742

[102] S. Deprez, M. B. de Ruiter, S. Bogaert, R. Peeters, J. Belderbos, D. De Ruysscher, S. Schagen, S. Sunaert, P. Pullens, and E. Achten, "Multi-center reproducibility of structural, diffusion tensor, and resting state functional magnetic resonance imaging measures," *Neuroradiology*, vol. 60, no. 6, pp. 617–634, 6 2018. [Online]. Available: http://link.springer.com/10.1007/s00234-018-2017-1

[103] S. Noble, M. N. Spann, F. Tokoglu, X. Shen, R. T. Constable, and D. Scheinost, "Influences on the TestRetest Reliability of Functional Connectivity MRI and its Relationship with Behavioral Utility," *Cerebral Cortex*, vol. 27, no. 11, pp. 5415–5429, 11 2017. [Online]. Available: https://academic.oup.com/cercor/article/27/11/5415/4139668

[104] J. Jovicich, L. Minati, M. Marizzoni, R. Marchitelli, R. Sala-Llonch, D. Bartrés-Faz, J. Arnold, J. Benninghoff, U. Fiedler, L. Roccatagliata, A. Picco, F. Nobili, O. Blin, S. Bombois, R. Lopes, R. Bordet, J. Sein, J.-P. Ranjeva, M. Didic, H. Gros-Dagnac, P. Payoux, G. Zoccatelli, F. Alessandrini, A. Beltramello, N. Bargalló, A. Ferretti, M. Caulo, M. Aiello, C. Cavaliere, A. Soricelli, L. Parnetti, R. Tarducci, P. Floridi, M. Tsolaki, M. Constantinidis, A. Drevelegas, P. M. Rossini, C. Marra, P. Schönknecht, T. Hensch, K.-T. Hoffmann, J. P. Kuijer, P. J. Visser, F. Barkhof, and G. B. Frisoni, "Longitudinal reproducibility of default-mode network connectivity in healthy elderly participants: A multicentric resting-state fMRI study," *NeuroImage*, vol. 124, pp. 442–454, 1 2016. [Online]. Available: https://www.sciencedirect.com/science/article/pii/S1053811915006199

[105] R. Marchitelli, L. Minati, M. Marizzoni, B. Bosch, D. Bartrés-Faz, B. W. Müller, J. Wiltfang, U. Fiedler, L. Roccatagliata, A. Picco, F. Nobili, O. Blin, S. Bombois, R. Lopes, R. Bordet, J. Sein, J.-P. Ranjeva, M. Didic, H. Gros-Dagnac, P. Payoux, G. Zoccatelli, F. Alessandrini, A. Beltramello, N. Bargalló, A. Ferretti, M. Caulo, M. Aiello, C. Cavaliere, A. Soricelli, L. Parnetti, R. Tarducci, P. Floridi, M. Tsolaki, M. Constantinidis, A. Drevelegas, P. M. Rossini, C. Marra, P. Schönknecht, T. Hensch, K.-T. Hoffmann, J. P. Kuijer, P. J. Visser, F. Barkhof, G. B. Frisoni, and J. Jovicich, "Test-retest reliability of the default mode network in a multi-centric fMRI study of healthy elderly: Effects of data-driven physiological noise correction techniques," *Human Brain Mapping*, vol. 37, no. 6, pp. 2114–2132, 6 2016. [Online]. Available: http://doi.wiley.com/10.1002/hbm.23157

[106] L. Huang, X. Wang, M. N. Baliki, L. Wang, A. V. Apkarian, and T. B. Parrish, "Reproducibility of Structural, Resting-State BOLD and DTI Data

between Identical Scanners," *PLoS ONE*, vol. 7, no. 10, p. e47684, 10 2012. [Online]. Available: http://dx.plos.org/10.1371/journal.pone.0047684

[107] J. A. Turner, E. Damaraju, T. G. Van Erp, D. H. Mathalon, J. M. Ford, J. Voyvodic, B. A. Mueller, A. Belger, J. Bustillo, S. C. McEwen, S. G. Potkin, F. I. BIRN, and V. D. Calhoun, "A multi-site resting state fMRI study on the amplitude of low frequency fluctuations in schizophrenia," *Frontiers in Neuroscience*, vol. 7, p. 137, 8 2013. [Online]. Available: http://journal.frontiersin.org/article/10.3389/fnins.2013.00137/abstract

[108] R. A. Feis, S. M. Smith, N. Filippini, G. Douaud, E. G. P. Dopper, V. Heise, A. J. Trachtenberg, J. C. van Swieten, M. A. van Buchem, S. A. R. B. Rombouts, and C. E. Mackay, "ICA-based artifact removal diminishes scan site differences in multi-center resting-state fMRI," *Frontiers in Neuroscience*, vol. 9, p. 395, 10 2015. [Online]. Available: http://journal.frontiersin.org/Article/10.3389/fnins.2015.00395/abstract

[109] K. Jann, D. G. Gee, E. Kilroy, S. Schwab, R. X. Smith, T. D. Cannon, and D. J. Wang, "Functional connectivity in BOLD and CBF data: Similarity and reliability of resting brain networks," *NeuroImage*, vol. 106, pp. 111–122, 2 2015. [Online]. Available: https://www.sciencedirect.com/science/article/pii/S1053811914009458

[110] B. Biswal, F. Zerrin Yetkin, V. M. Haughton, and J. S. Hyde, "Functional connectivity in the motor cortex of resting human brain using echo-planar mri," *Magnetic Resonance in Medicine*, vol. 34, no. 4, pp. 537–541, 10 1995. [Online]. Available: http://doi.wiley.com/10.1002/mrm.1910340409

[111] M. D. Fox and M. E. Raichle, "Spontaneous fluctuations in brain activity observed with functional magnetic resonance imaging," *Nature Reviews Neuroscience*, vol. 8, no. 9, pp. 700–711, 9 2007. [Online]. Available: http://www.nature.com/articles/nrn2201

[112] M. D. Greicius, B. Krasnow, A. L. Reiss, and V. Menon, "Functional connectivity in the resting brain: a network analysis of the default mode hypothesis." *Proceedings of the National Academy of Sciences of the United States of America*, vol. 100, no. 1, pp. 253–8, 1 2003. [Online]. Available: http://www.ncbi.nlm.nih.gov/pubmed/12506194http://www.pubmedcentral.nih.gov/articlerender.fcgi?artid=PMC140943

[113] C. F. Beckmann, M. DeLuca, J. T. Devlin, and S. M. Smith, "Investigations into resting-state connectivity using independent component analysis." *Philosophical transactions of the Royal Society of London. Series B, Biological sciences*, vol. 360, no. 1457, pp. 1001–13, 5 2005. [Online]. Available: http://www.ncbi.nlm.nih.gov/pubmed/16087444http://www.pubmedcentral.nih.gov/articlerender.fcgi?artid=PMC1854918

[114] Z. Shehzad, A. M. C. Kelly, P. T. Reiss, D. G. Gee, K. Gotimer, L. Q. Uddin, S. H. Lee, D. S. Margulies, A. K. Roy, B. B. Biswal, E. Petkova, F. X. Castellanos, and M. P. Milham, "The Resting Brain: Unconstrained yet Reliable," *Cerebral Cortex*, vol. 19, no. 10, pp. 2209–2229, 10 2009. [Online]. Available: https://academic.oup.com/cercor/article-lookup/doi/10.1093/cercor/bhn256

[115] A. R. Mayer, M. V. Mannell, J. Ling, C. Gasparovic, and R. A. Yeo, "Functional connectivity in mild traumatic brain injury," *Human Brain Mapping*, vol. 32, no. 11, pp. 1825–1835, 11 2011. [Online]. Available: http://doi.wiley.com/10.1002/hbm.21151

[116] S. J. Broyd, C. Demanuele, S. Debener, S. K. Helps, C. J. James, and E. J. Sonuga-Barke, "Default-mode brain dysfunction in mental disorders: A systematic review," *Neuroscience & Biobehavioral Reviews*, vol. 33, no. 3, pp. 279–296, 3 2009. [Online]. Available: https://www.sciencedirect.com/science/article/pii/S0149763408001504

[117] J. A. Contreras, J. Goñi, S. L. Risacher, O. Sporns, and A. J. Saykin, "The Structural and Functional Connectome and Prediction of Risk for Cognitive Impairment in Older Adults," *Current Behavioral Neuroscience Reports*, vol. 2, no. 4, pp. 234–245, 12 2015. [Online]. Available: http://link.springer.com/10.1007/s40473-015-0056-z

[118] E. Bullmore and O. Sporns, "Complex brain networks: graph theoretical analysis of structural and functional systems," *Nature Reviews Neuroscience*, vol. 10, no. 3, pp. 186–198, 3 2009. [Online]. Available: http://www.nature.com/articles/nrn2575

[119] M. Rubinov and O. Sporns, "Complex network measures of brain connectivity: Uses and interpretations," *NeuroImage*, vol. 52, no. 3, pp. 1059–1069, 2010. [Online]. Available: http://dx.doi.org/10.1016/j.neuroimage.2009.10.003

[120] O. Sporns, "Contributions and challenges for network models in cognitive neuroscience," *Nature Neuroscience*, vol. 17, no. 5, pp. 652–660, 5 2014. [Online]. Available: http://www.nature.com/articles/nn.3690

[121] Y. He, Z. Chen, G. Gong, and A. Evans, "Neuronal networks in Alzheimer's disease," pp. 333–350, 8 2009. [Online]. Available: http://journals.sagepub.com/doi/10.1177/1073858409334423

[122] A. Fornito, A. Zalesky, and E. T. Bullmore, *Fundamentals of brain network analysis*. Academic Press, 2016. [Online]. Available: https://books.google.com/books?hl=en&lr=&id=Hc-cBAAAQBAJ&oi=fnd&pg=PP1&dq=Brain+Network+Analysis+Fornito+Zalesky+Bullmore&ots=AMzDxn2Z5b&sig=vJoHDyoBEzc-L96_YGj-Ne_C7yM#v=onepage&q=BrainNetworkAnalysisFornitoZaleskyBullmore&f=false

[123] U. Braun, M. M. Plichta, C. Esslinger, C. Sauer, L. Haddad, O. Grimm, D. Mier, S. Mohnke, A. Heinz, S. Erk, H. Walter, N. Seiferth, P. Kirsch, and A. Meyer-Lindenberg, "Testretest reliability of resting-state connectivity network characteristics using fMRI and graph theoretical measures," *NeuroImage*, vol. 59, no. 2, pp. 1404–1412, 1 2012. [Online]. Available: https://www.sciencedirect.com/science/article/pii/S105381191100961X

[124] J.-H. Wang, X.-N. Zuo, S. Gohel, M. P. Milham, B. B. Biswal, and Y. He, "Graph Theoretical Analysis of Functional Brain Networks: Test-Retest Evaluation on Short- and Long-Term Resting-State Functional MRI Data," *PLoS ONE*, vol. 6, no. 7, p. e21976, 7 2011. [Online]. Available: https://dx.plos.org/10.1371/journal.pone.0021976

[125] D. H. Schultz and M. W. Cole, "Higher Intelligence Is Associated with Less Task-Related Brain Network Reconfiguration," *The Journal of Neuroscience*, vol. 36, no. 33, pp. 8551–8561, 2016. [Online]. Available: http://www.jneurosci.org/lookup/doi/10.1523/JNEUROSCI.0358-16.2016

[126] O. Mira-Dominguez, B. D. Mills, S. D. Carpenter, K. A. Grant, C. D. Kroenke, J. T. Nigg, and D. A. Fair, "Connectotyping: Model based fingerprinting of the functional connectome," *PLoS ONE*, vol. 9, no. 11, 2014.

[127] E. S. Finn, X. Shen, D. Scheinost, M. D. Rosenberg, J. Huang, M. M. Chun, X. Papademetris, and R. T. Constable, "Functional connectome fingerprinting: Identifying individuals using patterns of brain connectivity," *Nature Neuroscience*, vol. 18, no. 11, pp. 1664–1671, 2015. [Online]. Available: http://dx.doi.org/10.1038/nn.4135

[128] E. S. Finn, D. Scheinost, D. M. Finn, X. Shen, X. Papademetris, and R. T. Constable, "Can brain state be manipulated to emphasize individual differences in functional connectivity?" *NeuroImage*, vol. 160, no. March, pp. 140–151, 2017. [Online]. Available: http://dx.doi.org/10.1016/j.neuroimage.2017.03.064

[129] E. M. Gordon, T. O. Laumann, B. Adeyemo, A. W. Gilmore, S. M. Nelson, N. U. Dosenbach, and S. E. Petersen, "Individual-specific features of brain systems identified with resting state functional correlations," *NeuroImage*, vol. 146, pp. 918–939, 2017. [Online]. Available: http://dx.doi.org/10.1016/j.neuroimage.2016.08.032

[130] L. Waller, H. Walter, J. D. Kruschwitz, L. Reuter, S. Müller, S. Erk, and I. M. Veer, "Evaluating the replicability, specificity, and generalizability of connectome fingerprints," *NeuroImage*, vol. 158, pp. 371–377, 9 2017. [Online]. Available: https://www.sciencedirect.com/science/article/pii/S1053811917305840

[131] E. M. Gordon, T. O. Laumann, A. W. Gilmore, D. J. Newbold, D. J. Greene, J. J. Berg, M. Ortega, C. Hoyt-Drazen, C. Gratton, H. Sun, J. M. Hampton, R. S. Coalson, A. L. Nguyen, K. B. McDermott, J. S. Shimony, A. Z. Snyder, B. L. Schlaggar, S. E. Petersen, S. M. Nelson, and N. U. Dosenbach, "Precision Functional Mapping of Individual Human Brains," *Neuron*, vol. 95, no. 4, pp. 791–807, 2017. [Online]. Available: http://dx.doi.org/10.1016/j.neuron.2017.07.011

[132] J. Zimmermann, J. Griffiths, M. Schirner, P. Ritter, and A. McIntosh, "Subject-Specificity of the Correlation Between Large-Scale Structural and Functional Connectivity," *Network Neuroscience*, pp. 1–35, 4 2018. [Online]. Available: https://www.mitpressjournals.org/doi/abs/10.1162/NETN_a_00055

[133] T. D. Satterthwaite, C. H. Xia, and D. S. Bassett, "Personalized Neuroscience: Common and Individual-Specific Features in Functional Brain Networks," *Neuron*, vol. 98, no. 2, pp. 243–245, 4 2018. [Online]. Available: https://www.sciencedirect.com/science/article/pii/S0896627318302915

[134] A. S. Greene, S. Gao, D. Scheinost, and R. T. Constable, "Task-induced brain state manipulation improves prediction of individual traits," *Nature Communications*, vol. 9, no. 1, p. 2807, 12 2018. [Online]. Available: http://www.nature.com/articles/s41467-018-04920-3

[135] J. Gonzalez-Castillo and P. A. Bandettini, "Task-based dynamic functional connectivity: Recent findings and open questions," *NeuroImage*, no. August, pp. 1–8, 2017. [Online]. Available: http://dx.doi.org/10.1016/j.neuroimage.2017.08.006

[136] E. Amico and J. Goñi, "The quest for identifiability in human functional connectomes," *Scientific Reports*, vol. 8, no. 1, p. 8254, 12 2018. [Online]. Available: http://www.nature.com/articles/s41598-018-25089-1

[137] V. Pallarés, A. Insabato, A. Sanjuán, S. Kühn, D. Mantini, G. Deco, and M. Gilson, "Extracting orthogonal subject- and condition-specific signatures from fMRI data using whole-brain effective connectivity," *NeuroImage*, vol. 178, pp. 238–254, 9 2018.

[138] D. O. Svaldi, J. Goñi, A. Bharthur Sanjay, E. Amico, S. L. Risacher, J. D. West, M. Dzemidzic, A. Saykin, and L. Apostolova, "Towards Subject and Diagnostic Identifiability in the Alzheimers Disease Spectrum Based on Functional Connectomes." Springer, Cham, 9 2018, pp. 74–82. [Online]. Available: http://link.springer.com/10.1007/978-3-030-00689-1_8

[139] T. Vanderwal, J. Eilbott, E. S. Finn, R. C. Craddock, A. Turnbull, and F. X. Castellanos, "Individual differences in functional connectivity during naturalistic viewing conditions," *NeuroImage*, vol. 157, pp. 521–530, 8 2017. [Online]. Available: https://www.sciencedirect.com/science/article/pii/S1053811917304962

[140] X. Shen, E. S. Finn, D. Scheinost, M. D. Rosenberg, M. M. Chun, X. Papademetris, and R. T. Constable, "Using connectome-based predictive modeling to predict individual behavior from brain connectivity," *Nature Protocols*, vol. 12, no. 3, pp. 506–518, 2 2017. [Online]. Available: http://www.nature.com/doifinder/10.1038/nprot.2016.178

[141] K. Yoo, M. D. Rosenberg, W.-T. Hsu, S. Zhang, C.-S. R. Li, D. Scheinost, R. T. Constable, and M. M. Chun, "Connectome-based predictive modeling of attention: Comparing different functional connectivity features and prediction methods across datasets," *NeuroImage*, vol. 167, pp. 11–22, 2 2018. [Online]. Available: https://www.sciencedirect.com/science/article/pii/S1053811917309175

[142] L. M. Shah, J. A. Cramer, M. A. Ferguson, R. M. Birn, and J. S. Anderson, "Reliability and reproducibility of individual differences in functional connectivity acquired during task and resting state," *Brain and Behavior*, vol. 6, no. 5, 5 2016. [Online]. Available: http://doi.wiley.com/10.1002/brb3.456

[143] E. Amico, D. Marinazzo, C. Di Perri, L. Heine, J. Annen, C. Martial, M. Dzemidzic, M. Kirsch, V. Bonhomme, S. Laureys, and J. Goñi, "Mapping the functional connectome traits of levels of consciousness," *NeuroImage*, vol. 148, pp. 201–211, 3 2017. [Online]. Available: https://www.sciencedirect.com/science/article/pii/S1053811917300204

[144] P. Coupé, J. V. Manjón, E. Gedamu, D. Arnold, M. Robles, and D. L. Collins, "Robust Rician noise estimation for MR images." *Medical image analysis*, vol. 14, no. 4, pp. 483–93, 8 2010. [Online]. Available: http://www.ncbi.nlm.nih.gov/pubmed/20417148

[145] P. Coupe, P. Yger, S. Prima, P. Hellier, C. Kervrann, and C. Barillot, "An Optimized Blockwise Nonlocal Means Denoising Filter for 3-D Magnetic Resonance Images," *IEEE Transactions on Medical Imaging*, vol. 27, no. 4, pp. 425–441, 4 2008. [Online]. Available: http://ieeexplore.ieee.org/document/4359947/

[146] N. Wiest-Daesslé, S. Prima, P. Coupé, S. P. Morrissey, and C. Barillot, "Rician Noise Removal by Non-Local Means Filtering for Low Signal-to-Noise Ratio MRI: Applications to DT-MRI." Springer, Berlin, Heidelberg, 2008, pp. 171–179. [Online]. Available: http://link.springer.com/10.1007/978-3-540-85990-1_21

[147] T. B. Jones, P. A. Bandettini, L. Kenworthy, L. K. Case, S. C. Milleville, A. Martin, and R. M. Birn, "Sources of group differences in functional connectivity: An investigation applied to autism spectrum disorder," *NeuroImage*, vol. 49, no. 1, pp. 401–414, 1 2010. [Online]. Available: https://www.sciencedirect.com/science/article/pii/S1053811909008416

[148] J. D. Power, K. A. Barnes, A. Z. Snyder, B. L. Schlaggar, and S. E. Petersen, "Spurious but systematic correlations in functional connectivity MRI networks arise from subject motion," *NeuroImage*, vol. 59, no. 3, pp. 2142–2154, 2 2012. [Online]. Available: https://www.sciencedirect.com/science/article/pii/S1053811911011815

[149] J. D. Power, A. Mitra, T. O. Laumann, A. Z. Snyder, B. L. Schlaggar, and S. E. Petersen, "Methods to detect, characterize, and remove motion artifact in resting state fMRI," *NeuroImage*, vol. 84, pp. 320–341, 1 2014. [Online]. Available: https://www.sciencedirect.com/science/article/pii/S1053811913009117

[150] H. J. Jo, Z. S. Saad, W. K. Simmons, L. A. Milbury, and R. W. Cox, "Mapping sources of correlation in resting state FMRI, with artifact detection and removal." *NeuroImage*, vol. 52, no. 2, pp. 571–82, 8 2010. [Online]. Available: http://www.ncbi.nlm.nih.gov/pubmed/20420926http://www.pubmedcentral.nih.gov/articlerender.fcgi?artid=PMC2897154

[151] X. Shen, F. Tokoglu, X. Papademetris, and R. T. Constable, "Groupwise whole-brain parcellation from resting-state fMRI data for network node identification," *NeuroImage*, vol. 82, pp. 403–415, 2013. [Online]. Available: https://ac.els-cdn.com/S1053811913005818/1-s2.0-S1053811913005818-main.pdf?_tid=ae5a71b2-cb19-11e7-8e37-00000aacb362&acdnat=1510869862_99b0ab31b7cdafb9151e03e618315d12

[152] B. T. Thomas Yeo, F. M. Krienen, J. Sepulcre, M. R. Sabuncu, D. Lashkari, M. Hollinshead, J. L. Roffman, J. W. Smoller, L. Zöllei, J. R. Polimeni, B. Fischl, H. Liu, and R. L. Buckner, "The organization of the human cerebral cortex estimated by intrinsic functional connectivity," *Journal of Neurophysiology*, vol. 106, no. 3, pp. 1125–1165, 9 2011. [Online]. Available: http://www.physiology.org/doi/10.1152/jn.00338.2011

[153] R. c. Team, "R: A Language and Environment for Statistical Computing," 2013. [Online]. Available: http://www.r-project.org/

[154] P. E. Shrout and J. L. Fleiss, "Intraclass correlations: Uses in assessing rater reliability." *Psychological Bulletin*, vol. 86, no. 2, pp. 420–428, 1979. [Online]. Available: http://doi.apa.org/getdoi.cfm?doi=10.1037/0033-2909.86.2.420

[155] K. O. McGraw and S. P. Wong, "Forming inferences about some intraclass correlation coefficients." *Psychological Methods*, vol. 1, no. 1, pp. 30–46, 1996. [Online]. Available: http://doi.apa.org/getdoi.cfm?doi=10.1037/1082-989X.1.1.30

[156] B. T. Yeo, F. M. Krienen, J. Sepulcre, M. R. Sabuncu, D. Lashkari, M. Hollinshead, J. L. Roffman, J. W. Smoller, L. Zollei, J. R. Polimeni, B. Fischl, H. Liu, and R. L. Buckner, "The organization of the human cerebral cortex estimated by intrinsic functional connectivity," *Journal of neurophysiology*, vol. 106, pp. 1125–1165, 2011. [Online]. Available: http://jn.physiology.org/content/106/3/1125.short

[157] R. B. Mars, R. E. Passingham, and S. Jbabdi, "Connectivity Fingerprints: From Areal Descriptions to Abstract Spaces," *Trends in Cognitive Sciences*, vol. 22, no. 11, pp. 1026–1037, 11 2018. [Online]. Available: https://www.sciencedirect.com/science/article/pii/S1364661318302092

[158] C. Sripada, M. Angstadt, S. Rutherford, D. Kessler, Y. Kim, M. Yee, and E. Levina, "Basic Units of Inter-Individual Variation in Resting State Connectomes," *Scientific Reports*, vol. 9, no. 1, p. 1900, 12 2019.

[159] J. Beckman, S. Bari, Y. Chen, M. Dark, and B. Yang, "The Impacts of Representational Fluency on Cognitive Processing of Cryptography Concepts," Tech. Rep. [Online]. Available: https://www.usenix.org/system/files/conference/laser2017/laser2017_beckman.pdf

[160] A. Pierce, "Exploring the Cybersecurity Hiring Gap," Ph.D. dissertation, 1 2016. [Online]. Available: https://scholarworks.waldenu.edu/dissertations/3198

[161] D. C. Rowe, B. M. Lunt, and J. J. Ekstrom, "The role of cybersecurity in information technology education," in *Proceedings of the 2011 conference on Information technology education - SIGITE '11*. New York, New York, USA: ACM Press, 2011, p. 113. [Online]. Available: http://dl.acm.org/citation.cfm?doid=2047594.2047628

[162] M. Suby and F. Dickson, "2015 (ISC)2 global information workforce study," Tech. Rep., 2015. [Online]. Available: http://www.boozallen.com/insights/2015/04/2015-isc2-global-information-workforce-study

[163] M. Suby, "50 Years of Growth, Innovation and Leadership The 2013 (ISC) 2 Global Information Security Workforce Study," *Frost & Sullivan in partnership with Booz Allen Hamilton for ISC2*, 2013. [Online]. Available: https://iamcybersafe.org/wp-content/uploads/2017/01/2013-ISC2-Global-Information-Security-Workforce-Study.pdf

[164] D. L. Burley and D. L., "Cybersecurity education, part 1," *ACM Inroads*, vol. 5, no. 1, pp. 41–41, 3 2014. [Online]. Available: http://dl.acm.org/citation.cfm?doid=2568195.2568210

[165] K. Evans and F. Reeder, *A human capital crisis in cybersecurity: Technical proficiency matters*, 2010. [Online]. Available: https://books.google.com/books?hl=en&lr=&id=zsGHmE1oi1cC&oi=fnd&pg=PR5&dq=A+Human+Capital+Crisis+in+Cybersecurity:+Technical+Proficiency+Matters.&ots=tDF-LeBoCl&sig=j1K82iL5YYKGLEPjhKY7_1UoNag

[166] A. McGettrick, L. N. Cassel, M. Dark, E. K. Hawthorne, and J. Impagliazzo, "Toward curricular guidelines for cybersecurity," in *Proceedings of the 45th ACM technical symposium on Computer science education - SIGCSE '14*. New York, New York, USA: ACM Press, 2014, pp. 81–82. [Online]. Available: http://dl.acm.org/citation.cfm?doid=2538862.2538990

[167] F. B. Schneider, "Cybersecurity Education in Universities," *IEEE Security & Privacy*, vol. 11, no. 4, pp. 3–4, 7 2013. [Online]. Available: http://ieeexplore.ieee.org/document/6573305/

[168] W. Wei, A. Mann, K. Sha, and T. A. Yang, "Design and implementation of a multi-facet hierarchical cybersecurity education framework," in *2016 IEEE Conference on Intelligence and Security Informatics (ISI)*. IEEE, 9 2016, pp. 273–278. [Online]. Available: http://ieeexplore.ieee.org/document/7745488/

[169] R. S. Cheung and H. Z. Lo, "Challenge Based Learning in Cybersecurity Education," Tech. Rep. [Online]. Available: http://worldcomp-proceedings.com/proc/p2011/SAM5063.pdf

[170] W. Wei, A. Mann, K. Sha, and T. A. Yang, "Design and implementation of a multi-facet hierarchical cybersecurity education framework," in *2016 IEEE Conference on Intelligence and Security Informatics (ISI)*. IEEE, 9 2016, pp. 273–278. [Online]. Available: http://ieeexplore.ieee.org/document/7745488/

[171] A. Sherman, M. Dark, A. Chan, R. Chong, T. Morris, L. Oliva, J. Springer, B. Thuraisingham, C. Vatcher, R. Verma, and S. Wetzel, "INSuRE: Collaborating Centers of Academic Excellence Engage Students in Cybersecurity Research," *IEEE Security & Privacy*, vol. 15, no. 4, pp. 72–78, 2017. [Online]. Available: http://ieeexplore.ieee.org/document/8012344/

[172] J. Piaget, "Part I: Cognitive development in children: Piaget development and learning," *Journal of Research in Science Teaching*, vol. 2, no. 3, pp. 176–186, 9 1964. [Online]. Available: http://doi.wiley.com/10.1002/tea.3660020306

[173] T. J. Moore, R. L. Miller, R. A. Lesh, M. S. Stohlmann, and Y. R. Kim, "Modeling in Engineering: The Role of Representational Fluency in Students' Conceptual Understanding," *Journal of Engineering Education*, vol. 102, no. 1, pp. 141–178, 1 2013. [Online]. Available: http://doi.wiley.com/10.1002/jee.20004

[174] D. Ausubel, J. Novak, and H. Hanesian, *Educational psychology: A cognitive view*, 1968. [Online]. Available: http://www.spbkbd.com/english/art_english/art_51_030211.pdf

[175] J. Bransford, A. Brown, and R. Cocking, *How people learn*, 2000. [Online]. Available: http://csun.edu/~SB4310/HowPeopleLearn.pdf

[176] G. Özdemir and D. B. Clark, "An Overview of Conceptual Change Theories," *Eurasia Journal of Mathematics, Science and Technology Education*, vol. 3, no. 4, pp. 351–361, 2007. [Online]. Available: https://s3.amazonaws.com/academia.edu.documents/42088543/EJMSTE_v3n4_Ozdemir_Clark.pdf?AWSAccessKeyId=AKIAIWOWYYGZ2Y53UL3A&Expires=1553715158&Signature=eovX6bT0q1AQrlOjK8D4Z8BcsvE%3D&response-content-disposition=inline%3Bfilename%3DAn_Overview_of_Concept

[177] L. Hsu, E. Brewe, T. M. Foster, and K. A. Harper, "Resource Letter RPS-1: Research in problem solving," *American Journal of Physics*, vol. 72, no. 9, pp. 1147–1156, 9 2004. [Online]. Available: http://aapt.scitation.org/doi/10.1119/1.1763175

[178] R. J. Spiro, P. J. Feltovich, M. J. Jacobson, R. L. Coulson, P. J. Feltovich, M. J. Jacobson, and R. L. Coulson, "Cognitive Flexibility, Constructivism, and Hypertext: Random Access Instruction for Advanced Knowledge Acquisition in Ill-Structured Domains," pp. 103–126, 10 2012. [Online]. Available: https://www.taylorfrancis.com/books/e/9781136476013/chapters/10.4324/9780203052600-11

[179] M. Dark, *A models and modeling perspective on skills for the high performance workplace*, 2003. [Online]. Available: https://scholar.google.com/scholar?hl=en&as_sdt=0%2C15&q=A+models+and+modeling+perspective+on+skills+for+the+high+performance+workplace.&btnG=

[180] D. Szűcs and U. Goswami, "Educational Neuroscience: Defining a New Discipline for the Study of Mental Representations," *Mind, Brain, and Education*, vol. 1, no. 3, pp. 114–127, 9 2007. [Online]. Available: http://doi.wiley.com/10.1111/j.1751-228X.2007.00012.x

[181] T. Rickard, S. Romero, G. Basso, C. Wharton, S. Flitman, and J. Grafman, "The calculating brain: an fMRI study," *Neuropsychologia*, vol. 38, no. 3, pp. 325–335, 3 2000. [Online]. Available: https://www.sciencedirect.com/science/article/pii/S0028393299000688

[182] M. Delazer, F. Domahs, L. Bartha, C. Brenneis, A. Lochy, T. Trieb, and T. Benke, "Learning complex arithmetican fMRI study," *Cognitive Brain Research*, vol. 18, no. 1, pp. 76–88, 12 2003. [Online]. Available: https://www.sciencedirect.com/science/article/pii/S0926641003002155

[183] M. O. J. Thomas, A. J. Wilson, M. C. Corballis, V. K. Lim, and C. Yoon, "Evidence from cognitive neuroscience for the role of graphical and algebraic representations in understanding function," *ZDM*, vol. 42, no. 6, pp. 607–619, 10 2010. [Online]. Available: http://link.springer.com/10.1007/s11858-010-0272-7

APPENDICES

A. HAE AND MRS EVALUATION

Table A.1.: Percentage of data points excluded for each of the two regions of interest (ROIs) in the male and female CSA pools, based on CRLB criteria, insufficient voxel overlap and missed imaging sessions.

CSA Group	ROI	Metabolite	Sessions				
			Pre	In1	In2	Post1	Post2
Male	DLPFC	Ins	8.51	23.40	21.28	17.02	29.79
		tNAA	6.38	21.28	17.02	14.89	29.79
		tCho	6.38	19.15	17.02	14.89	27.66
		tCr	6.38	19.15	17.02	14.89	27.66
		Glx	6.38	19.15	17.02	14.89	27.66
	M1	Ins	14.89	6.38	10.64	17.02	25.33
		tNAA	14.89	6.38	10.64	19.15	21.28
		tCho	14.89	6.38	10.64	12.77	23.40
		tCr	14.89	6.38	10.64	12.77	21.28
		Glx	14.89	6.38	10.64	12.77	21.28
Female	DLPFC	Ins	6.90	6.90	17.24	10.34	13.79
		tNAA	6.90	6.90	17.24	10.34	13.79
		tCho	6.90	6.90	13.79	10.34	10.34
		tCr	6.90	6.90	13.79	10.34	13.79
		Glx	6.90	6.90	13.79	10.34	13.79
	M1	Ins	3.45	10.34	17.24	6.90	20.69
		tNAA	3.45	10.34	10.34	6.90	17.24
		tCho	0.00	6.90	6.90	6.90	17.24
		tCr	3.45	6.90	6.90	6.90	17.24
		Glx	3.45	6.90	10.34	6.90	17.24

Table A.2.: The 25^{th}, 50^{th}, 75^{th} and 90^{th} percentiles of PTA (g) of all HAE that exceeded 10g.

	25^{th} Percentile	50^{th} Percentile	75^{th} Percentile	90^{th} Percentile
Male CSA (football)	25.1	33.0	47.0	67.0
Female CSA (Soccer)	23.9	30.0	43.3	62.2

Table A.3.: Median $cPTA_{Th,j,i}$ for male and female CSA at Th = 20g, 50g and 70g and *j-th* session = *In1-2*, *Post1*.

Session	In1			In2			Post1		
Th (g)	20	50	70	20	50	70	20	50	70
Male CSA	2639.0	939.9	561.6	7624.0	2929.0	1303.0	12770.0	5169.0	2262.0
Female CSA	1492.0	396.4	168.30	3273.0	1333.0	721.0	4137.0	1707.0	758.7

Table A.4.: Median $aPTA_{Th,j,i}$ for male and female CSA at Th = 20g, 50g and 70g and *j-th* session = *In1-2*, *Post1*.

Session	In1			In2			Post1		
Th	20	50	70	20	50	70	20	50	70
Male CSA	41.12	70.40	90.69	39.07	70.58	90.61	38.95	71.02	91.03
Female CSA	35.17	67.19	84.11	36.30	69.60	85.29	36.18	68.72	88.37

Table A.5.: Wilcoxon signed rank test statistic W and (p_{FDR}) assessing the across-session stability for each metabolite concentration, in each of two regions of interest (ROIs) in the male and female NCA pools.

Population	ROI	Metabolite-Concentration				
		Ins	tNAA	tCho	tCr	Glx
Male NCA	DLPFC	69 (0.447)	68 (0.447)	69 (0.447)	60 (0.670)	36 (0.447)
	M1	58 (0.951)	80 (0.453)	54 (0.951)	46 (0.951)	45 (0.951)
Female NCA	DLPFC	52 (0.566)	39 (1.000)	34 (0.917)	54 (0.566)	57 (0.566)
	M1	65 (0.106)	65 (0.106)	57 (0.220)	51 (0.380)	62 (0.129)

Table A.6.: Wilcoxon signed rank test statistic W and (p_{FDR}) assessing the across-session stability for each metabolite concentration ratio to [tCr], in each of two regions of interest (ROIs) in the male and female NCA pools.

Population	ROI	[Metabolite]-Ratio of Concentration to [tCr]			
		Ins	tNAA	tCho	Glx
Male NCA	DLPFC	58 (0.808)	57 (0.808)	46 (0.808)	37 (0.808)
	M1	59 (0.903)	75 (0.690)	67 (0.782)	55 (0.903)
Female NCA	DLPFC	44 (0.733)	25 (0.602)	17 (0.369)	44 (0.733)
	M1	55 (0.235)	59 (0.235)	45 (0.677)	69 (0.064)

Table A.7.: Friedman χ^2 score (p-value) assessing the presence of a dependence on session for each metabolite concentration, in each of two regions of interest (ROIs) in the male and female CSA pools. Metabolites exhibiting significant dependence on session within the given CSA pool and ROI are marked in bold.

Population	ROI	Metabolite-Concentration				
		Ins	tNAA	tCho	tCr	Glx
Male CSA	DLPFC	5.23 (0.264)	4.10 (0.392)	4.15 (0.385)	9.14 (0.058)	**9.6 (0.047)**
	M1	2.88 (0.578)	2.98 (0.561)	2.89 (0.576)	3.15 (0.533)	2.74 (0.602)
Female CSA	DLPFC	1.26 (0.738)	3.41 (0.332)	3.99 (0.262)	3.91 (0.271)	2.71 (0.439)
	M1	4.24 (0.237)	0.02 (0.999)	2.54 (0.467)	3.00 (0.392)	**11.03(0.009**

Table A.8.: Friedman χ^2 score (p-value) assessing the presence of a dependence on session for each metabolite concentration ratio to [tCr], in each of two regions of interest (ROIs) in the male and female CSA pools. Metabolite ratios exhibiting significant dependence on session within the given CSA pool and ROI are marked in bold.

Population	ROI	[Metabolite]-Ratio of Concentration to [tCr]			
		Ins	tNAA	tCho	Glx
Male CSA	DLPFC	1.48 (0.83)	3.26 (0.54)	**15.01 (0.0046)**	4.39 (0.356)
	M1	2.93 (0.57)	1.5 (0.827)	2.33 (0.675)	1.02 (0.91)
Female CSA	DLPFC	1.68 (0.642)	5.40 (0.145)	2.05 (0.562)	2.21 (0.529)
	M1	2.34 (0.505)	1.26 (0.738)	1.10 (0.778)	**10.99 (0.012)**

B. IDENTIFIABILITY RESULTS FOR YALE DATASET

Fig. B.1.: ***Purdue dataset.*** Averaged (100 iterations) intra-class correlation coefficient (ICC) values, computed for each FC edge, for the original (Orig) and reconstructed (Recon) on the *Training* and *Validation* sets, for resting-state functional connectomes without global signal regression (*NoGSR*; (A) and (B)) and with global signal regression (*GSR*; (C) and (D)). Edges are arranged by Yeo's resting-state functional networks [156]. As before, notable benefit is observed for the reconstruction to enhance identifiability, independent of the exclusion/inclusion of global signal regression.

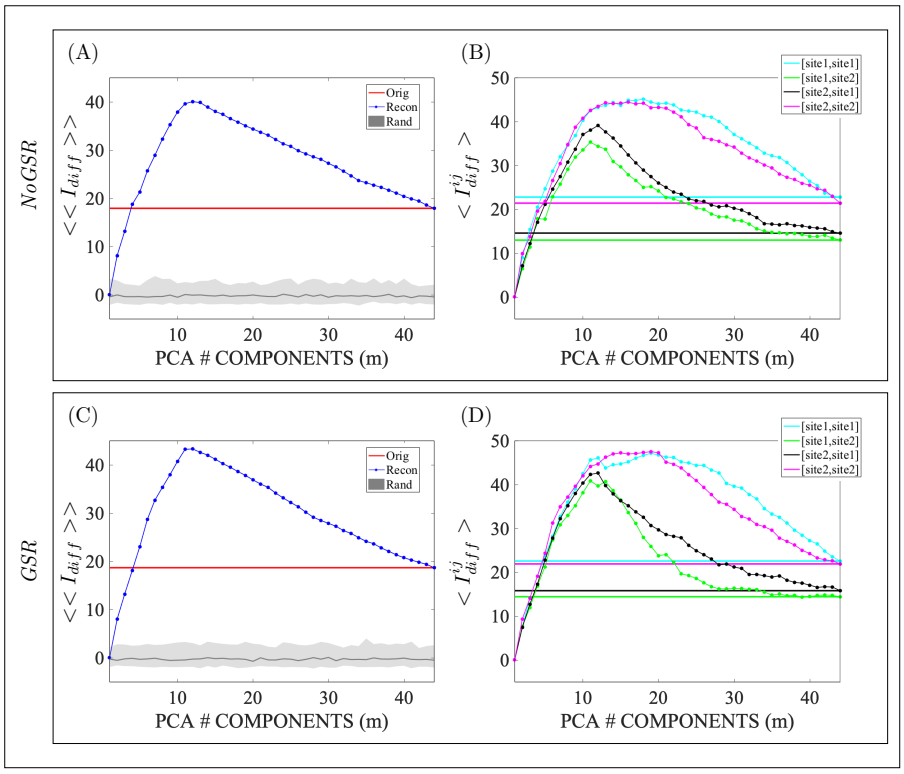

Fig. B.2.: Yale dataset. Multi-site differential identifiability ($<< I_{diff} >> *100$) and differential identifiability of each [site$i$, site$j$] pair, ($< I^{ij}_{diff} > *100$) for training data as a function of the number of principal components (PCs) used for reconstruction for resting-state data without global signal regression (*NoGSR*; (A) and (B)); and with global signal regression (*GSR*; (C) and (D)). In all figures solid lines denote $<< I_{diff} >>$ and $< I^{ij}_{diff} >$ as computed from the original FCs, whereas lines with circles denote the differential identifiability for reconstructed FCs as a function of **m**, the included number of components. In (A) and (C), the gray (shaded) area denotes the 95% confidence interval for $<< I_{diff} >>$ over 100 random permutations of the test-retest FC pairs at each value of **m**. It may be observed that the benefit of reconstruction on differential identifiability was not dependent on the exclusion/inclusion of global signal regression.

Table B.1.: Yale dataset. Maximum percentage differential identifiability ($< I^{ij*}_{diff} > *100$), explained variance (R^2) and number of principal components for each [site$i$, site$j$] pair (m^{ij*}) for Training datasets without global signal regression ($NoGSR$) and with global signal regression (GSR).

	[site$i$, site$j$]	$< I^{ij*}_{diff} >$	m^{ij*}	R^2
$NoGSR$	[site1, site1]	45.1	18	0.75
	[site1, site2]	35.3	11	0.63
	[site2, site1]	39.1	12	0.65
	[site2, site2]	44.4	16	0.72
GSR	[site1, site1]	47.1	19	0.76
	[site1, site2]	40.9	11	0.64
	[site2, site1]	42.6	12	0.66
	[site2, site2]	47.5	19	0.76

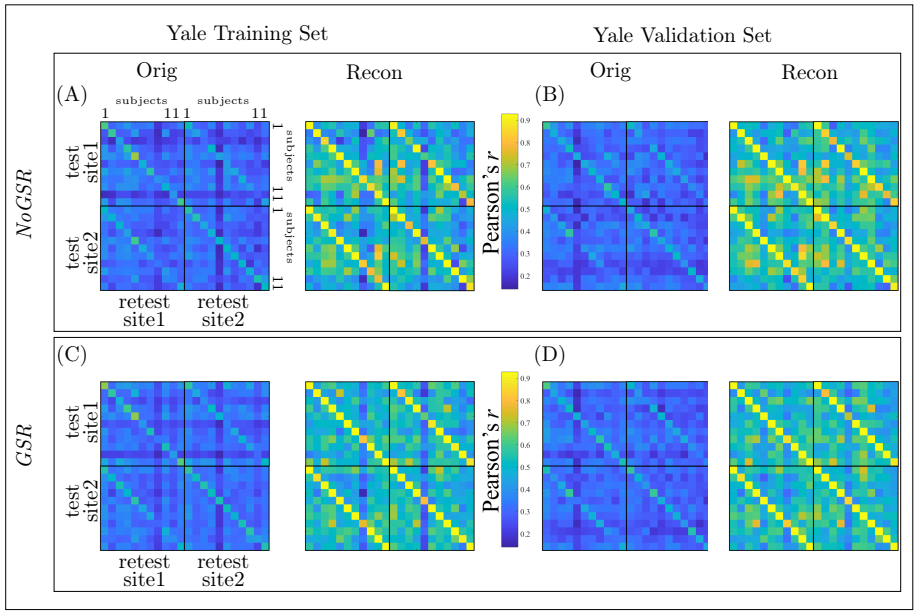

Fig. B.3.: Yale dataset. Identifiability matrices (**I**) of the original (Orig) and reconstructed (Recon) data for the *Training*, (A) and (C), and *Validation*, (B) and (D) sets of resting-state functional connectomes without global signal regression (*NoGSR*; (A) and (B)) and with global signal regression (*GSR*; (C) and (D)). The Identifiability matrix (**I**) has a blockwise structure where each block is I^{ij}, representing the identifiability for the [site$i$, site$j$] pair. Note that identifiability was meaningfully improved across sites regardless of the exclusion/inclusion of global signal regression.

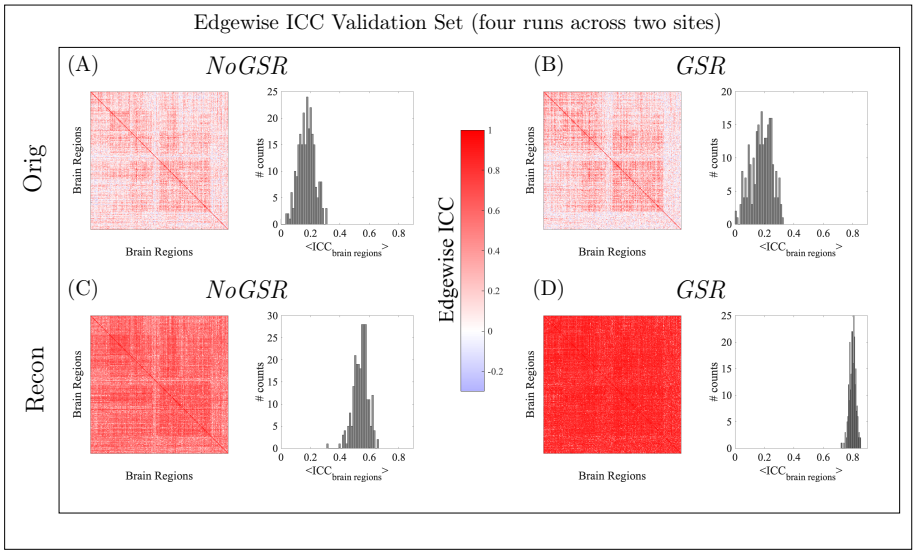

Fig. B.4.: Yale dataset. Averaged (100 iterations; see Methods for bootstrap details) intra-class correlation coefficient (ICC) values, computed for each FC edge from four visits across two sites, for the *Validation* set original (Orig; (A) and (B)) and reconstructed (Recon; (C) and (D)) data without global signal regression (*NoGSR*; (A) and (C)) and with global signal regression (*GSR*; (B) and (D)). Note that the benefit from reconstruction to enhance identifiability is, again, not dependent on exclusion/inclusion of global signal regression.

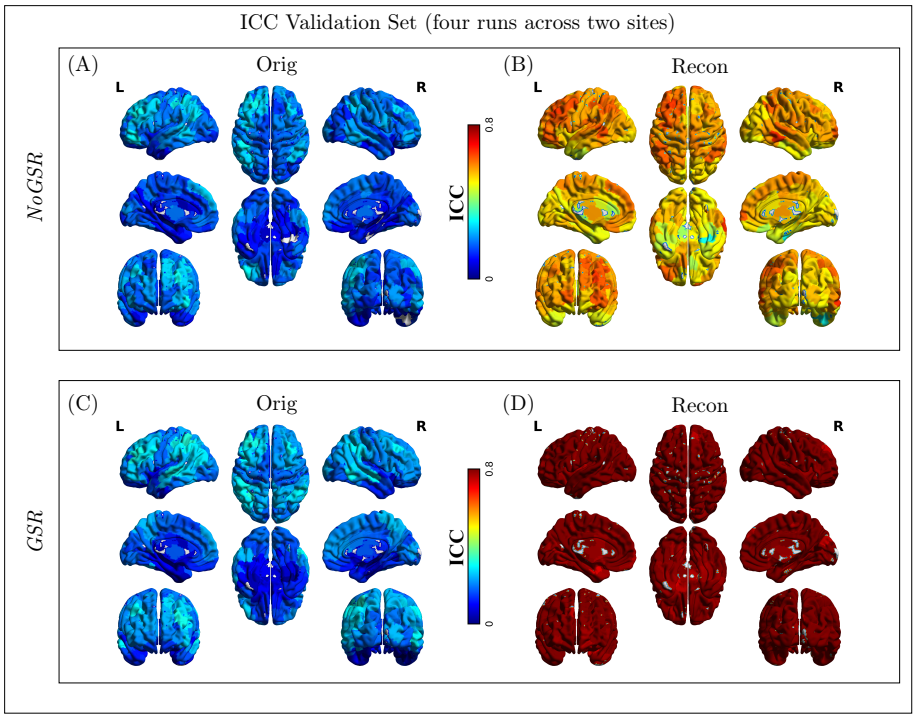

Fig. B.5.: Yale dataset. Brain rendering of intraclass correlation coefficient (ICC), computed from all four visits across the two sites for the *Validation* set original (Orig; (A) and (C)) and reconstructed (Recon; (B) and (D)) data without global signal regression (*NoGSR*; (A) and (B)) and with global signal regression (*GSR*; (C) and (D)). The strength per brain region—computed as the mean of edgewise ICC values (ICC computed for each FC edge and averaged over 100 iterations; see Methods for Bootstrap procedure)—provides an assessment of overall reproducibility of the functional connections of each brain region. FC reproducibility was appreciably improved, regardless of exclusion/inclusion of global signal regression.

C. THE IMPACTS OF REPRESENTATIONAL FLUENCY ON COGNITIVE PROCESSING OF CRYPTOGRAPHY CONCEPTS

The material presented in this chapter is published in [159].

C.1 Introduction

Cybersecurity is considered a top priority by the US government to defend its virtual borders. A shortage of qualified IT security professionals has long been a problem nationally and internationally [160–162]. Furthermore, the workforce shortfall is widening. According to a 2015 workforce study, 62% of respondents stated that their organizations have too few information security professionals compared to the 56% in 2013 [163].

Cybersecurity education has been and continues to be a primary focus for fortifying the workforce. The implications are many and include: the need for more students to become aware of and interested in cybersecurity; the need for a higher proportion of the students who are interested in cybersecurity to convert to a declared cybersecurity major in college; and the need to retain students in that major to boost graduation numbers so that more enter the workforce. However, quantity is not the only challenge in cybersecurity workforce development. It is equally, if not more, important that the work-force have the breadth and depth of skills needed to perform in the workforce. Cybersecurity education needs breadth that covers both technical and nontechnical skills spanning computer science, computer engineering, information systems, psychology, business and management, and many other related disciplines [164]. According to [165] we have a shortage of the highly technically skilled people required to operate and support systems we have already deployed, we

also face an even more desperate shortage of people who can design secure systems, write safe computer code, and create the ever more sophisticated tools needed to prevent, detect, mitigate, and reconstitute systems after an attack. [166] and [167] also emphasize that cybersecurity experts need deep technical skills coupled with capabilities to recognize and respond to complex and emergent behavior, mastery in using abstractions and principles, assessing risk and handling uncertainty, problem-solving, and reasoning; coupled with facility in adversarial thinking.

It is a challenge to educate cybersecruity graduates to assure that they: 1) have broad and deep technical skills, 2) are facile in abstraction, problem-solving, reasoning, and adversarial thinking, and 3) able to learn and perform in this complex and emergent domain. Teaching cyberscurity requires the educator to present the abstract concept to students in a crystal clear way, and to extend the abstract concept to practice to let the students learn the knowledge in context.

Given the newness of the field, cybersecuritys pedagogical best practices have not yet been adequately investigated [168]. In the past 10-15 years, articles focused on teaching practice have increased. For example, [169] discuss challenge based learning methodology to improve learning via a multi-disciplinary approach which encourages students to collaborate with their peers, ask questions, develop a deeper understanding of the subject and take actions in solving real-world challenges. Wei et.al proposed a multi-faceted hierarchical education framework to teach cybersecurity with the desired level of breath and depth [170]. [171] present a unique teaching collaborative among 13 universities that intends to teach students agile research and development skills in cyberecurity. While there has been considerable growth in the investigation and reporting on cybersecurity teaching, we find that there is little to no substantive work on cybersecurity learning and thinking.

This work is grounded in cognitive theory and investigates students mental models in one knowledge area of cybersecurity, i.e., cryptography. We developed Model-Eliciting Activities (MEAs), investigated students representational fluency and the relationship of students development of schema and changes in their cognitive process-

ing and control when encountering cryptography concepts. In this paper, we report on studentsmental models using functional magnetic resonnance imaging (fMRI) analysis of students brain activities while solving complex security problems, as well as learning data from classroom tests.

C.2 Literature Review

The Importance of Conceptual Understanding of Cryptography in Cybersecurity

Cryptography is an important subject in cybersecurity. And while cryptography is important for everyone in the field to understand, it can be an especially challenging subject to learn. The domain includes several key concepts, such as symmetric key cryptography, asymmetric key cryptography, types of ciphers, cryptanalysis and attacks, hashing, digital signatures, etc. Each of these concepts is comprised of sub concepts, which build with other sub concepts to form conceptual understanding of a key concept. Furthermore, the conceptual understanding of these concepts and sub concepts requires mathematical, language, and analytic thinking. Both breadth and depth of cryptography knowledge must be considered.

Conceptual understanding is defined as the abstract mental representation of given phenomena. Conceptual understanding occurs in the mind and the mind continuously (re)forms mental representations. The veracity of learners conceptual understanding is the fidelity of the conceptual understanding to the external world. If conceptual understanding matters, then conceptual learning is where we need to start.

Cognitive Theory, Conceptual Learning and Measurement Thereof

Cognitive theories of conceptual learning are grounded in Piagets work on logical mental frameworks (also called schemas and mental models) as structures in the brain that organize information and interactions among information. Interacting with new information, according to Piaget, modifies these schema, which is learning [172]. Conceptual learning is the acquisition of information about concepts and their

interactions, and the ongoing modification about the body of conceptual knowledge as new concepts and their interactions are encountered [173].

Correct categorization involves making links to prior knowledge and so may require adjustment or correction of prior knowledge. Ausubels assimilation theory contrasts rote learning (temporary acquisition of disorganized or poorly understood isolated or arbitrarily related concepts) with meaningful learning (long-term acquisition of organized, interrelated concepts into existing cognitive structures) [174]. Conceptual learning is the process of identifying and correctly categorizing concepts such that they can later be used to make predictions or decisions [175, 176].

The study [173] have shown that providing learners with instruction in representational fluency can build conceptual understanding. Representations are the different forms in which a concept, principle, or phenomenon can be expressed and communicated. Common representations include graphic, pictorial, verbal, mathematical, and concrete. Each representation presents the phenomenon it is in-tended to describe in a different mode. Deep(er) under-standing of the given concept requires understanding of and among various representations. Beyond comprehending representations, even deeper understanding means being fluent in shifting back and forth among the variety of relevant representations.

The concept of fluency is often associated with the ability to express oneself in the spoken and written word, and to move effortlessly (automatically) between the two representations. A person who is fluent in a language has this ability; they can translate from English to Chinese and back, and from written to spoken word and back (where written may be in English and spoken in Chinese).

The idea of fluency has been extended to other fields such as physics, chemistry, engineering, and mathematics. For example, a study [177] on experts and novices found that physics problem solvers who are fluent in their use of different representations can easily translate between them, and can assess the usefulness of a particular representation in different situations. Similarly, [178] found that when learners develop

multiple representations they are better able to transfer knowledge to new domains with increased cognitive flexibility.

Representational fluency in the STEM fields can include: a) visualizing and conceptualizing transformation processes abstractly; b) understanding systems that do not exhibit any physical manifestations of their functions; c) transforming physical sensory data to symbolic representations and vice versa; d) quantifying qualitative data, e) qualifying quantitative data; f) working with patterns; g) working with continuously changing qualities and trends; and h) transferring principles appropriately from one situation to the next [179]. Regardless what the transformation, representational fluency connotes continuous adaptation and flexibility of the conceptual model, and the ability to perform with facility, adeptness, and expertise. Representational fluency is an important aspect of deep conceptual understanding that has been shown to promote transfer of learning and the development of expertise.

The authors in [180] advocate for the role of neuroscience in the study of mental models. The mental frameworks theorized by [172] would require activity in the brain. As learners mental schema change to incorporate new information derived from experiences, brain function in the learners brains changes. That is, learning changes the structures of the brain.

Advances in neuroscience offer researchers new tools, such as fMRI, to measure brain activity. To date, fMRI has been used in studies of cognitive processing of mathematics. The study [181] sought to understand what areas of the brain are involved in mathematical computation while [182] built on [181] by using fMRI to measure changes in cognitive processing after instructing students in multiplication in one and two digit numbers. These studies are examples of how neuroscience is being used to understand cognitive processing, so that later it can be applied to evaluate the impacts of instruction on learning.

Our study seeks to understand where cryptography is processed in the brain as a basis for understanding what instructional methods maximize cryptography learning in students.

C.3 Methods

C.3.1 Research Questions

This exploratory study first investigated where in the brain cryptography is processed. Second, we investigated the impact of representational form on cognitive processing. More specifically, we investigated whether cognitive processing increased when students were asked to translate cryptography concepts between representational forms (language to math, math to graphical, etc.) in comparison to cognitive processing of concepts using the same representational form (language to language, math to math, etc.). Third we investigated whether teaching cryptography using multiple representations changed how and/or where cryptography concepts were processed in the brain in comparison to instruction that was not focused on generating representational fluency.

The research team used fMRI scans of students to answer the research questions. In order to investigate impact of teaching using multiple representations, learners were taught five cryptography topics using multiple representations, and four topics were taught using single representations to convey concepts. Data gathered from learners classroom performance were used in support of the fMRI analysis, as discussed below.

C.3.2 fMRI Component

Variables and Operationalization

Independent Variables

As a descriptive question, determining where cryptography concepts are processed in the brain did not have an independent variable. When considering whether translation between representational forms in the context of cryptography impacted cognitive processing, the research team defined a binary variable, Representational Translation. Either the students had to make a translation be-tween representations, or they did not. We implemented this variable as questions that the students were asked to an-

swer while under fMRI scanning. Students were required to make a Representational Translation when, as shown in Figure 1, Representation 1 and Representation 2 were presented in different representational forms.

Questions asked of students during fMRI were generated from material that was taught using both the representational fluency-focused instructional method, as well as the method that did not focus on the use of multiple representations in instruction. Instructional Method was defined as the independent variable in terms of our third research question regarding the impact of instruction focused on representational fluency on cognitive processing of cryptography concepts.

Dependent Variables

For our research questions, the dependent variable was Cognitive Processing of Cryptography Concepts, which illustrates where in the brain and with what intensity cryptography is processed. The variable was analyzed in different ways based on the question asked, but was implemented by comparing different periods of activity in the fMRI scan based on the question being considered against brain activity measured as the subject observed the crosshair pattern following each question as shown in Figure 1.

Population and Sample

Nine out of the 12 students from a graduate-level, semester-long network security course participated in fMRI scans.

MRI Acquisitions

Scans were administrated at the University MRI Facility using 3T GE Discovery MR750 and a 32-channel brain array (Nova Medical). Scans consisted of a high-resolution (1mm isotropic) T_1 weighted anatomical scan for registration and tissue segmentation purposes and six functional scans (TR/TE = 1500/28msec; flip angle = 72°; 35 slices at 3.5mm; field of view (FOV)= 24 cm and matrix = 64x64). Each functional run focused on one topic and consisted of nine yes/no matching questions (nine blocks) using three different representational forms. The functional runs were presented in random order. The subjects were able to see the questions inside

the scanner through fiber optic goggles (NordicNeuroLab; Bergen, Norway) and responded with their answers through a four-button keypad. Subjects responses were directly transmitted to a computer for storage. Each block began with 15 seconds of crosshair display during which subjects were instructed to relax and focus on the display. The subjects were then presented with a question in one of the representational form for nine seconds, the ISI was of 1.5 seconds and then they were presented with another slide consisting of a question in the same or different representation form for nine seconds. After the second representation subjects then had nine seconds to decide if both the representations (R1 and R2) presented the same concept or not and answered yes or no by pressing one of the designated buttons on the keypad.

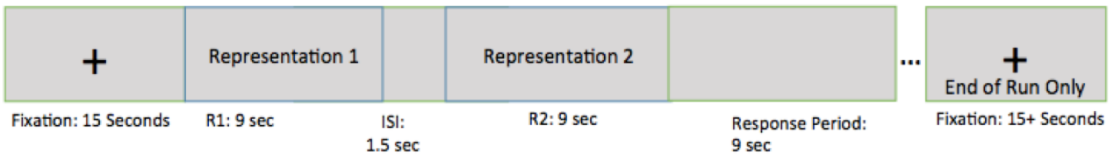

Fig. C.1.: The protocol of a block.

fMRI data analysis

fMRI scans were processed with an in-house MATLAB code adapted from afni_proc.py, using AFNI and FSL. The pipeline consisted of brain extraction, outlier detection, despiking, slice timing correction, motion correction, alignment to the T_1-weighted anatomical scan, tissue segmentation into gray matter, white matter and cerebral spinal fluid (CSF), and spatial smoothing within each tissue type (isotropic Gaussian filter with Full Width Half Maximum (FWHM) of 4mm). Anatomical and fMRI scans of all subjects were aligned to a standard template (skull stripped 1 mm^3 ICBM152) so that brain activation patterns from different subjects could be grouped together for analysis. Data were motion corrected using three motion parameters (three translational and three rotational for each x-y-z axes) and their derivatives as regressors in General Linear Model (GLM). Block regressors were used for each of the nine transitions and crosshairs in GLM.

Brain activations obtained from crosshair slides were treated as Baseline activations. Brain activations for each representation were obtained by comparing the $\beta_{Representation}$ versus $\beta_{Baseline}$ obtained from GLM of all subjects and all runs, using paired voxel-wise 3D t-tests followed by voxel-wise False Discovery Rate (FDR) correction. Adjacent voxels with $p_{FDR} < 0.05$ and cluster size greater than 100 voxels were considered as significant brain activations against the baseline and are as shown in the figures.

fMRI data gathered was analyzed differently for dependent variable, Cognitive Processing of Cryptography Concepts, based on which question was being investigated. When investigating where in the brain cryptography concepts are processed, activation patterns were gathered during the presentation of the first representation of each question. Activation present during the resting period following the question (noted as the second crosshair pattern in Figure 1) was subtracted from activation patterns noted during Representation 1. Data were separated based on the representation presented in Representation 1 in Figure 1, then the data were aggregated for all student participants (n=9) by representation n=18 per student), for a total of 162 individual data points per representation.

Evaluating whether translation between representations within questions impacted cognitive processing of cryptography, the period of time during the presentation of Representation 2 and the Response Period (as shown in Figure 1) was used to gather cognitive processing data and activation noted during the second crosshair pattern was subtracted from the gathered cognitive processing data. Data were grouped by the independent variable Representational Translation and aggregated for all students. In this case, three questions per topic did not require Representational Translation. So, the total number of data points for non-translation was n=18. Six per topic did require translation for a total translation n=36. Each student answered questions on the same six topics.

Finally, cognitive processing data were gathered and analyzed by the Instructional Method independent variable. In this case, the same data gathering process was used

as for analysis of Representational Translation, except that the data were grouped by the instructional method in which the topic was taught. In terms of this comparison, each student was given questions from three topics that were taught using the treatment instructional method that focused on representational fluency and three topics that were taught with the control instructional methodology. This analysis consisted of nine questions over three topics aggregated for nine students, or n=243. However, the research team delimited these comparisons by comparing only questions with the same structure to each other. For example, the fMRI results for all questions on a topic that required the subject to translate a concept from language to math (or vice versa) were aggregated to determine cognitive processing of cryptography concepts during that translation process. Therefore, the effective n=27 (three translations per topic, nine subjects in total) treatment data points and n=54 control data points.

C.3.3 Classroom Component

Research Question

Classroom data were used only in support of analysis of the fMRI results produced from this study; therefore, the research questions are the same as those discussed as part of the fMRI component earlier.

Variables and Operationalization

Independent Variables

The independent variable in this experiment was the method of instruction. Instructional methods were as-signed by the researchers to the following topics taught in class: Zero-Knowledge Proof (ZKP), Pohlig-Hellman Ciphers (PH), Rivest Shamir Adleman Cryp-tosystems (RSA), Digital Cash (DC), and Public Key Infrastructure (PKI). All other content taught during the semester was taught using two representational forms not focused on representational fluency.

Dependent Variables

The dependent variable was students pre to post-test learning gain. Learning gain was determined by normalizing students points scored on the pre and post-tests into a percentage interval variable, subtracting the pretest score from the post-test score, and averaging the differences of the twelve students for each question. Pre to post-test score differences were aggregated by instructional method and compared using a t-test.

Populations and Samples

Twelve of twelve students from a graduate-level, advanced network security course offered in the Spring 2017 semester at a large university in the Midwestern United States consented to allow their pre and post-test exam scores to be used in this research.

Setting

Data for this experiment were gathered in one section of a graduate-level advanced networking course at a large public university in the Midwestern United States. The course was not a required course. The control topics were taught using a combination of lectures delivered by projecting slides containing individual representational forms (language, graphics, or math) to deliver concepts to learners. Instruction of the treatment topics taught: Zero-Knowledge Proof (ZKP), Pohlig-Hellman Ciphers (PH), Rivest Shamir Adleman Cryptosystems (RSA), Digital Cash (DC), and Public Key Infrastructure (PKI) using activities consisting of multiple representations and focused on representational fluency. No other aspects of the instruction or scored evaluation of the students in the classroom differed between the control and treatment groups. Student performance was evaluated using a pretest and post-test, which also served as the students final exam.

Population

The population from which subjects were drawn for this experiment consisted of all students enrolled in the Universitys graduate advanced network security course offered by the college of Technology in the Spring of 2017. Enrolled students were predominantly 18-24-year-old. Because the experiment required subjects to consent

to the use of their scores on course homework, projects, and exams, those students who gave their signed consent to release their scores to the research team comprised the sample in each class section. All 12 students in the course consented to allow use of their classroom scores in this study.

C.4 Results

C.4.1 Brain Location: Cognitive Processing of Cryptography

In order to answer the question, Where in the brain are cryptography concepts processed?, the research team analyzed blood oxygen level data (BOLD) of participants, representing brain activity, taken during the fMRI while the participants were processing cryptography questions. Measurement of blood flow to the bran, the measurement on which fMRI is based, serves as a proxy for changes in brain activity. Increased blood flow to an area of the brain indicates increased brain activity, cognitive processing, where decreased activity is signaled by reduced blood flow to areas of the brain. In this re-search, questions were presented using graphical, language, and mathematics representations as shown in Figure C.1, which generated distinct patterns of brain activation, so we address the research question by representation.

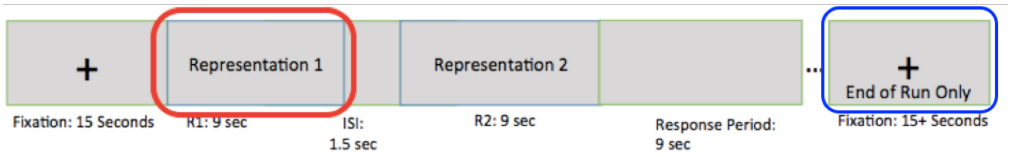

Fig. C.2.: Activation Comparisons by Representation.

This analysis used brain activation detected during the presentation of the first of two slides in each question, and the resting cross hair pattern following the question as illustrated in Figure C.2.

The research team aggregated the BOLD signal data for all questions by the type of the first representation, that is math, graphical, or language, across the nine

student participants. Cryptography concepts presented using mathematical, English Language and graphical representation produced BOLD activation patterns shown in Figure C.3.

Clusters of activation were noted at a significance level of $\alpha = 0.05$. Corresponding Broadmann Areas and usages are listed in Tables C.1, C.2 and C.3 below.

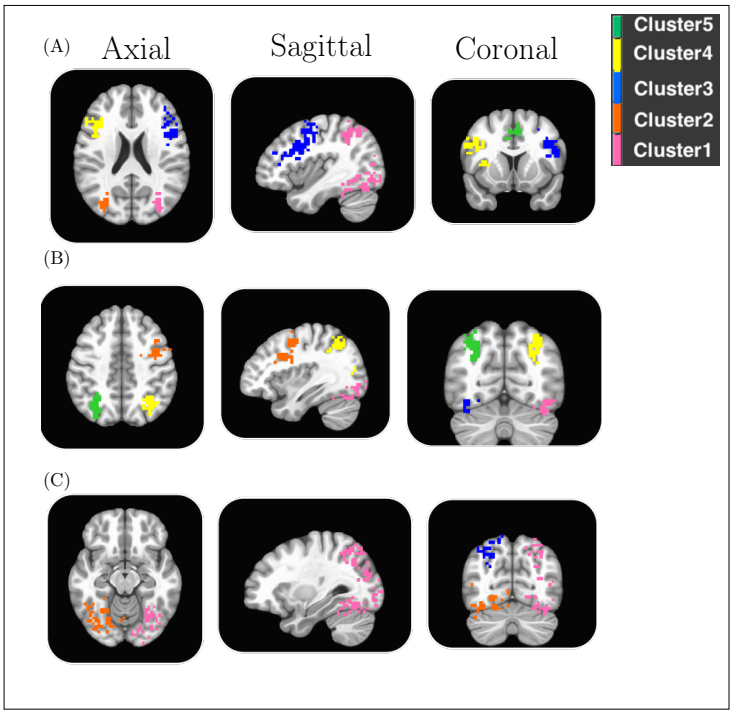

Fig. C.3.: Brain Activation of Cryptography Concepts presented using (A) Mathematical (B) Language and (C) Graphical Representations.

C.4.2 Brain Activation in Cryptography Processing During Translation of Representational Forms

The research team compared students cognitive processing on cryptography questions in which they were forced to make a translation between representational forms in order to answer the question against cognitive processing activity on questions in

Table C.1.: Math Processing Areas of Activation

Cluster	Broadmann Area	Gyrus	Usage
1	Left 39	Left Middle Temporal	Accessing word meaning
2	Right 39	Right Middle Temporal	Accessing word meaning
3	Left 9	Left Inferior Frontal	Representation of numbers
4	Right 44	Right Inferior Frontal	Executive Processing
5	Left 9	Left Medial Frontal	Executive Processing

Table C.2.: Language Processing Areas of Activation

Cluster	Broadmann Area	Gyrus	Usage
1	Left 17	Left Inferior Occipital	Visual Processing
2	Left 44	Left Inferior Frontal	Executive Language Processing
3	Right 37	Right Lingual Gyrus	Visual Processing
4	Left 3	Left Inferior Parietal	Somatosensory Processing
5	Right 1,2	Right Superior Parietal	Somatosensory Processing

Table C.3.: Graphics Processing Areas of Activation

Cluster	Broadmann Area	Gyrus	Usage
1	Left 30	Left Middle Occipital	Visual Processing
2	Right 7	Right Superior Parietal	Facial Stimuli
3	Right 37	Right Lingual	Visual and Letter Processing

which no such translation was necessary. We had hypothesized, based on [183], that questions requiring such a translation would produce more intense cognitive activity in similar brain regions than those that did not require representational translation. Our comparison of brain activation in this study did not support this hypothesis. Only brain activation patterns in the Language to Language questions, the Language

to Math, and the Math to Graphical analyses showed significant activation beyond baseline. Figure C.4 show the brain areas of significant activation in this comparison.

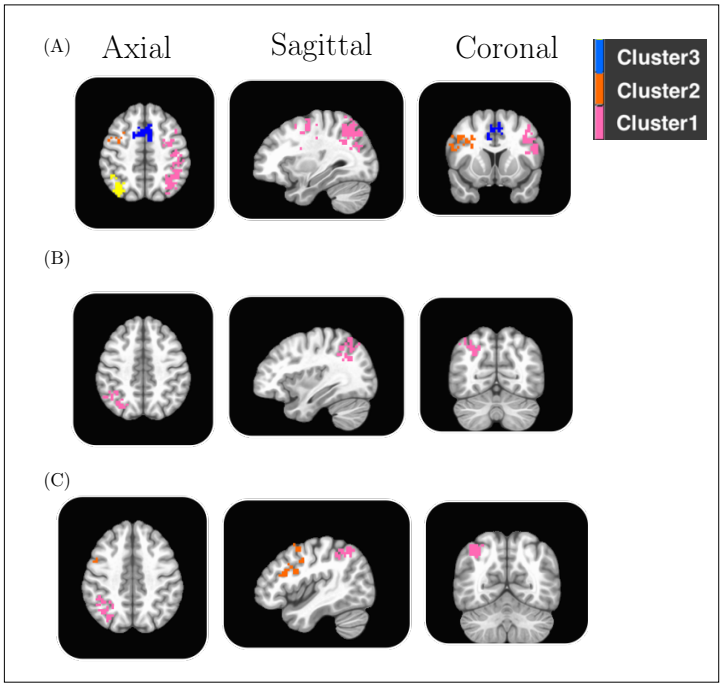

Fig. C.4.: Brain Activation for (A) Language to Language, (B) Language to Math and (C) Math to Graph Comparisons of Cryptography Concepts.

C.4.3 Cryptography Learning by Instructional Method

In support of the fMRI brain activation data comparison between topics instructed using MEA and focused on representational fluency and those taught using traditional lecture-based instruction, the research team also compared learning gains using the course pre-test and post-test. We hypothesized that teaching cryptography concepts using representational fluency would produce different patterns of cognitive activation compared against topics taught without a focus on representational fluency. For this

comparison, pre and post-test scores were aggregated from the twelve students in the class, and across all topics that were instructed using MEA and compared to those that were instructed using the traditional method of instruction not focused on representational fluency. This analysis showed an average learning gain of 10.83% on topics instructed using MEA and 3.56% on topics instructed using methods not focused on representational fluency. These learning gains are not significant at $\alpha = 0.05$ (t=1.19, p=0.24). Comparing pre-test scores based on instructional method indicated a similar level of knowledge, on average, of material that would be instructed using MEA ($\mu = 0.57$, $\sigma = 0.23$) versus topics that would be instructed using other methods ($\mu = 0.57$, $\sigma = 0.25$).

C.5 Discussion and Conclusion

The purpose of this work is to design and evaluate if and how representational fluencies are related to cognitive learning. The team specifically examined the following research questions:

Where does the cryptography occur in the brain?

The fMRI scan analyses showed that cryptography concepts, if represented using different formats, i.e. language, graph, and math notations, activate different parts of the brain. The results were statistically significant, even when the sample size was merely 9. The activation maps also echo similar distributions as the previous study on math and physics concepts. This may suggest that from cognitive perspective, cryptography is fundamentally not very different from math and physics. Or put it differently, brain activations are directly related to the form of the representations rather than the underlying complex cryptography concepts or algorithms.

Where do the transitions of different representations occur in the brain? Among nine possible representation fluencies, the re-search team discovered that three of them are statistically significant. They are from language to language, from language to math, and from math to graph. This suggest for the group of students that

participated fMRI scans, longer and stronger brain activities were recorded when students were asked to translate the same concept from language to language, from language to math, and from math to graph. Interestingly, the translation from math to language and the translation from graph to math were not shown the same statistical significance. If the research results are reliable, it can be inferred that representation translations are uni-directional. That is the brain reacts differently when translating language to math than translating math to language. If we further assume stronger or longer brain activations are related to more difficult tasks, then it may suggest the three transitions that showed statistically significance might be the ones that students having trouble with.

How does representational fluency impact the class-room learning results? The classroom learning results showed an average of 10.38% gains between pretests and post tests when the instructional methods were delivered using MEAs that representational fluencies. In contrast, the gains were merely 3.56% when conventional instructional methods were adopted in the classroom. However, the p value of the paired t-test was 0.26: too large for the research team to declare the findings are statistically significant. There were two major reasons accounted for this non-significance. The first was due to small sample size of 12. They second was the very high 57% average pretest scores. Students participated in this study were all graduate students and it would not be too surprising that they may possess strong prior knowledge. The high pretest scores may also relate to how the grade was calculated and normalized. Further study is needed with a bigger sample size, and preferably at undergraduate level to fully understand the impact the representational fluencies on the classroom learning results.

C.6 Future Work

The results of this study present several avenues for future research. Given the limitations of this experiment, future work could validate our findings regarding where

cryptography concepts are processed in the brain. Our failure to find significant results relating to cognitive processing activation during representational translations or cognitive processing related to representational fluency leave these areas open for additional research. In particular, it is possible that different types of classroom instruction or classroom measures of that instruction could also be performed in order to evaluate the effects on cognitive processing and learning. With a cognitive processing baseline set in this work for processing of cryptography, many aspects of learning can be compared against these baselines toward the goal of increasing cryptography learning in information security students.

VITA

VITA

Sumra Bari is a PhD candidate at the school of Electrical and Computer Engineering, Purdue University, IN, USA. She received her Bachelors degree in Electrical Engineering from University of Engineering and Technology (UET) Lahore, Pakistan in 2011 and Masters degree from Purdue University, West Lafayette, IN in 2015. Her research interests include image and signal processing, neuro-imaging, machine learning and network science.